Dissertation
submitted to the
Combined Faculties for the Natural Sciences and for Mathematics
of the Ruperto-Carola University of Heidelberg, Germany
for the degree of
Doctor of Natural Sciences

presented by

Diplom-Ingenieur (FH) Michael Angstmann
born in Mannheim, Germany

Date of oral-examination: _____

Characterization of cell-matrix interactions during multipotent mesenchymal stromal cell (MSC) differentiation

Referees: Prof. Dr. Stefan Wölfl
PD Dr. Frank Breitling

Abstract

For their huge variety of functions mesenchymal stromal/stem cells (MSCs) are attractive candidates for tissue engineering and cell therapy. Although *in vitro* differentiation of MSCs is well established and has been extensively studied, little is known about stem cell niches. So how are these niches defined in tissues and which cell-matrix contacts determine the fate of MSCs therein? To approach this task, herein the adhesive behavior of MSCs was evaluated under varying conditions employing non-invasive impedance monitoring in real-time, using fibroblast and keratinocytes as non-specific controls. Major focus was on changes in adhesion and migration of MSCs induced to differentiate into adipogenic and osteogenic lineages, the effects of extracellular matrix (ECM) contacts on this response, and the correlation of impedance profiles with specific differentiation markers including the predictive value of these recorded profiles. Finally, the influence of the MSC source was evaluated by comparing different cell populations derived from bone marrow and fat tissue.

MSCs roughly resembled fibroblast adhesion while keratinocytes differed significantly, which was reflected by impedance recordings. Inducing differentiation, impedance profiles of MSCs driven into the osteogenic lineage revealed a continuous rise of impedance due to matrix deposition and strong cell-matrix contacts and furthermore by maturation and formation of a mineralized matrix. Adipogenic differentiation was marked by shallower initial slopes and eventually declining profiles, corresponding to more compact and roundish cells with lowered cell-cell contacts. Concordance of impedance profiles and differentiation markers of the varying differentiation potential of MSCs from different donor and age underlined the reliability of the system. MSC migration was delayed during adipogenesis or by increasing cell attachment in response to TNFα treatment. Pre-coating with ECM proteins revealed favored osteogenesis on collagen I and IV, whereas adipogenesis was increased on fibronectin, which was also reflected by impedance recordings.

Overall, the present thesis revealed distinct differences of cell attachment during the process of differentiation and the guidance of differentiation by cell-matrix contacts and evaluated the potential of impedance measurements as a valuable tool for real-time, non-invasive high throughput screening of cell properties and identification of receptors involved in the regulation differentiation processes.

Zusammenfassung

Aufgrund ihrer vielfältigen Funktionen sind mesenchymale Stammzellen (MSCs) interessant für die künstliche Gewebskonstruktion und die Zelltherapie. Obwohl die *in vitro* Differenzierung von MSCs gut etabliert und weitreichend untersucht wurde, ist wenig bekannt über die Stammzellnischen. Wie sind diese Nischen im Gewebe definiert und welche Matrix-Kontakte bestimmen das Schicksal der MSCs? Um dieser Frage nachzugehen wurde das Adhäsionsverhalten von MSCs unter verschiedensten Bedingungen mit Hilfe von Impedanz-Messungen untersucht. Fibroblasten und Keratinozyten dienten als unspezifische Kontrollen. Das Hauptaugenmerk lag auf den Veränderungen der Zelladhäsion und Migration während der Differenzierung in Fett- oder Knochen-Zelllinien, den Effekten von extrazellulären Matrix (EZM)-Kontakten auf diese Veränderungen und der Korrelation der Impedanz-Profile mit spezifischen Differenzierungsmarkern, bzw. wie diese Profile der Abschätzung der Differenzierung dienen können. Desweiteren wurden Zellen aus Knochen- und Fettgewebe verglichen um den Einfluss der Zellherkunft zu untersuchen. Während sich Keratinozyten klar unterschieden, stimmte die Adhäsion von MSCs im Wesentlichen mit dem Verhalten von Fibroblasten überein, was sich auch in Impedanz-Messungen widerspiegelte. Nach Induktion wiesen die Profile der osteogenen Differenzierung aufgrund von Reifung und Bildung einer mineralisierten Matrix und starken Zell-Matrix-Kontakten einen kontinuierlichen Anstieg der Impedanz auf. Adipogenese zeichnete sich durch anfänglich schwächere Steigung und später abfallende Profile aus. Dies deckte sich mit kompakteren und runden Zellen sowie geringeren Zell-Zell-Kontakten. Übereinstimmende Impedanzprofile mit dem Differenzierungsgrad der Zellen aus unterschiedlichen Spendern und unterschiedlichem Alter bestätigen diesen Ansatz. Migration von MSCs konnte durch Induktion der Adipogenese oder durch Verstärkung der Zellanheftung durch TNFα-Behandlung verzögert werden. Zellinteraktionen mit EZM-Proteinen zeigten, dass die Osteogenese auf Kollagen I und IV bevorzugt wird, wohingegen die Adipogenese auf Fibronektin erhöht war. Diese Ergebnisse konnten durch Impedanzmessungen bestätigt werden.

Die vorliegende Arbeit zeigt wesentliche Unterschiede der Zellanheftung während des Verlaufs und die Steuerung der Differenzierung durch Zell-Matrix-Kontakte auf und untersuchte die Möglichkeiten von Impedanz zur nicht-invasiven Hochdurchsatzbestimmung von Zelleigenschaften in Echtzeit und zur Identifizierung von Rezeptoren die an der Regulierung der Abläufe der Differenzierung beteiligt sind.

Für meinen Papa.

Acknowledgements

I would like to acknowledge Prof. Dr. Stefan Wölfl and PD Dr. Frank Breitling for the willingness to supervise my PhD-Thesis. Thank you for attending the progress of the project and for providing hints and directions.

I am deeply indebted to my supervisor Prof. Dr. Christian Maercker for giving me this highly interesting project for my PhD thesis. I cannot sufficiently express my admiration and gratitude for all his encouragement, guidance and invaluable support throughout the thesis. He had always an open ear for discussions and propositions for the ongoing project. In addition, I would like to thank PD Dr. Dirk Breitkreutz, who was always willing to spend his free-time to discuss results and share his great enthusiasm for science and his extensive knowledge of matrix biology. Thank you both for putting your valuable time into this work.

Thanks to Irena Brinkmann and PD Dr. Karen Bieback not only for generously providing the cells, but moreover for the extraordinary cooperation and the nice atmosphere during our meetings. I am especially grateful to Prof. Dr. Petra Boukamp and Prof. Dr. Margareta Müller from the DKFZ Heidelberg, for letting me use their well equipped laboratories, where most of the present work was done. They helped me with my research and lighted up the project from a further point of view. I am most grateful for all your support and suggestions for my thesis. It is my big pleasure to thank all members of the Boukamp and Müller group for the great atmosphere in and outside of the lab, especially the 'Puma-Box' a.k.a. Agnieszka Dobrogowski, Benedikt Müller, Dennis Dauscher, and Marco Nici, for their outstanding performance and for making the lab a special place to work. Thanks for being a wonderful team. Special thanks must also go to 'animal trainer'

Sonja Depner who kept the thing running, gave useful hints and always had an open ear for the daily sorrows in the lab. Also thanks to our neighboring box with Alice Meides, Claudia Gutschalk, Nina Linde and Renate Becker. Thanks to all technicians for keeping the lab running. Thank you Iris Martin, Katrin Schmidt, Meike Schwan, Silke Haid, and so many other lab members for all your assistance which has always been highly appreciated. This work also would not be possible without the continuous support and help of Andreas Holloschi, Ariane Tomsche and Ina Schäfer at the Hochschule Mannheim to whom I would like to express my sincere gratitude.

Lastly, I would like to express my deepest gratitude to my parents, my sister and friends who supported me in any respect throughout the years and during the hardest times.

Contents

List of Abbreviations **vii**

List of Figures **x**

List of Tables **xi**

1 Introduction **1**

1.1 Mesenchymal stromal cells 1

1.1.1 Differentiation of MSCs 3

1.1.1.1 Adipogenic differentiation 4

1.1.1.2 Osteogenic Differentiation 5

1.2 The extracellular matrix and the stem cell niche 6

1.2.1 Proteins of extracellular matrix 7

1.2.1.1 Collagens 7

Collagen Type I 8

Collagen Type IV 9

1.2.1.2 Laminin 9

1.2.1.3 Fibronectin 10

1.3 Impedance measurements 12

2 Aims of this work **14**

3 Materials and Methods **15**

3.1 Materials 15

3.1.1 General materials 15

3.1.2 Materials for the cell culture 16

3.1.3 Chemicals and solutions for the cell culture 16

3.1.4 Chemicals and solutions for staining . . . 17
3.1.5 Primary antibodies for immunofluorescence staining . . . 18
3.1.6 Secondary antibodies for immunofluorescence staining . . . 18
3.1.7 Chemicals and solutions for protein analysis . . . 18
3.1.8 Primary antibodies for protein detection . . . 20
3.1.9 Secondary antibodies for protein detection . . . 20
3.1.10 Chemicals for PCR . . . 20
3.2 Cells and cell lines . . . 21
3.2.1 Mesenchymal stromal cells . . . 21
3.2.2 Fibroblasts . . . 21
3.2.3 The human epidermal cell line HaCaT . . . 21
3.3 Cell culture . . . 22
3.3.1 Cell Counting . . . 23
3.3.2 Cryopreservation of cells . . . 23
3.3.3 In vitro differentiation of MSCs . . . 23
3.4 Impedance measurements . . . 24
3.4.1 Normalization of xCELLigence impedance data . . . 25
3.5 Coating of ECM-proteins . . . 26
3.6 Multiple Substrate Array . . . 26
3.7 Migration assays . . . 26
3.8 Light microscopy and immunofluorescence . . . 27
3.9 Protein analysis . . . 28
3.10 Gene expression analysis . . . 30
3.10.1 PCR for nidogen-1 gene expression . . . 30
3.10.2 RT-qPCR of adipogenic marker genes . . . 31

4 Results **33**

4.1 Discrimination between cell type and cell number by impedance monitoring 33
4.1.1 Monitoring changes in cell adhesion . . . 35
4.1.1.1 Confirmation of molecular switch by gene and protein expression analysis . . . 35
4.2 Monitoring of MSC differentiation . . . 37
4.2.1 Differentiation potential of MSCs is dependent on passage number 37

4.2.2 Induction of differentation reflected by impedance 37
4.2.3 MSCs behavior depends on donor tissue 38
4.2.4 Confirmation of impedance data by specific staining, protein and RNA analysis 40
4.3 Cell adhesion on ECM proteins monitored by impedance measurements 44
4.3.1 Extracellular matrix proteins affect MSC differentiation 44
4.3.1.1 Adhesion on Collagen I depends on coating density . . . 45
4.3.2 Confirmation and quantification of adipogenesis and osteogenesis 47
4.4 Cell migration monitored by impedance 55
4.4.1 Expression of adhesion molecule affects cell migration 55
4.4.2 Migration of MSCs 56

5 Discussion **58**

References **73**

Appendix **87**

Abbreviations

AC	alternating current
ADRP	adipose differentiation related protein
AIM	adiopgenic induction medium
ALP	alkaline phosphatase
AMM	adipogenic maintenance medium
ARS	Alizarin Red S
ASC	adipose tissue derived mesenchymal stromal cell
BGP	β-glycerophosphate
BM	basement membrane
BMP	bone morphogenic protein
BMSC	bone marrow derived mesenchymal stromal cell
BSP	bone sialoprotein
C/EBP	CCAAT/enhancer binding protein
CAFs	carcinoma associated fibroblasts
cAMP	3'-5' cyclic adenosine monophosphate
CCL5	chemokine (C-C motif) ligand 5
Cbfa-1	core-binding factor-1
CFU-F	colony forming unit-fibroblastic cell
C_m	cell membrane capacitance
dH_2O	distilled H_2O
DMEM	Dulbecco's modified eagle medium
ECIS	electric cell-substrate impedance sensing
ECL	enhanced chemiluminescence
ECM	extracellular matrix
EDTA	ethylenediaminetetraacetic acid
e.g.	exempli gratia - for example
EGF	epidermal growth factor
ERK	extracellular signal-regulated kinases
FACIT	fibril-associated collagens with interrupted triple helices
FCS	fetal calf serum
Fn	fibronectin

GAPDH	glyceraldehyde-3-phosphate dehydrogenase
GMPs	good manufacturing practices
GvHD	graft versus-host-disease
HGF	hepatocyte growth factor
HLA-DR	human leucocyte antigen DR
hTERT	human telomerase reverse transcriptase
IBMX	3-isobutyl-l-methyl-xanthine
i.e.	id est - that is
IGF	insulin-like growth factor
IL	interleukin
ISCT	International Society for Cellular Therapy
kHz	kilo Hertz
LDV	leucine - aspartic acid - valine sequence
LE	laminin type EGF (epidermal growth factor)-like domain
LG	laminin G-like domain
MCP-1	monocyte chemotactic protein 1
mRNA	messenger ribonucleic acid
MSA	multiple substrate arrays
MSC-GM	mesenchymal stem cell growth medium
MSC	mesenchymal stromal/stem cell
NC-1	non-triple helical domain
OCN	osteocalcin
OIM	osteogenic induction medium
OPN	osteopontin
ORO	Oil Red O
OSE2	osteoblast-specific cis-acting element 2
PBS	phosphate buffered saline
PCR	polymerase chain reaction
PDGF	platelet derived growth factor
PER	perilipin
PKA	protein kinase A
POX	peroxidase
PPAR	peroxisome proliferative activated receptor

R_b	barrier resistance
RGD	arginine-glycine-aspartate sequence
RT	room temperature
RTCA DP	Real time cell analyzer Dual Plate
RT-qPCR	real time quantitative polymerase chain reaction
Runx2	runt-related transcription fator 2
SDF-1	stromal derived factor-1
TNF	tumor necrosis factor
TRAIL	TNF-related apoptosis-inducing ligand
U	units
VEGF	vascular endothelial growth factor

List of Figures

1.1 Principle of impedance measurement 12

4.1 Cell density and cell type affect impedance profiles 34
4.2 Attachment of cells on MSA 34
4.3 Impedance profiles of nidogen-inducible cells. 35
4.4 Expression of nidogen 36
4.5 MSC differentiation induces early and specific changes in impedance . . 37
4.6 Induction of MSC differentiation 38
4.7 MSC differentiation from different sources 39
4.8 Cells on electrodes 40
4.9 ORO and von Kossa stain of BMSCs and ASCs 41
4.10 Western blot of differentiated MSCs 42
4.11 Adipogenic gene expression of BMSCs and ASCs 43
4.12 Extracellular matrix molecules influence impedance differentiation profiles of MSC 44
4.13 Fibroblasts on extracellular matrix molecules monitored via impedance . 45
4.14 Concentration of collagen I affects impedance profiles 46
4.15 Denatured vs. native collagen I coating in impedance measurement . . . 47
4.16 Phase contrast microscopy of BMSCs on ECM proteins 48
4.17 Attachment of BMSCs on MSA on different ECM-proteins 48
4.18 Matrix influence on early adipogenic differentiation 49
4.19 ORO staining of d21 samples 50
4.20 Quantification of ORO staining on various collagen I concentrations . . . 51
4.21 Extracellular matrix molecules influence MSC differentiation: osteogenesis 52
4.22 Relative gene expression of adipogenic markers on ECM coatings 54
4.23 Wounding of HaCaT cells and fibroblasts 56

4.24 Migration of differentiating MSCs 57
4.25 Migration factors influence on MSCs 57

List of Tables

3.1.1 General materials 15
3.1.2 Materials for the cell culture 16
3.1.3 Chemicals and solutions for the cell culture 16
3.1.4 Chemicals and solutions for staining 17
3.1.5 Primary antibodies for immunofluorescence staining 18
3.1.6 Secondary antibodies for immunofluorescence staining 18
3.1.7 Chemicals and solutions for protein analysis 18
3.1.8 Primary antibodies for protein detection 20
3.1.9 Secondary antibodies for protein detection 20
3.1.10 Chemicals for PCR 20
3.6 Nidogen-1 primer 30
3.7 PCR program 30
3.8 RT-qPCR program 31
3.9 Primer sequences with specified probe numbers 32

1 Introduction

1.1 Mesenchymal stromal cells

Since their first description by Friedenstein et al. in 1970, mesenchymal stromal/stem cells (MSCs) have evolved from connective-tissue generating cells to a promising resource for therapeutic applications. Their adaptive mesodermal differentiation potential, immune regulatory properties and trophic functions make MSCs attractive candidates for novel cell therapies (Kern et al., 2006; Sensebé et al., 2010; Zhao et al., 2010). By selecting adhesive stromal cells, MSCs are readily isolated from various human tissues, including bone marrow and adipose tissue. They can be propagated *in vitro* maintaining their differentiation capacity and genetic stability (Kern et al., 2006; Bieback et al., 2009), though clonal nature defined as CFU-Fs (colony forming unit-fibroblastic cells) and true multipotent stemness are questionable in some cases (Bianco et al., 2010). Function and MSC behavior depend on the tissue of origin, age and individual characteristics of the donor, but also conditions of isolation and early propagation (Kern et al., 2006; Bieback et al., 2009; Gregory et al., 2005), all of which have to be addressed to qualify MSC isolates. Strategies to yield more homogeneous populations e.g. by clonal amplification or cell sorting are often hampered by paucity of suitable well-defined surface markers allowing for prospective isolation. Very crucial for expansion of MSCs is maintenance of stemness, i.e. self renewal capacity and specific tissue precursor properties, as prerequisites for clinical application. As promising approach for extending life span *in vitro* hTERT has been inserted in MSCs (Hung et al., 2010), which could foster tissue engineering but may *in vivo* increase the risk for developing cancer.

To provide common standards in the field of MSC more homogeneous, the International Society for Cellular Therapy (ISCT) defined minimal criteria for these cells. According to these criteria, MSCs must be (1) multipotential *in vitro* i.e. they must be able to differentiate at least into adipogenic, osteogenic and chondrogenic lineages and (2)

plastic-adherent. Additionally, surface markers of MSCs were defined and accordingly (3) MSCs must express CD105, CD73 and CD90. For excluding contamination, mainly by several types of hematopoietic cells, (4) they should lack CD45, CD34, CD14 or CD11b, CD79α or CD19 and HLA-DR (Dominici et al., 2006). Furthermore, an uniform terminology was agreed on to avoid further confusion. During the nearly 40 years after the first report of MSCs, several terms can be found in the literature: Introduced as osteogenic stem cells (Friedenstein et al., 1970), Caplan coined the popular term of mesenchymal stem cells (Caplan, 1991) while now MSCs should be addressed as multipotent 'mesenchymal stromal cells', and this term and definition is used throughout this thesis.

Since the 1990s MSCs have been used in various therapeutic approaches of tissue engineering and clinical regenerative medicine due to their potential to differentiate into diverse cell types like osteoblasts, adipocytes, or chondrocytes (Prockop, 1997; Pittenger et al., 1999; Gregory et al., 2005): Infusion of MSCs improved the outcome in children with osteogenesis imperfecta (Horwitz et al., 2002). Direct injection of concentrated bone marrow for the treatment of long-bone fractures supported bone healing when applying MSCs from bone marrow (Hernigou et al., 2005) and also MSCs in combination with tissue engineering was succesfully applied for bone replacement (Quarto et al., 2001). MSCs transplanted into infarcted heart and stimulated to differentiate into cardiomyocytes by 5-azacytidine reduced the size of damaged tissue (Tomita et al., 1999) and MSCs can also differentiated *in vitro* into functional beating cardiomyocytes (Makino et al., 1999; Planat-Benard et al., 2004a). Furthermore, MSC mediated enhancement of epithelial wound healing was shown. However, it needs to be clarified, whether MSCs contribute to wound healing by transdifferentation, for example into cornea cells (Arnalich-Montiel et al., 2008). Alternatively paracrine effects could stimulate neighboring stromal cells (Oh et al., 2008), by either recruiting macrophages or endothelial lineage cells (Chen et al., 2008) or, most likely through multiple combined pathways. MSCs can not only be implanted in diverse anatomical sites for tissue repair using their differentiation potential to resume physiological processes, reports have shown prevention of graft versus-host-disease (GvHD) and enhanced engraftment in haematopoietic stem cell transplantation in combination with MSCs (Le Blanc et al., 2008; Muller et al., 2008; Kim et al., 2004). Moreover, in response to cytokines and other soluble factors, they can also migrate into inflammatory sites and tumor surrounding

stroma (Mishra et al., 2009). Thus, genetically manipulated MSCs could deliver drugs to the tumor microenvironment for interference with tumor growth (Hall et al., 2007; Bexell et al., 2009).

However, besides envisaged therapeutic benefits, MSCs also carry potential risks. Spontaneous differentiation into osteogenic lineage including increased calcification by MSCs injected into rat hearts, demonstrated pitfalls in therapeutic application of MSCs (Breitbach et al., 2007). Not only development of 'wrong' tissues can occur, there are also reports that MSCs resident in tumor stroma converted into cells resembling carcinoma associated fibroblasts (CAFs) (Galiè et al., 2008; Mishra et al., 2009), though distinct markers to trace their fate or function are still elusive. Among other factors, CAFs secrete stromal derived factor-1 (SDF-1) that stimulates tumor cell proliferation and migration via SDF-1 receptor (CXCR4) (Orimo et al., 2005). Moreover, SDF-1 recruits endothelial precursors from bone marrow, favoring tumor angiogenesis. Other biomarkers suggest a strong relationship of MSCs with perivascular cells or pericytes which are essential for functional maturation of blood vessels (Brachvogel et al., 2005; Bexell et al., 2009; Paquet-Fifield et al., 2009; Bianco et al., 2010). Underlining MSC plasticity, mesenchymal-epithelial transitions have been reported, possibly generating also malignant epithelial cells, but this is still a controversial issue and in several cases cross-contamination in culture has been uncovered (Orimo et al., 2005; Rubio et al., 2008; Garcia et al., 2010). For all applications a challenging problem remains that cell isolates represent mixed populations, containing early precursors with a wide potential, cells committed already to distinct lineages or more specialized fibroblastoid cells (Bianco et al., 2010).

1.1.1 Differentiation of MSCs

The ability of MSCs to differentiate into cells of various tissue types as major hallmark of their properties is the most obvious benefit for clinical application. Besides fulfilling the minimal criteria for MSCs to give rise to adipogenic, osteogenic and chondrogenic cells (Gregory et al., 2005), differentiation into myocytes (Zuk et al., 2001), hepatocytes (Banas et al., 2007; Seo et al., 2005), neurons (Safford et al., 2004), pancreatic cells (Timper et al., 2006) and also into endothelial cells (Planat-Benard et al., 2004b) was

shown in various studies. In this thesis the main focus is on adipogenic and osteogenic differentiation.

1.1.1.1 Adipogenic differentiation

Differentiation along the adipogenic pathway is not only one of the crucial characteristics of MSCs, but might also be of clinical relevance for example in fat grafting for the treatment of contour deformities (Yoshimura et al., 2008). Early adipogenic differentiation is marked by increased levels of CCAAT/enhancer binding protein β (C/EBPβ) and CCAAT/enhancer binding protein δ (C/EBPδ) which in turn activate as heterodimers peroxisome proliferative activated receptor γ (PPARγ), one of the major proteins in adipocyte maturation and maintenance. PPARγ is thought to play a role in the growth arrest at G0/G1 phase typically seen for cells at the onset of adipogenic differentiation. This is followed by cell doubling for clonal amplification of committed cells (Pairault and Green, 1979). PPARγ activates C/EBPα, both leading to activation of adipogenic specific genes like adiponectin, perilipin, leptin, fatty acid synthase and fatty acid binding protein. But C/EBPα also serves as negative effector by decreasing the early adipogenic markers C/EBPβ and δ. By accelerating the degradation of β-catenin, PPARγ participates in suppression of Wnt-signaling, thus inhibiting osteogenesis (Liu and Farmer, 2004).

Morphologically adipogenic differentiation is accompanied by drastic changes of the cell shapes from an elongated fibroblast-like morphology into more roundish cells containing large accumulations of lipid droplets. The conversation into mature adipocytes is preceded by a decreased assembly of the cytoskeletal proteins actin and tubulin (Gregoire et al., 1998; Spiegelman and Ginty, 1983). For adipogenic differentiation *in vitro*, usually MSCs at confluent stage are stimulated with a cocktail of factors which trigger or accelerate adipogenesis such as dexamethasone, insulin, 3-isobutyl-l-methyl-xanthine (IBMX), and indomethacine. The glucocorticosteroide dexamethasone increases expression of the early adipogenic markers C/EBPδ and decreases glyceraldehyde-3-phosphate dehydrogenase (GAPDH) mRNA. The phospohodiesterase inhibitor IBMX increases the level of 3'-5' cyclic adenosine monophosphate (cAMP) which in turn activates protein kinase A (PKA). Perhaps of more input IBMX directly acts on the adipogenic differentiation process by increasing C/EBPβ levels. Indomethacine accelerates adipo-

genesis by increasing C/EBPβ expression in a prostaglandin-independent manner and by inhibiting of cAMP degradation but it might also be a direct agonist for PPARγ. In addition indomethacine increases levels of ADRP (Adipocyte differentiation-related protein, also termed adipophilin) which leads to accumulation of triglycerides and fat storage. Finally, due to its inhibitory activity on cyclooxygenases indomethacine also acts as negative effector of osteogenesis (Styner et al., 2010; Lehmann et al., 1997; Gregory et al., 2005). Insulin and also insulin-like growth factor (IGF)-1 are not only major regulators of glucose uptake, thus fueling lipid metabolism, but might also play a role in stimulation of the clonal amplification of committed adipogenic cells.

1.1.1.2 Osteogenic Differentiation

Their potential to differentiate into osteoblasts and the resulting ability to form bone matrix qualifies MSCs for therapeutical application supporting bone repair after injuries. At the cellular level the ossification process can be divided into three major stages of differentiation: (i) proliferation of precursor cells and mature osteoblasts, (ii) production and maturation of extracellular matrix (ECM), and (iii) cell-mediated mineralization of the matrix (Aubin, 2001). Each stage is accompanied by expression of a specific set of genes. Central player in osteogenesis is runt-related transcription fator 2 (Runx2), also termed Cbfa-1, which is activated via bone morphogenic proteins (BMPs) or ERK 1 and 2 dependent pathways (Lee et al., 2000; Salasznyk et al., 2004). Underlining its importance knock out of Runx2 leads to accumulation of immature osteoblasts and preventing of bone formation in mice (Komori et al., 1997; Otto et al., 1997). Activated Runx2 binds to osteoblast-specific cis-acting element 2 (OSE2) and induces several osteogenesis related proteins (Ducy et al., 1997; Hoshiba et al., 2009). One of those, osteopontin (OPN) shows two peaks of high gene expression, the first between day 4 and 6 after induction of differentiation and the second at late phase when matrix and mineralization are almost fully developed. Similarly, increased levels of bone sialoprotein (BSP) are also detectable in a very early and at late phase. In contrast, alkaline phosphatase (ALP) is expressed exclusively during early stages, initiating mineralization of the ECM by hydrolyzation of organic phosphates (Stanford et al., 1995). The ALP level decreases when mineralization is fully developed (Aubin, 2001). At this late stage again Runx2 induced genes are highly expressed as BSP and

other osteogenic specific markers like osteocalcin (OCN). Complete osteogenic differentiation *in vitro* is marked by deposits of calciumphosphate and hydroxyapatite in the mineralized matrix of cultured cell layers. Although cultivation of MSCs in medium containing dexamethasone, ascorbic acid and β-glycerophosphate (BGP) was shown to be efficient for *in vitro* osteogenic differentiation (Pereira et al., 1995; Colter et al., 2000), these conditions might not reflect the *in vivo* signals. Contradictory results for the role of bone morphogenic protein (BMP)2 in osteogenesis have been reported (Gregory et al., 2005; Hanada et al., 1997; Diefenderfer et al., 2003) whereas osteogenic differentiation has been also induced by other factors like 1α,25-dihydroxyvitamineD3 or 9-cis retinoic acid (Jørgensen et al., 2004; Titorencu et al., 2007). During the process of induced *in vitro* differentiation ascorbic acid increases the production of collagen and ALP activitiy in cells undergoing osteogenic differentiation (Maniatopoulos et al., 1988; Chan et al., 1990). The secreted collagens (mainly type I collagen) bind to integrin $\alpha 1\beta 1$ at the cell surface, activating intracellularly ERK proteins which in turn initiate a signaling cascade which ends in activation of Runx2 (Salasznyk et al., 2004). For matrix mineralization BGP serves as organic phosphate source for the osteogenic cells. Though dexamethasone is not essential for osteogenic differentiation, it apparently increases the osteogenic output of cells which differentiate. However, for its stimulating effect on adipogenic differentiation and the known negative influence of glucocorticoides on bones, the role of dexamethasone might be of ambivalent nature (Aubin, 2001).

1.2 The extracellular matrix and the stem cell niche

A central role for the pool of stem cells and their fate plays the stem cell niche, the environment in which genuine stem cells are located including surrounding cells, the composition of the surrounding ECM as well as growth factors bound or produced there. The stem cell niche not only maintains the self-renewal properties and regulates proliferation but also prevents or, upon appropriate stiumuli, directs stem cell differentiation (Warstat et al., 2010). Stem cells which are triggered to migrate out of their niche by extrinsic factors like cytokines or growth factors may enter circulation or can start to proliferate and differentiate into different lineages after homing at specific sites. For therapeutic application the maintenance of stemness of the cells *in vitro* is of crucial importance. Thus, major issues are, (1) providing an environment which allows

proliferation of the stem cells without losing their potential to differentiate and (2) the developing of factor-conditioned supports or matrices which are favorable for certain lineages. This will be of highest interest for either tissue engineering or direct clinical application of MSCs. Due to its protein composition the extracellular matrix (ECM) provides a scaffold for tissues and the cells within it. The composition of ECM macromolecules varies from tissue to tissue and through specific cell-matrix contacts the ECM plays also a regulatory role in cell adhesion, proliferation, migration, differentiation and cell behavior in general. In the context herein, these interactions with the ECM are essential for stem cells mediating their homing in the stem cell niche (Warstat et al., 2010). Concordantly, cultivation of MSCs on certain ECM proteins can improve the maintenance of differentiation potential *in vitro* (Volloch and Kaplan, 2002) but also promote (Salasznyk et al., 2004; Mizuno and Kuboki, 2001) or inhibit certain differentiation pathways (Mauney and Volloch, 2009, 2010; Santiago et al., 2009) which is further refined by structural and mechanical substrate properties like stiffness or elasticity (Engler et al., 2006; Rowlands et al., 2008). These signals from the outside (ECM) into the cell are mainly mediated by integrins (outside-in signaling) which triggers the cellular responses such as growth or maintenance of stemness, migration and differentiation.

1.2.1 Proteins of extracellular matrix

The ECM is made up by a large number of proteins and its composition varies from tissue to tissue, determining ECM function. ECM proteins can be grouped into collagens and other glycoproteins, both capable of self-assembly, and less structured proteoglycans. Due to their extended use this section further describes ECM proteins collagen I and IV as well as laminin and fibronectin.

1.2.1.1 Collagens

Collagens are the most abundant proteins in vertebrates, being present amply in all connective tissues and in varying amounts in virtually all organs. Collagen terms for a group of several subfamilies of trimeric proteins sharing structural and functional properties. All collagens express domains with triple helical conformation giving rise to rigid, rod-like molecular structures. Collagens such as fibrillar (type I, II, III, V and VI collagen) or short chain collagens (type VIII and X collagen) express only one

triple-helical domain spanning almost the entire length of the molecule. Other collagens such as basement membrane (BM) collagens (type IV collagens, several isoforms), FACITs (fibril-associated collagens with interrupted triple helices: type IX, XII, XIV, XVI and XIX collagen) or MACITs (membrane-associated collagens with interrupted triple helices: type XIII and XVII) are composed of show short triple helical domains which are interrupted by non-helical sequences (Kühn, 1995). The subunits of these superhelices, called α-chains contain the repetitive sequence motif (Gly-X-Y)$_n$, frequently with proline in the X or Y position besides any other amino acids. This is an absolute prerequisite for the typical rod-like collagen structure being stabilized through regularly spaced hydrogen-bonds. In addition collagens are stabilized by a high content of hydroxyproline through specific hydroxylation of proline in Y-position. This is raising the number of hydrogen-bonds and thus the degree of hydroxylation is further increasing the thermal denaturation temperature. Usually, collagens form fibrils, filaments or networks. The formation of these supramolecular aggregates occurs either by pure self-assembly or together with other extracellular components such as decorin or the 'minor' collagen types (FACITs). Collagens mostly contribute to the stable scaffold of ECM-structures, but also to the anchorage of cells to the ECM. Direct adhesion of cells to collagen occurs in a conformation dependent manner, mostly recognizing distinct triple-helical binding sites by integrins, in particular integrin $\alpha1\beta1$ and $\alpha2\beta1$. In addition, collagens can exhibit regulatory functions as well (Kreis and Vale, 1999). Thus, different types of collagens have an influence on cell differentiation and migration during development, in most cases also mediated via integrins.

Collagen type I is the predominant collagen in striated collagen fibrils. Its fibrillar structure makes collagen I the major protein in various tissues. It forms rope-like structures in tendon, sheet-like structures in skin, and in bone collagen I makes up to 90% of the total protein matrix which is aligned and reinforced by calcium hydroxyapatite. Thus, it provides the essential scaffold for ordered mineralization and provides bone a certain degree of elasticity. The molecular structure of collagen I is dominated by a long uninterrupted triple helical domain built by heterotrimers of two $\alpha1$(I) and one $\alpha2$(I) chain, also an $\alpha1(I)_3$ isoform exists but at low abundancy. Intracellularly synthesized heterotrimeric procollagens are secreted and propeptide regions are removed by N- and C-proteinases in the extracellulare space. These mature triple-helical molecules assemble into cross-banded fibrils, stabilized by further cross-linking

of specific lysine/hydroxylysine residues and non-helical as well as helical domains. Direct interactions of collagen I and cells is mainly mediated via integrin $\alpha1\beta1$ and $\alpha2\beta1$ (Staatz et al., 1991; Mecham, 2011).

Collagen Type IV, a major component of basement membranes, is a network-forming collagen and consists of variable combinations of six different α chains. The major part of type IV collagen is made up by a hetero-trimeric isoform consisting of two $\alpha1$(IV) and one $\alpha2$(IV) chain. Two further combinations of α-chains are found, which are from minor incidence: $\alpha3$(IV)$\alpha4$(IV)$\alpha5$(IV) and $\alpha5$(IV)$\alpha6$(IV). Structurally the α-chains can be separated into 3 domains: the N-terminal cysteine rich (7S) domain, a central triple helical domain and a non-triple helical domain (NC-1) at the C-terminal end of the molecule (Khoshnoodi et al., 2008). Network assembly of collagen IV is initiated by covalent cross-linking through its 7S domains, forming dimers and in a further step tetramers. Aggregation of tetramers is accomplished through end-to-end interactions of the C-terminal NC1-domains, finally forming a chicken-wire like network. Additionally, the network is stabilized by lateral associations between triple helical domains (Timpl et al., 1981). While the $\alpha1(\text{IV})_2\alpha2$(IV)-form is highly abundant, the $\alpha3$(IV) to $\alpha6$(IV)-chains are found only in specialized BMs. Thus, the $\alpha3$(IV)$\alpha4$(IV)$\alpha5$(IV) network is expressed in lung, kidney and neuromuscular junctions and the $\alpha5$(IV)$\alpha6$(IV) chains are restricted to BMs lining epidermal and smooth muscles cells, adipocytes, and kidney tubules (Kühn, 1995; Miner, 2011). In BMs the networks of collagen IV are closely linked, which is largely mediated by nidogen, further stabilizing BM structure (Breitkreutz et al., 2004; Nischt et al., 2007).

1.2.1.2 Laminin

Up to now, of the large glycoyprotein family of laminins at least 15 members are known. Each isoform consists of an α-, β- and γ-polypeptide chain, forming a heterotrimeric glycoprotein. Five different α-chains, four β-chains and three γ chains have been identified, which give the laminins a large variety of functional and biological activities. Nomenclature of laminins was revised in 2005 changing names from numeral ordered laminins according to their discovery to a 3-digit system based on their chain composition (Aumailley et al., 2005). So, laminins-5, -6 and -10, being most abundant in the basement membrane zone of adult skin (McMillan et al., 2003; Miner and Yurchenco,

2004), have been renamed laminin-332 (Lm-322), Lm-311, and Lm-511 for examples. Apparently β- and γ- chains are assembled first in the cell, while the addition of the α-chain is required for secretion. Genuine, i.e. unprocessed laminins have a cross- or T-shaped structure. The rod-like arm consists of the coiled-coil domains of the three different chains, held together by hydrophobic and polar interactions, and five globular laminin G-like domain (LG)-modules (LG1-LG5) at the C-terminus of the α-chain. The two or three short arms, are contributed by either the β and γ or all three chains, containing repeats of laminin type EGF (epidermal growth factor)-like domain (LE)-modules, interrupted by one or two globular L4 modules which are all individually stabilized by interchain disulphide bonds (Kreis and Vale, 1999; Ghohestani et al., 2001; Aumailley and Rousselle, 1999). The first step of polymeric self-assembly and network formation is mediated by interactions of the N-terminal 'sticky' ends (LN domains) of the short arms. In the BM zone, connection to the collagen IV networks occurs through nidogen binding at the γ1III4-module of laminin though nidogen-binding presumably also adapts laminin conformation for interactions (Breitkreutz et al., 2004). Laminins not only contribute to the formation of networks but are also directly involved in cell adhesion via integrins, especially the integrins $\alpha3\beta1$, $\alpha6\beta1$, $\alpha6\beta4$ and $\alpha7\beta1$ (Miner, 2011). The function of the individual laminins is considerably modified by proteolytic processing, especially clipping off LG4 and LG5 or N-terminal parts of the α and γ short arms. This processing is particularly extensive on Lm-332. While Lm-111 is prominent (mostly in the BM) during embryonic development, the most abundant laminin in human adults is Lm-511. Whereas the $\alpha1$ and $\alpha5$ chain apparently cannot compensate for each other despite of high sequence homology, the $\beta1$ and $\gamma1$ chains are essential in BM formation. Defects in the expression of $\alpha5$-chain are related to various developmental defects which are generally embryonic lethal (Miner and Yurchenco, 2004; Rebustini et al., 2007). Though the underlying mechanisms are not fully understood, this clearly points out that a functional basement membrane is essential for proper tissue function and signaling to adjacent cells.

1.2.1.3 Fibronectin

Another major protein of the extracellular matrix is the ubiquitous glycoprotein fibronectin (Fn). Two large subunits connected through disulfide bonds on the C-terminal

end form the basic dimeric structure of fibronectin. Each subunit can be divided into several domains which in turn contain different functional modules, responsible for crosslinking of fibronectin molecules, binding of cells or other ECM molecules like collagens, fibrin and heparin. Various isoforms of fibronectin-subunits are found which is caused by alternative splicing giving rise to 20 different fibronectin mRNAs. Cell binding of fibronectin occurs mainly through an RGD motif in the 'type III fibronectin (FnIII) repeat' in the cell binding module which is interacting with various integrins, primarily $\alpha5\beta1$ integrins, on the cell surface (Mao and Schwarzbauer, 2005). Binding of a LDV sequence motife with integrins $\alpha4\beta1$ or $\alpha4\beta7$ to a LDV sequence motif could be also detected in the alternatively spliced FnV region (Humphries et al., 2006; Leiss et al., 2008). In contrast to the self-assembling networks of collagens or laminins, these interactions of fibronectin with cells are a prerequisite for fibril formation in the extracellular matrix of tissues. As long as not bound to cells the cryptic binding site for fibronectin self-assembly is hidden in the molecular structure. Getting bound to cells the fibronectin molecules are stretched by cell mediated tension via integrins and intracellular actin stress fibers, which is exposing the binding module. The fibronectin molecules can now interact with other to form fibrilar networks around cells, thus connecting neighboring cells and contributing to matrix (ECM) organization (McDonald, 1988; Singh et al., 2010). This function is essential for keeping fibronectin monomeric and soluble e.g. to prevent formation of clumps in the bloodstream by spontaneous self-assembly (Alberts et al., 2007; Xu et al., 2009). Defects in fibronectin expression have severe effects particularly on the interactions of vascular cells with the ECM. Mice not expressing fibronectin are unable to form mature blood vessels and die at an early embryonic stage (George et al., 1993). Furthermore, fibronectin participates in wound healing, where conditional knockout of fibronectin was shown to provoke impairment of thrombus formation, growth and stability after injuries (Ni et al., 2003).

1.3 Impedance measurements

The principle of impedance measurement to monitor cell behavior electrically in tissue culture was first reported by the pioneering work of Giaever and Keese (1984) and was further developed into an own field of biosensors using this method called electric cell-substrate impedance sensing (ECIS) (Giaever and Keese, 1993). Based on this principle today several systems, each equipped with its own specific features like additional sensors for pH, temperature, glucose or oxygen-consumption evolved (Kirstein et al., 2006; Thedinga et al., 2007; Wiest et al., 2006). To monitor cell behavior electrically cells are grown in tissue culture vessels in which bottom (gold) electrodes are incorporated.

An alternating current (AC) signal of several kHz is applied on the electrodes and the resulting voltage can be measured to calculate the impedance, the AC equivalent to electric resistance. Therefore its unit is also Ohms (Ω). When cells are seeded in these culture wells and start to attach on the electrodes they serve mainly as insulators and restrict the current flow, thus increasing the impedance (Fig. 1.1). In general, impedance is closely related with the covered area of the electrodes, thus mainly influenced by the cell number and size of the cells attached to the electrodes, but also cell-cell and cell-substrate/ECM interactions further contribute to the overall impedance values. Therefore, the impedance profiles, varying in magnitude and initial slopes depending on cell morphology and attachment of the cells, reflect cell type and cell state and this method may be used as a valuable tool to characterize cells in a continuous but non-invasive manner (Giaever and Keese, 1993). Further interpretation of impedance data can be obtained if the phase of voltage

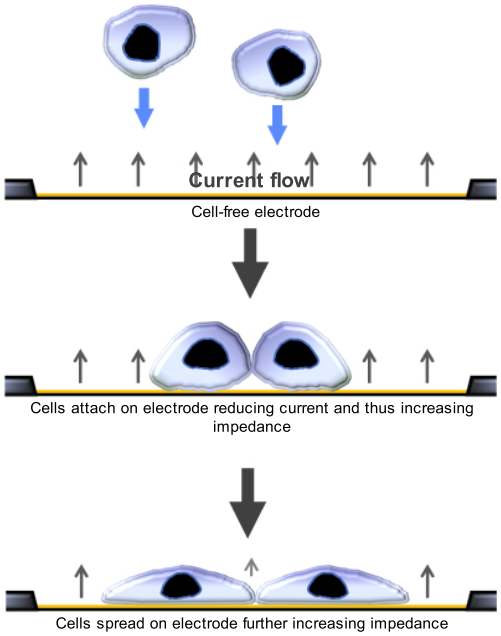

Figure 1.1: Principle of impedance measurement

is also considered. Measuring voltage and the phase of the voltage, impedance can be broken down into a pure resistive part **R**

$$R = \frac{V(inphase)}{I}$$

and a capacitive portion $\mathbf{X}_c$

$$X_c = \frac{V(outphase)}{I}$$

with

I electric current

and finally the **impedance Z** is given as

$$Z = \sqrt{R^2 + X_c^2}$$

herein X_c depends on the applied frequency of the AC, this parameter allows calculation of the capacitive proportion C of the impedance

$$X_c = \frac{1}{2\pi f C}$$

with

f frequency of the applied alternating current.

Based on this, a mathematical model was developed which determines three parameters further describing impedance data (for details see Giaever and Keese (1991) and Lo et al. (1995)). Therein, the current flows beneath the cells are defined by the cell-substrate parameter α which mainly depends on the cell size and the space between the cells and the substratum. The spaces and formed junctions between the cells determines the current flowing through the cell layer and defines the barrier resistance R_b. Finally, due to the plasma membrane the membrane capacitance C_m can be considered as well.

However, in this thesis two different impedance based systems were used both only measuring the parameter of impedance Z without regard to other parameters. The ECIS system (Applied Biophysics) allows microscopic evaluation of the cells but only a small fraction of the bottom of the well is covered with measuring electrodes, whereas the xCELLigence system (Roche) covers approximately 80% of the growth area but microscopy is hardly restricted due to the close gold layers. Further description of the systems can be found in 3.4.

2 Aims of this work

In the last decade multipotent mesenchymal stromal cells (MSCs) developed more and more to attractive candidates for therapeutical applications and tissue engineering. This is closely related to their mesodermal differentiation potential but also to further characteristics like immunomodulary properties. Differentiation of cells is often accompanied by changes in cell morphology, adhesion and changes of interactions with their environment including extracellular matrix- and cell-to-cell contacts.

This present thesis evaluates how cell adhesion is influenced during differentiation processes by interactions with proteins of the extracellular matrix or vice versa how these cell-matrix interactions further contribute to direction of cell differentiation. The process of differentiation of MSCs is monitored in a non invasive manner using real time impedance measurements in live cell chips. Impedance mainly reflects cell layer resistance against alternating current and, to a minute extent, cell surface electric capacity. For the present work the question was raised if impedance-based assays can determine changes in cell morphology and interactions during differentiation processes of MSCs and how this correlates to differentiation of the cells, determined by traditional histochemical staining, gene, and protein expression profiling. Furthermore, mobilization or migration from their stem cell niche and the guidance of migration into sides of injured tissue is mainly triggered by secretion of certain factors from inflammatory tissue. The migratory properties of MSCs during differentiation and in response to certain extrinsic factors were studied.

Overall this thesis aims on further characterization of MSC differentiation and, furthermore, cell-matrix interplay during differentiation and evaluates the readiness of impedance tools for studying cell differentiation mainly via changes in cell morphology and adhesive properties.

3 Materials and Methods

The present thesis was accomplished in a molecular-biological laboratory, classified biosafety level S1, considering all safety precautions. All used chemicals were of analytical grade or met the requirements for cell culture.

3.1 Materials

3.1.1 General materials

Name	**Information / Supplier**
Camera	Digital true color camera, ColorView212; SIS
Camera	Digital b/w camera F-View; SIS
Camera	Digital camera Camedia C-2020; Olympus
Devoloper	Agfa
Electrophoresis chamber	MiniVE System; Hoefer
Electrophoresis chamber	Model H5; Bethesda Research
Film processor	Classic E.O.S Typ 5270; Agfa
Fixer	Agfa
Fluorescence - and Lightmicroscope	AX-70; Olympus
Fluorescence - and Lightmicroscope	DM RD; Leica Microsystems
Spectrophotometer	Fluoroskan; Ascent Labsystems
Incubator	CO_2-Incubator CB210; Binder
Light Cycler 480	Roche
Lightmicroscope	BX-51; Olympus
Lightmicroscope	IX-70; Olympus
NanoDrop	NanoDrop 3300; Thermo Scientific
pH Meter	PB-11; Sartorius
Power supply	PowerPac Basic; BioRad
Power supply	GPS200/400; Pharmacia
Thermal Cycler	PTC-200; BioRad
Transfer system	BioRad
UV illuminator	MultiImage Light Cabinet; Fisherbrand

3.1.2 Materials for the cell culture

Name	Information / Supplier
μ-Slide	μ-Slide 8 well coated; ibidi
8W10E+	ibidi / Applied Biophysics
8W1E	ibidi / Applied Biophysics
Cell counter	Casy® Modell TTC; Schärfe Systme GmbH
Cell culture flasks	T25-, T75, T175 cell culture flasks; Greiner BioOne
Cell culture dishes	15 cm-, 10 cm- 6 cm-, 3.5 cm- tissue culture treated dishes; BD Bioscience
Coverslips	24x60mm; Menzel Gläser
Coverslips	round, 13 mm diameter; Neolab, Karl Hecht GmbH
ECIS instrument	ECIS Model 1600; ibidi / Applied Biopyhsics
E-plate 16	Roche
Freezing container	Mr. Frosty Freezing Container; Nunc
Freezing vials	Cryotube; Nunc
Microscope slide	76x26mm; R.Langenbrinck
MSA-Slide	Multiple Substrate Array; Biocat
Multi-well plates	6-well, 24-well, 96-well plate; BD Biosciences
Polypropylen-falcon	15 mL vials; BD Biosciences
Polypropylen-falcon	50 mL vials; BD Biosciences
Cell lifter	Costar
Silicon inserts	ibidi
xCELLigence instrument	Real time cell analyzer (RTCA); Roche

3.1.3 Chemicals and solutions for the cell culture

Chemical	Information / Supplier
Acetic Acid	Sigma-Aldrich
AIM	Adipogenic Induction Medium containing dexamethasone, h-insulin (recombinant), indomethacine, IBMX, L-glutamine, Growth Supplements, Gentamicin, Amphotericin B; Lonza
AMM	Adipogenic Maintenance Medium containing h-Insulin (recombinant), L-glutamine, Growth Supplements, Gentamicin, Amphotericin B; Lonza
Blasticidin S	Invitrogen
CASYton	Schärfe System GmbH
Collagen type I	from rat tail tendon; Roche
Collagen type IV	from human placenta; Sigma-Aldrich
Collagenase Type I	Sigma-Aldrich

DMEM	Dulbecco's Modified Eagle's Medium, 4.5g/l glucose, with L-glutamine; Lonza
DMSO	Dimethyl sulfoxide; Sigma-Aldrich
Doxycycline	Sigma-Aldrich
EDTA	0.05% in PBS + 1μl/ml phenol red; Serva
FCS	fetal calf serum; Gibco
Fibronectin	from human plasma; Roche
Ficoll-Hypaque-Plus	GE Healthcare BioScience;
Glycerol	Roth
Laminin	from Engelbreth-Holm-Swarm sacroma (mouse); Roche
MSC-GM	Mesenchymal Stem Cell Growth Medium containing L-glutamine, Gentamicin, Amphotericin B; Lonza
OIM	Osteogenic Induction Medium, containing dexamethasone, β-glycerophosphate, ascorbate, L-glutamine, Growth Supplements, Penicillin/Streptomycin; Lonza
PBS	Serva
PDGF	recombinant human PDGF-AB; Peprotech
Penicillin/Streptomycin	10000 U/10000 μg/ml; Biochrom
SDF-1α	recombinant human SDF-1α; Peprotech
TNFα	recombinant human TNFα; Peprotech
Triton X-100	Gerbu
Trypsin	0.1% in 0.05% EDTA/PBS; Roche
Zeocin	Invitrogen

3.1.4 Chemicals and solutions for staining

Chemicals	**Information / Supplier**
Alizarin Red S Solution	40 mM Alizarin Red S (Sigma-Aldrich) in H_2O, pH 4.1 adjusted with 10% ammonium hydroxide
Antibody solution	2% BSA in PBS
Blocking solution	5% BSA, 0.02% Tween20 in PBS
BSA	Bovine serum albumine; PAA
Formaldehyde	3.7% Paraformaldehyde; Merck in PBS
Hoechst33258	Serva
Isopropanol	Sigma-Aldrich
Mounting medium	Dako
Oil Red O Stock Solution I	3% Oil Red O (w/v) (Sigma) in isopropanol
Oil Red O Stock Solution II	0.5% Oil Red O (w/v) (Sigma) in 60% Triethyl phosphate (v/v) (Fluka)
Phalloidin	FITC-labeled phalloidin; Sigma-Aldrich

Pyrogallol solution	Sigma-Aldrich
Silver nitrate	Sigma-Aldrich
Sodium thiosulfate	Merck
Triton X-100	0.5%, Gerbu
Tween20	MP Bio
Whatman paper 42	Whatman

3.1.5 Primary antibodies for immunofluorescence staining

antigen	**produced in**	**dilution**	**Cat-#**	**Supplier**
Nidogen-1	rabbit	1:500	n/a	gift from R. Nischt, Cologne
Vimentin	guinea pig	1:100	GP53	Progen
Cytokeratin	guinea pig	1:100	GP14	Progen

3.1.6 Secondary antibodies for immunofluorescence staining

		produced in	**dilution**	**Cat-#**	**Supplier**
anti-guinea pig	Cy3	donkey	1:800	706-165-148	Dianova
anti-rabbit	Cy3	donkey	1:1000	111-165-144	Dianova

3.1.7 Chemicals and solutions for protein analysis

	Information / Supplier
Acrylamide	40% Acrylamide/Bis solution 37.5:1 (2.6%C); BioRad
Aprotinin	Sigma-Aldrich
APS	ammonium persulfate; Serva
β-mercaptoethanol	Merck
Blocking buffer	5% skim milk powder in TBS-T
Blot membrane	Nitrocellulose membrane; Whatman
Bradford reagent	Protein Assay; Biorad
Bromphenol blue	Serva
BSA	Bovine serum albumine; PAA
Collection gel	0.95 ml collection gel buffer, 2.6 ml H_2O, 0.3 ml acrylamide, 22.5 μl 10% APS, 7.5 μl TEMED
Collection gel buffer	0.5 M Tris-HCl pH 8.8, 0.4% SDS
ECL	Enhanced Chemiluminescense, GE Healthcare
EDTA	Serva
Glycerol	Roth
Glycine	Gerbu
Leupeptin	Biomol
Loading buffer	20% glycerol, 10% β-mercaptoethanol, 25% collection gel buffer, 6% SDS, bromphenol blue in dH_2O

Lysis buffer	10 mM Tris pH 7.2, 150 mM NaCl, 1% Triton X-100, 0.1% sodium desoxycholate, 0.1% SDS, 5 mM EDTA, containing 100 nM sodium orthovanadate, 10 nM Pefabloc, 1 μg/μl Leupeptin, 1 μg/μl Pepstatin, 1 μg/μl Aprotinin
Methanol	Sigma-Aldrich
Pefa bloc	Biomol
Pepstatin	Biomol
Ponceau S	5x Concentrate solution; Fluka
Protein Marker	PeqGold Protein Marker V, PeqLab
Running buffer	30 mM Tris, pH 8.3, 500 mM glycine, 0.1%SDS
Separation gel, 10%	2.5 ml separation gel buffer, 0.75 ml 50% glycerol, 4.25 ml H_2O, 2.5 ml acrylamide, 100 μl 10% APS, 10 μL TEMED
Separation gel, 6%	2.5 ml separation gel buffer, 0.75 ml 50% glycerol, 5.25 ml H_2O, 1.5 ml acrylamide, 100 μl 10% APS, 10 μl TEMED
Separation gel buffer	1.5 M Tris-HCl, pH 6.8, 0.4% SDS
Skim milk powder	Roth
Sodium chloride	Sigma-Aldrich
Sodium desoxycholate	Merck
Sodium dodecyl sulfate (SDS)	Gerbu
Sodium ortho vanadate	Sigma-Aldrich
Strip buffer	62.5 mM Tris, pH 6.7, 2% SDS, 1% β-mercaptoethanol
TBS	150 mM NaCl, 20 mM Tris
TBS-T	TBS, 0.1% Tween 20
TEMED	N,N,N',N'-Tetramethylethylenediamine; Sigma-Aldrich
Transfer buffer	30 mM Tris, 500 mM glycine, 20% methanol
Tris	Sigma-Aldrich
Tris-HCl	Sigma-Aldrich
Triton X-100	Gerbu
Tween 20	MP Biomedicals
X-Ray films	Super RX Fuji medical x-ray film; Fujifilm

3.1.8 Primary antibodies for protein detection

antigen	produced in	dilution	Cat-#	Supplier
ACT	rabbit	1:1000	sc-1616	Santa Cruz
ADRP	mouse	1:1000	AP125	Progen
BSP	mouse	1:1000	ab58825	Abcam
OPN	rabbit	1:1000	ab8448	Abcam
PER	guinea pig	1:2000	GP29	Progen
TUB	mouse	1:200	T4026	Sigma-Aldrich

3.1.9 Secondary antibodies for protein detection

		produced in	dilution	Cat-#	Supplier
anti-guinea pig	POX	rabbit	1:10000	A-5545	Sigma-Aldrich
anti-mouse	POX	donkey	1:10000	715-035-150	Dianova
anti-rabbit	POX	donkey	1:10000	711-035-152	Dianova

3.1.10 Chemicals for PCR

Chemicals	Information /Supplier
Agarose	Biozym
cDNA synthesis	Transcriptor High Fidelity cDNA Synthesis Kit; Roche
CoralLoad PCR buffer	Qiagen
DNA ladder	100 bp Plus DNA ladder, Fermentas
dNTPs	Sigma-Aldrich
Omniscript RT Kit	Qiagen
Primer	Thermo Scientific
Probes	Human Universal Probe Library; Roche
QIAshredder	Qiagen
RNase Inhibitor	Protector RNase Inhibitor; Roche
RNeasy Mini Kit	Qiagen
RT-qPCR reaction	Light Cycler 480 Probes Master; Roche
SYBRSafe	Invitrogen
TAE	40 mM Tris base, 20 mM acetic acid and 1 mM EDTA buffer
Taq DNA-Polymerase	Qiagen
96-well plates	for RT-qPCR, FrameStar; Axon
96-well cover foil	Axon

3.2 Cells and cell lines

3.2.1 Mesenchymal stromal cells

Mesenchymal stromal cells (MSCs) were generously provided by Karen Bieback's laboratory at University Hospital Mannheim. Cells were isolated from bone marrow (BMSCs, 3 donors) or adipose tissue (ASCs, 2 donors) as described previously, complying ethical standards (Kern et al., 2006). In brief, bone marrow aspirates were diluted with 2 mM EDTA-PBS and mononuclear cell fractions were isolated by centrifugation on Ficoll-Hypaque-Plus density gradients. Lipoaspirates were digested with 0.075% collagenase type I for 30-45 minutes at 37℃, blocking activity with basal medium, and stromal fractions were peletted, resuspended and filtered through gauze. Both BMSCs and ASCs suspended in complete mesenchymal stem cell growth medium (MSC-GM) were seeded at a density of 1 x 10^6 cells/cm^2 into T75 or T175 culture flasks. Non-adherent cells were removed with first medium change within 3 days after plating and the resulting fibroblastoid cells expanded in MSC-GM. All MSC isolates used herein fulfilled the minimal criteria defined by the ISCT (Dominici et al., 2006; Kern et al., 2006; Bieback et al., 2010).

3.2.2 Fibroblasts

Human fibroblasts were isolated from the dermis of healthy human skin obtained from the Department of Dermatology, University of Heidelberg (Smola et al., 1993). Wild type mouse fibroblasts were isolated from adult mice by outgrowth from explants of back skin samples (Angstmann, 2007). Its counterparts double knock out mouse fibroblasts isolated from newborn mice, deficient in nidogen-1 and nidogen-2 were generously provided by R. Nischt, Cologne (Nischt et al., 2007).

3.2.3 The human epidermal cell line HaCaT

The human epidermal cell line HaCaT was developed from a long-term primary culture of human adult skin keratinocytes, isolated from non-affected skin of a 62 year old melanoma male patient (Boukamp et al., 1988). Culturing in low calcium medium (0.2 mM) resulted in reduction of terminal differentiation of the keratinocytes. Furthermore, elevation of culture temperature to 38.5℃ caused increased proliferation and prolonged

the average life span, presumably by inducing genetic instability. Those modified culture conditions led to a spontaneous, immortalized human keratinocyte line, still restoring high differentiation potential while being not tumorigenic or invasive. At least in part, immortalization was due to the later found independent, distinct mutations in the p53 gene in both alleles. The name HaCaT indicates the initial culture conditions for establishing the cell line: human, adult, low calcium, and elevated temperature. Based on this immortalized cell line, HaCaT-ND1 cells, inducible in nidgogen-1 expression, were generated. Upon addition of tetracycline using the T-REx-system (Invitrogen) the extracellular matrix protein nidogen-1 (also entactin) is expressed (Angstmann, 2007; Regl et al., 2002; Yao et al., 1998).

3.3 Cell culture

All cells, mesenchymal stromal cells, HaCaT cell lines, mouse and human fibroblasts were cultured under standard conditions in a humified atmosphere at 37°C, 5% CO_2, 95% air.

Mesenchymal stromal cells were cultured in complete MSC-GM optimized for MSC cultivation containing antibiotics. MSCs were split at about 80-90% confluency by washing two times with phosphate buffered saline (PBS) and incubation with 0.1% trypsin. The trypsin reaction was stopped by adding equal amounts of complete growth medium. For subcultivation MSCs were seeded at densities of 2000 cells/cm^2 in fresh cell culture flasks. Skin derived keratinocytes and fibroblasts were cultured in 1x Dulbecco's modified eagle medium (DMEM) containing 10% fetal calf serum (FCS), 100 U/ml penicillin and 100μ/ml streptomycin. Fibroblasts were split when reaching confluency at a ration of 1:3 - 1:5 and HaCaT cells at a ratio of 1:10. To remove residual serum and ECM with bound calcium and magnesium, fibroblasts were washed twice with 0.05% EDTA while keratinocytes were incubated first in 0.05% EDTA for 15 minutes at room temperature. Fibroblasts were detached by incubation with 0.1% trypsin at 37°C for 3-5 minutes. HaCaT cells were incubated in 0.05% trypsin for about 7 minutes and trypsin reaction was stopped by adding complete growth medium. For maintenance of selection pressure on transfected HaCaT-ND1 cells medium was supplemented with 6 μg/ml Blasticidin S and 25 μg/ml Zeocin. For keratinocyte cultures designated for nidogen expression, 1 μg/ml of the inducing agent doxcycline was added.

3.3.1 Cell Counting

If desired, cells were counted using the automatic cell counter system CASY®-1. Routinely, 50 μl of trypsinized cell suspension were diluted 1:200 in isotonic CASYton solution. Cell numbers were calculated by the CASY®-1 system automatically.

3.3.2 Cryopreservation of cells

Cells were detached from culture dishes as described above for regular subcultivation. After inactivation of trypsin cell suspensions were centrifuged for 5 min at 1000 x g. The supernatant was removed carefully and cell pellets were resuspend in freezing medium. Keratinocytes and fibroblasts were frozen in 1xDMEM, 20% FCS, 10% glycerol at a final concentration of 2 x 10^6 cells/ml. For MSCs final concentration was set to 0.5 x 10^6 cells/ml in FCS containing 20% DMSO. Aliquots of 1 ml were transferred into cryotubes and pre-cooled for 1 h at 4°C. The freezing was performed gradually, decreasing temperature 1°C per minute in a freezing container. Frozen samples were stored in liquid nitrogen. For recultivation, cells were thawed in a 37°C water bath rapidly and transferred immediately to a 100 mm culture dish containing complete growth medium. To remove residual cryoprotectant medium was changed 24 h after thawing.

3.3.3 In vitro differentiation of MSCs

For gene and protein expression as well as histochemical analysis 3-4 x 10^3 cells/cm^2 were seeded and kept in MSC-GM for 24 hours. Adipogenic differentiation was induced in confluent cultures by adipogenic induction medium, containing recombinant human insulin, dexamethasone, indomethacin, and 3-isobutyl-l-methyl-xanthine (IBMX) (AIM). Three days later, AIM was replaced by adipogenic maintenance medium lacking dexamethasone, IBMX and indomethacine (AMM) for 2 days. After 3 induction/maintenance cycles and 4-7 additional day in AMM, adipogenic differentiation was fully developed. Uninduced control cultures were kept in MSC-GM throughout. For osteogenesis confluent cultures were incubated in osteogenic induction medium, containing dexamethasone, ascorbate and β-glycerophosphate (OIM). Fresh OIM was added twice a week for 21 days, while negative controls were fed with MSC-GM on the same schedule.

3.4 Impedance measurements

Measurements were done in two different systems, recording changes in electrical resistance of cell layers on sensing gold electrodes (Atienza et al., 2005). Using the ECIS Model 1600 and appropriate software, cells were analyzed in eight well-plates, each well (0.8 cm^2) with 40 electrodes of 250 μm diameter (ECIS 8W10E+ arrays). For measurement an oscillator sets an AC signal of 1-V amplitude at a frequency of 45 kHz in series with a 1 MΩ resistor resulting in an approximately constant current of 1 μA. Measuring signals are obtained through a lock-in amplifier and impedance data are collected at a computer. ECIS device allowed microscopic observation of samples, but titration curves revealed that cells had to be seeded at high densities for effective measurements. To improve cell attachment, wells were incubated with complete MSC-GM for 4 hours. Medium was removed and 0.5 ml cell suspension was applied to each well (0.5 - 1 x 10^5 cells/well equal to 0.6125 - 1.25 x 10^5 cells/cm^2), suspending fibroblasts or MSCs directly in differentiation media (AIM or OIM) or control media (MSC-GM). Accordingly, for impedance data of keratinocyte cultures wells were preincubated with DMEM, 10%FCS for 4 hours and cells were seeded at densities of 2 x 10^5 cells/well (2.5 x 10^5 cells/cm^2). Directly after cell plating arrays were placed in an incubator (37°C, 5% CO_2) and impedance was recorded in duplicate samples at 45 kHz. Secondly, the xCELLigence RTCA DP instrument was employed. In this 3 x 16 well-device (E-Plate 16; 0.2 cm^2/well), cell containments have a much higher electrode density covering 80% of the surface area (Atienza et al., 2005). Here cell titration revealed that much lower seeding densities were required, but light microscopy was not possible. Cell preparation and conditioning of xCELLigence wells was as described above except that 5 x 10^3 cells/well (2.5 x 10^4 cells/cm^2) were seeded and first allowed to settle for 30 min at room temperature (RT) before transfer to the incubator. Measurements were done in quadruplicates at 50 kHz (37°C, 5% CO_2).

For comparative analysis, ECIS impedance data were normalized by dividing recorded impedance values by the impedance measured at time zero of recording or at the point of adding induction media, respectively. Defining these reference values as 1.0, the later time points indicate changes in the relative impedance which is dimensionless. Due to the supplier-defined readout of the xCELLigence system the corresponding values had

to be recalculated first, as detailed in 3.4.1, to obtain profiles which are comparable for both systems.

3.4.1 Normalization of xCELLigence impedance data

The xCELLigence readout is defined by the manufacturer as "Cell Index"

$$CI = \frac{R_{tn} - R_{t0}}{F}$$

with

R_{t0} Background resistance measured at time point zero

R_{tn} Resistance measured at time point "n"

F Frequency dependent constant of the instrument

According to supplier's information F is 15 Ω. Based on the background value R_{t0} determined beforehand, R_{tn} can be calculated from the CI values for each measured time point using the rearranged formula from above.

$$R_{tn} = CI * F + R_{t0}$$

As for ECIS recording, normalized curves (relative impedance, dimensionless) were obtained by dividing the recorded impedance values (R_{tn}) by the background impedance at time zero (R_{t0}), so by definition the relative impedance at time point zero is again 1.0.

3.5 Coating of ECM-proteins

Cell adhesion, growth and differentiation was monitored on the extracellular matrix proteins collagen type I, collagen type IV, fibronectin, and laminin. For stock solutions collagens were dissolved in 0.2% sterile acetic acid (2 mg/ml) over night at 4℃ and fibronectin in sterile water (1 mg/ml), while laminin was supplied in solution (0.5 mg/ml). For denaturing of type I collagen, stock solution of collagen I was heated to 56℃ for 8 hours. For impedance measurements, the wells of E-plate 16 were coated with 100 μl/cm^2 of 50 μg/ml protein in PBS at RT for 45 minutes (corresponding to 5 μg/cm^2), adding plain PBS to control wells. Liquids were aspirated, wells washed twice with PBS, and cells plated on freshly coated, non-dried surfaces, measuring impedance in quadruplicates. For comparison cells were seeded on coated cover slips at comparable densities.

3.6 Multiple Substrate Array

Cell attachment on a variety of ECM proteins was determined on multiple substrate arrays (MSA). The assembled culture devices contain 14 wells with the proteins collagens I-VI, laminin, fibronectin (all those from different tissue sources), vitronectin, and heparan sulfate proteoglycan, each microspotted in quadruplicates on a glass surface. To evaluate the influence of differentiation media on cell adhesion and spreading 1 x 10^4 BMSCs per well were seeded on MSA slides in AIM, OIM, and in MSC-GM as control. For comparison fibroblasts and HaCaT cells were seeded on MSA slides in DMEM, 10% FCS. After 4 hours incubation at 37℃ (95% air, 5% CO_2) cells were washed in PBS, fixed with 3.7% formaldehyde and further processed for staining and immunofluorescence as described in 3.8.

3.7 Migration assays

For migration studies, cells were seeded in duplicates as described above in ECIS 8W1E arrays containing only one central single sensing electrode (250 μm diameter) in each well (Keese et al., 2004). 5 x 10^4 MSCs and fibroblasts or 2 x 10^5 keratinocytes were seeded and grown to plateau values of impedance recordings. These confluent cell layers

were wounded by a pulse of 4V (45 kHz) for 20 seconds for MSCs and fibroblasts or 3 times 20 second pulses for keratinocyte cultures, respectively, causing complete cell detachment from the electrode. Recordings were resumed immediately after the pulse to monitor repopulation of the wounded area. To study the influence of soluble factors on migration, media were supplemented with 100 ng/ml SDF-1, 10 ng/ml platelet derived growth factor (PDGF)-AB or 50 ng/ml tumor necrosis factor α (TNFα), respectively. In parallel, μ-slides equipped with removable silicon-inserts providing two separated growth areas were used. 8,000 cells per insert well were seeded and after reaching confluency, silicon inserts were removed to allow cells to migrate into the artificial cell-free gap. To document closing of the gap, microscopy pictures were taken every 24 hours and newly populated area was determined by image analysis using ImageJ software (http://rsbweb.nih.gov/ij/).

3.8 Light microscopy and immunofluorescence

Cells grown on cover slips or in ECIS arrays were fixed with 3.7% formaldehyde for 15 minutes, washed with dH_2O and treated with 0.5% Triton X-100 for 5 minutes. After two washes with PBS, samples were blocked in blocking buffer composed of 5% BSA, 0.02% Tween20 in PBS, and then incubated with guinea pig antibodies against vimentin or keratin (1:100) in 2% BSA for 90 minutes at RT. After three washes in PBS and incubation in blocking buffer for 15 minutes, Cy3-labeled secondary donkey antibodies against guinea pig, were applied for 45 minutes in the dark, together with Hoechst 33258 (1:50) for nuclear staining. For actin filament staining, samples were incubated with FITC-conjugated phalloidin (1:50 dilution). After three washes in PBS for 10 minutes samples were covered with mounting medium.

For staining of lipid droplets, fixed samples were washed in 60% isopropanol for 3 minutes and stained for 5 minutes in Oil Red O (ORO) in isopropanol. Therefore, three parts of ORO stock solution I were diluted with two parts of dH_2O, filtrated through whatman paper. Excessive dye was removed and samples washed in tap water several times. Nuclei were counterstained in hematoxylin solution for 5 minutes and samples were washed again in tap water until wash solution remained clear. ORO staining protocol was modified for fluorescence detection of lipid droplets as reported previously (Koopman et al., 2001). Three parts of ORO stock solution II were diluted

with 2 parts of dH_2O, filtrated through whatman paper. Before mounting, processed immunofluorescence samples were incubated with ORO stain for 30 minutes, rinsed with dH_2O and finally under running tap water for 10 minutes. Pictures were taken with a Leica DM RD microscope equipped with Analysis software (Olympus).

Osteogenic differentiation was determined by staining fixed cells with 40 mM Alizarin red S, pH 4.1 for 20 minutes (Gregory et al., 2004). Samples were washed four times with dH_2O for 5 minutes and micrographs taken as above. Alternatively, for osteogenic von Kossa staining (Majumdar et al., 1998) fixed samples were incubated in 5% silver nitrate for 15 min, 2 times washing in dH_2O before developping in 1% pyrogallol solution for 5 min in the dark, washed twice with dH_2O and fixated in 5% sodium thiosulfate for 5 minutes. The intensity of red ORO or Alizarin staining was evaluated together with nuclear Hoechst stain in 21 day cultures using ImageJ software. At least 10 pictures were analyzed and statistical significance was determined by Student's t-test.

3.9 Protein analysis

For protein extraction, MSCs grown in the different media (MSC-GM, adiopgenic induction medium (AIM), osteogenic induction medium (OIM)) were harvested at day 0, 2, 5 and 14. After washing with ice-cold PBS, cells were scraped with a cell lifter and centrifuged for 5 min at 250 x g, 4℃. Cell pellets were suspended in lysis buffer, supplemented with protease inhibitors and incubated on ice for 60 minutes. Cell debris was removed by centrifugation for 10 min at 10,000 x g, 4℃ and supernatant was transfered into a new vial. Protein concentrations were determined by colorimetric assay according to Bradford. The protein content of protein lysates was calculated from a standard BSA curve as reference, covering the range of 0-4 μg/ml protein. The standards and 1:10 diluted samples with Bradford reagent were measured in a spectrophotometer at 595 nm.

Total protein (100 μg) was mixed with sample loading buffer, heated at 95℃ for 5 minutes and proteins were separated by electrophoresis in a 10% SDS-polyacrylamide gel. Proteins were transferred onto nitrocellulose membranes and protein transfer was checked with Ponceau S. Ponceau was removed by washing in blocking buffer and after

additional blocking for 1-2 hours, membranes were incubated with primary antibodies (guinea pig anti-perilipin, mouse anti-adipophilin, mouse anti bone sialoprotein, rabbit anti-osteopontin) at 4℃ over night. Unbound primary antibodies were removed by 3 times washing in blocking buffer for 10 minutes before incubation with peroxidase (POX)-conjugated secondary antibodies for 45 minutes at RT. Enhanced chemiluminescence (ECL) reaction was detected on x-ray films, developed in an AGFA film processor.

Mouse wild-type fibroblasts and keratinocytes, 3 days induced for nidogen-1 expression and uninduced controls were lysed as described above and 30 μg of total protein were separated in a 6% SDS-polyacrylamide gel. After protein transfer and blocking, membranes were incubated with rabbit anti-nidogen-1 antibody and detected with anti-rabbit POX-conjugated secondary antibodies. For loading controls bound antibodies were removed by incubation in 62.5 mM Tris, pH 6.7, 2% SDS, 1% β-mercaptoethanol at 56℃ for 10 minutes followed by several washing steps with blocking buffer to remove residues of β-mercaptoethanol. Membranes were incubated with rabbit anti-β actin or mouse anti-β-tubulin antibodies and detected as above.

3.10 Gene expression analysis

For isolation of RNA, cells were lysed in 350 μl RLT buffer containing 1% β-mercaptoethanol and RNA was isolated using the RNeasy Mini Kit from QIAgen. Concentrations of isolated RNA samples were determined using a NanoDrop fluorospectrometer.

3.10.1 PCR for nidogen-1 gene expression

Reagents for reverese transcription were from the Omniscript RT Kit. Two μg of RNA were incubated in 1x reverse transcription buffer, containing 0.5 mM of dNTP mix, 1 μM Oligo-dTs, 4 U Omniscript RT enzyme, and 10 U RNase-Inhibitor in a total volume of 20 μl. Reverse transcription reaction was carried out in a thermal cycler at 37°C for 60 minutes. For detection of nidogen-1 gene expression, 2 μl of reverse transcriptase reaction were used in 1x CoralLoad PCR buffer containing 1.5 mM $MgCl_2$, 0.2 mM of each dNTP, 0.4 μM of each primer (table 3.6) and 1.5 U Taq DNA polymerase. Conditions of PCR are described in tabel 3.7. PCR-product was separated in a 2% agarose gel in 1xTAE buffer, containing 1:10000 SYBR Safe and detected using an UV illuminator.

Table 3.6: Nidogen-1 primer

Primer	Sequence
Forward	5'-TGG CAG CAG AGT ATG TCC AG
Reverse	5'-GCT CCG TTG CTC TTC CAT AG

Table 3.7: PCR program

	Temperature [°C]	Time	Cycles
Pre-incubation	95	5 min	1
Amplification	95	1 min	35
	60	45 s	
	72	1 min	
Extension	72	10 min	1
Cooling	4	∞	

3.10.2 RT-qPCR of adipogenic marker genes

The relative expression of adipogenic marker genes (table 3.9) was analyzed after 24, 48 and 72 h, as well as 5, 7 and 14 days. One μg RNA was reverse transcribed using 2.5 μM anchored-oligo(dT)18 primer and the Transcriptor High Fidelity cDNA Synthesis Kit. For RT-qPCR a 20 μl reaction mix of 50 ng transcribed RNA, 0.2 μM primer and 0.1 μM probe (table 3.9) and 10 μl Light Cycler 480 Probes Master was applied to a Light Cycler 480 as indicated in table 3.8. Three genes (table 3.9), identified with geNorm (http://medgen.ugent.be/~jvdesomp/genorm/index.php) as the most stable expressed genes out of five tested, were taken to calculate a normalization factor. Primer efficiency has been determined and relative expression based on efficiency and the normalization factor was calculated as described in (Vandesompele et al., 2002). A cDNA mix of three adipocyte samples served as positive control to normalize PCR plates and RNase-free water as negative control.

Table 3.8: RT-qPCR program

	Temperature [°C]	Time	Ramp rate [°C/s]	Cycles
Pre-incubation	95	10 min	4,8	1
Amplification	95	10 s	4,8	45
	60	30 s	2,2	
	72	1 s	4,4	
Cooling	40	10 s	1,5	1

Table 3.9: Primer sequences with specified probe numbers

Gene	Primer sequence	Probe [1]
TATA box binding protein (TBP) [2]	F: 5'-cccatgactcccatgacc-3'	51
	R: 5'-tttacaaccaagattcactgtgg-3'	
beta-2-microglobulin (B2M) [2]	F: 5'- ttctggcctggaggctatc-3'	42
	R: 5'-tcaggaaatttgactttccattc-3'	
glyceraldehyde-3-phosphate	F: 5'-tccactggcgtcttcacc-3'	45
dehydrogenase (GAPDH) [2]	R: 5'-ggcagagatgatgacccttttt-3'	
peroxisome proliferative activated	F: 5'-caggaaagacaacagacaaatca-3'	7
receptor γ (PPARγ)	R: 5'-ggggtgatgtgtttgaacttg-3'	
perilipin	F: 5'-ggacacagtggtgcattacg-3'	64
	R: 5'-gtcccggaattcgctctc-3'	
adiponectin (ADPQ)	F: 5'-ggtgagaagggtgagaaagga-3'	85
	R: 5'-tttcaccgatgtctcccttag-3'	

[1] Human Universal Probe Library (Roche)

[2] Reference genes

F, forward; R, reverse

4 Results

4.1 Discrimination between cell type and cell number by impedance monitoring

To optimize conditions for impedance measurements different cell types were seeded at various densities. Immortalized human keratinocytes, skin derived human fibroblasts and human mesenchymal stem cells were used. Direct correlation with cell morphology was made in the electric cell-substrate impedance sensing (ECIS) system (see methods 3.4). The impedance recordings (xCELLigence) revealed nearly complete saturation for BMSCs at a seeding density of 5 x 10^3 cells/well (2.5 x 10^4 cells/cm^2), only marginally increasing at higher cell densities (Fig. 4.1). After an initial very rapid increase which matched with nearly full cell spreading within the first 4 hours (Fig. 4.2), at 10 hours curves tended to decrease, rising slowly but steadily again after approximately 24 hours (Fig.4.1 A). Seeding 2.5 x 10^4 fibroblasts/cm^2 showed a comparable peak, while the maximum was nearly doubled with 5 x 10^4 cells/cm^2, profiles declining later on to a lower plateau depending on the initial cell number (Fig. 4.1 B). With similar numbers of HaCaT cells (5 x 10^4 cells/cm^2) impedance rose markedly slower and reached plateaus with considerable delay after 45 hours (Fig. 4.1 C), well correlating to generally slower and less intense spreading of keratinocytes (Fig. 4.2). Thus, by plating more HaCaT cells sensing electrodes were covered within 5 to 10 hours giving rise to strong impedance values. This emphasizes that both cell number and spreading or morphology strongly influence impedance profiles. But the smaller surface and higher coverage with gold electrodes in the xCELLigence system allowed lower cell seeding (factor 10-20) and thus was used for statistical analysis. The ECIS system (cell titration not shown) in contrast allows the direct correlation with cell morphology and thus was used to monitor differentiation by cellular staining after recording.

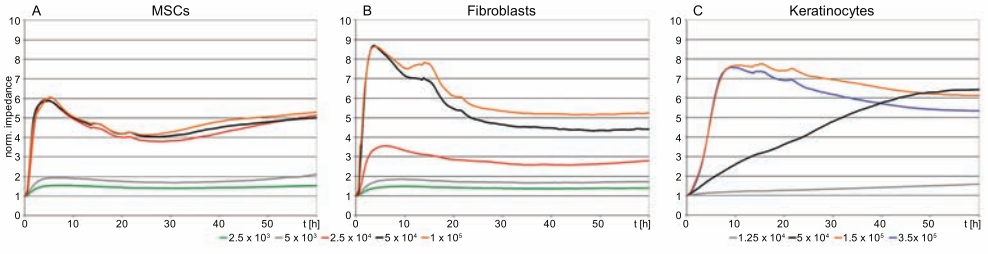

Figure 4.1: Cell density and cell type affect impedance profiles - For optimizing impedance measurements BMSCs (A), fibroblasts (B) and keratinocytes (C) were seeded at various densities in growth medium. Impedance profiles of means of quadruplicates (normalized values) were recorded continuously over 60 h (xCELLigence system).

For evalutation of cell morphology and spreading cells were seeded on protein spots (MSA-Slide). After 4 hours cells were stained for actin and vimentin or keratin, revealing generally good attachment and spreading of BMSCs and fibroblasts (both vimentin positive) on most ECM components (shown for collagen I; Fig. 4.2 A and B). For keratinocytes (stained for keratin) spreading was minimal at this point throughout (Fig. 4.2 C). Spreading of cells corresponded to impedance profiles which were less steep for keratinocytes compared to bone marrow derived mesenchymal stromal cell (BMSC)s and fibroblasts (Fig. 4.1).

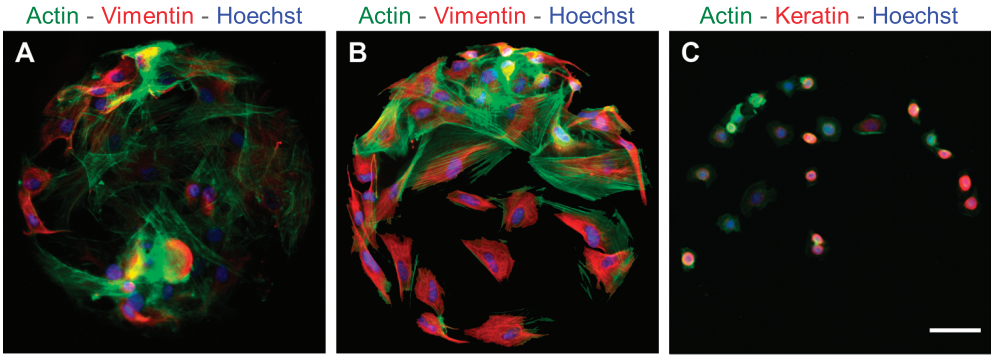

Figure 4.2: Attachment of cells on MSA - Attachment of BMSCs (A), fibroblasts (B) and keratinocytes (C) on rat tail collagen I spot (MSA-slide). 1 x 10^4 cells per MSA-well after incubation for 4 hours at 37°C. All cells were stained for actin-filaments (green), BMSCs and fibroblasts were stained for vimentin (red) (A and B) or keratinocytes for cytokeratine (red) (C). Nuclei, Hoechst dye (blue); scale bar = 50μm.

4.1.1 Monitoring changes in cell adhesion

To show cell adhesion effects on impedance measurement cells with altered expression of adhesion molecule were used in ECIS-system. HaCaT keratinocytes, naturally negative for nidogen expression, were stably transfected with the Tet-on system (Invitrogen) for inducible nidogen expression (Angstmann, 2007). For impedance measurements 2.5 x 10^5 cells per cm^2 were seeded and nidogen-1 expression was induced by addition of doxycycline. As controls non-induced cells were measured in parallel. Induction of nidogen-1 led to an increasing slope of impedance compared to not-induced nidogen-1 cells, indicating for changed adhesion properties of the cells in response to nidogen expression (Fig. 4.3).

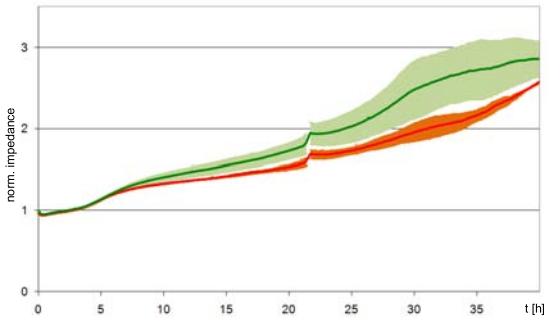

Figure 4.3: Impedance profiles of nidogen-inducible cells. - Nidogen-1 expressing cells (green line) show steeper profile compared to not-induced nidogen-1 transfected cells (red).

4.1.1.1 Confirmation of molecular switch by gene and protein expression analysis

For confirmation of nidogen expression in stable transfected HaCaT cells, gene and protein expression of nidogen-1 were verified by PCR and western blot analysis, as well as immunofluorescence staining of cultured cells. Although clones from single cell colonies were selected, heterogeneous not selected cell populations of stable transfected cells showed best expression of nidogen-1 compared to clonal cells (not shown). Nidogen-1 gene expression could be demonstrated by PCR revealing positive detection of 307 bp nidogen-1 product in induced cells (Fig. 4.4 A). Inducible expression of nidogen protein was shown in western blot experiments and immunofluorescence staining of cultivated cells. Western blot experiments showed hardly detectable nidogen-1 expression

in selected ND1-clones but was clearly detectable in unselected cultures (Fig. 4.4 B). Nidogen-1 expressing cells were stained for cytoskeleton protein actin (Phalloidin stain) and nidogen-1. As shown previously (Angstmann, 2007) nidogen was not expressed in all cells but nidogen is expressed in positive clusters (Fig. 4.4 C).

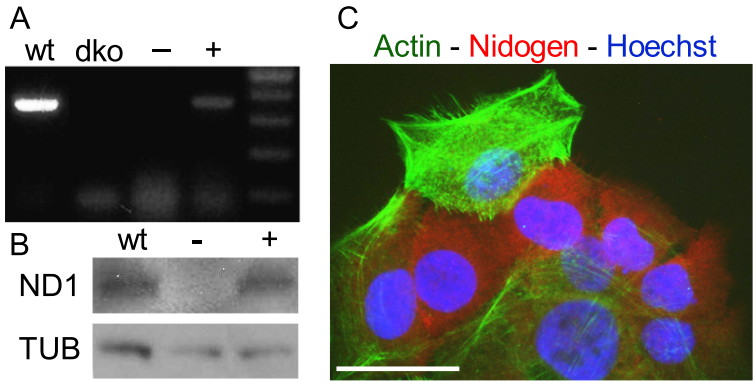

Figure 4.4: Expression of nidogen - (A) PCR of cDNA from wild-type mouse fibroblasts (wt) and induced HaCaT cells (+) showing nidogen-1 gene expression while samples from mouse with total knock out of nidogen expression (dko) and not induced HaCaT cells (-) were negative. (B) Western blot data confirmed nidogen-1 (ND1) protein expression in samples from wild-type mouse fibroblasts (wt) and induced keratinocyte cells (+), which was not detectable in not induced keratinocytes (-); loading control stained for β-tubulin (TUB) below. (C) Immunofluorescence staining for filamenteous actin (Phalloidin, green) and nidogen-1 (red) showing heterogeneous nidogen expression in induced HaCaT populations. Nuclei counterstained with hoechst dye (blue); scale bar: 25 μm.

4.2 Monitoring of MSC differentiation

4.2.1 Differentiation potential of MSCs is dependent on passage number

In order to follow early changes after induction of differentiation, BMSCs (passage 6), suspended in adiopgenic induction medium (AIM), osteogenic induction medium (OIM) or mesenchymal stem cell growth medium (MSC-GM) (two samples each) were seeded on ECIS chips at a density of 0.5 - 1 x 10^5 cells/well (0.6125 - 1.25 x 10^5 cells/cm^2) and impedance was monitored over 25 hours (Fig. 4.5). Over the first 5-8 hours impedance strongly increased under any conditions, though for cultures in AIM the slope was less steep (Fig. 4.5 A). After this early phase, profiles of osteogenic cells remained at a constant plateau, whereas those of adipogenic or non-induced cells decreased. Contrarily, the profiles of later BMSC passages (p15) did not substantially differ between AIM, OIM, and control media (Fig. 4.5 B).

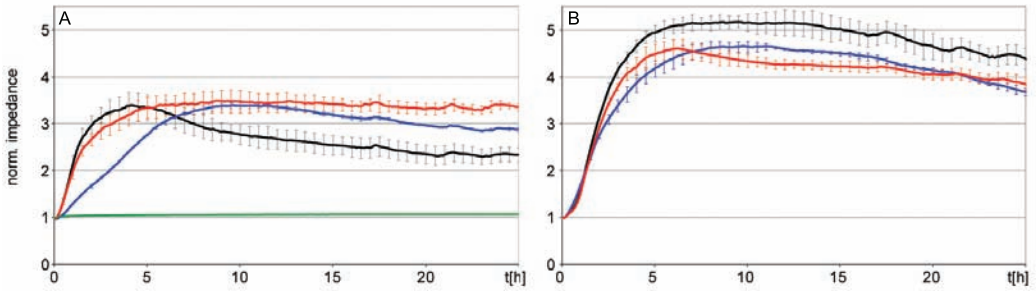

Figure 4.5: MSC differentiation induces early and specific changes in impedance
Impedance of low (A) and high passaged (B; population doublings higher 25) BMSCs in AIM (blue line), OIM (red), MSC-GM (black) and growth medium without cells (green).

4.2.2 Induction of differentation reflected by impedance

Seeding cells (p6) in GM and adding OIM or AIM after 3.5 hours indicated early influences of induction media, independent of initial cell adhesion (Fig. 4.6 A). While adipogenic induced cells develop less steep profiles as already seen before (Fig. 4.5 A) immediately after adding differentiation factors, slopes of osteogenic induction and control medium increased faster initially. In further progress, osteogenic cells remained at high level or are further increasing impedance while profiles of adipogenic induction and control medium declined. *In vitro* differentiation of MSCs is based on addition of

specific factors into the cell culture medium which induce the process of differentiation (see 1.1.1 and 3.3.3). Culturing of MSCs in adipogenic medium lacking one of these factors produce impedance profiles reflected the importance of these factors in adipogenic differentiation (Fig. 4.6 B). While lack of dexamethasone or insulin resulted in still declining impedance profiles similar to differentiation medium containing complete set of differentiation factors, whereas the lack of indomethacine or IBMX showed profiles with a steeper initial slope without the adipogenic typical decrease resembling more the profile of growth medium without any differentation factors.

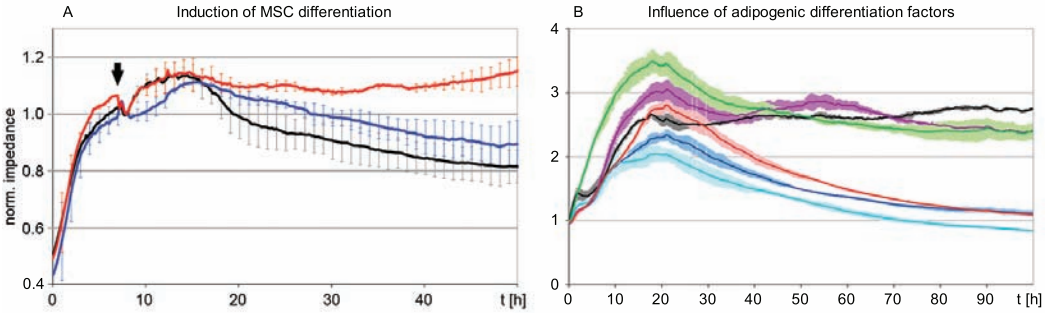

Figure 4.6: Induction of MSC differentiation - (A) Profiles of differentiating MSCs diverged after adding medium containing differentiation factors (arrow) to pre-plated BMSCs (p6). Differentiation was induced in AIM (blue line), OIM (red) and controls were cultured in MSC-GM (black). Graphs were normalized to the time point of induction, (B) BMSCs seeded in adipogenic differentiation medium lacking single factors usually included for differentiation: AIM without IBMX (green), without Indomethacine (purple), without dexamethasone (light blue) and without insulin (red). Controls of complete adipogenic differentiation medium in blue and growth medium in black.

4.2.3 MSCs behavior depends on donor tissue

To monitor MSC differentation from different tissues in long-term experiments, impedance was recorded for 14 days with BMSCs and ASCs from three and two donors, respectively. Cells were kept in MSC-GM for 26 hours before adding differentiation media (Fig. 4.7). Overlapping impedance profiles diverged after induction revealing typically a steeper slope in OIM, delayed slope in GM, and no increase rather than a decrease in AIM. With repeating adipogenic induction cycles the impedance profiles showed alternating a steep increase with subsequent plateau in adipogenic maintenance medium and in turn a decrease after adding AIM. Plain media effects could be excluded by

impedance measurements without cells (not shown). The more advanced profiles of BMSC-1, -2, -3 (Fig. 4.7 A; mean of three), and ASC-2 (Fig. 4.7 D) exhibited significant differences between osteogenic, adipogenic, and non-induced cells. But for ASC-1 (Fig. 4.7 C) osteogenic and control profiles were largely overlapping. BMSCs cultivated *in vitro* for more than 25 population doublings (p13) did not show the typical impedance profiles when exposed to differentiation medium (Fig. 4.7 B). Neither the continuously rising osteogenic profile even declining profile after initial peak, nor typical alternating impedance profile seen before during adipogenic differentiation were developed during differentiation of *in vitro* aged MSCs.

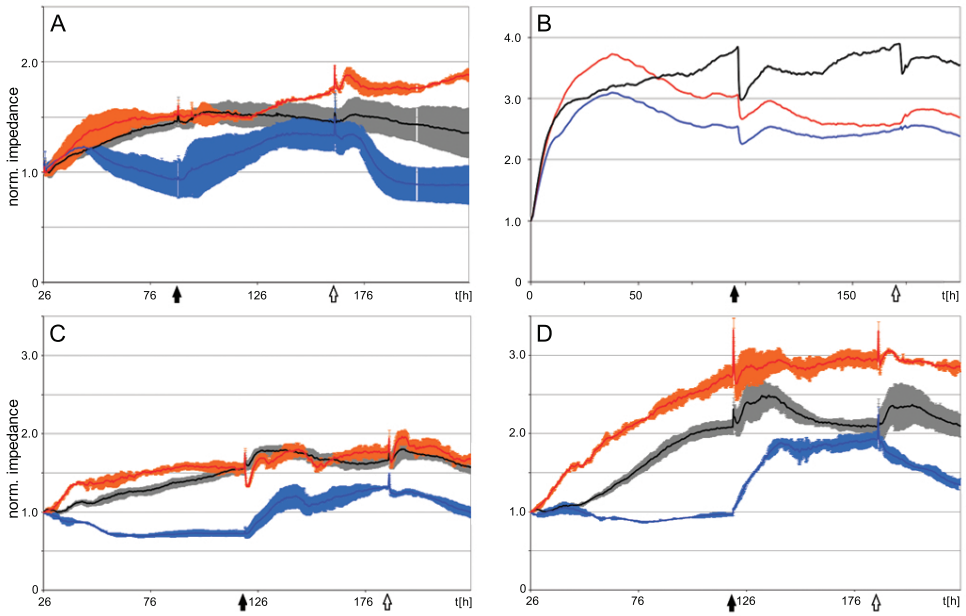

Figure 4.7: MSC differentiation from different sources - Impedance profiles of (A) low passaged BMSCs (mean of three donors), (C) ASC-1 and (D) ASC-2 (all ECIS system) compared to (B) high passaged BMSC in xCELLigence system recorded in duplicates for 14 days; Inducing differentiation after 26h, or immediately (B), (OIM: red line; AIM: blue) and non-induced controls (black); profiles over at least 10 days after induction. Medium changes are indicated by arrows, the switch from AIM to AMM is marked by black and back to AIM by white arrows.

4.2.4 Confirmation of impedance data by specific staining, protein and RNA analysis

To correlate impedance to cell number and morphology cultures were examined by microscopy. Staining at the endpoint (day 5) for actin filaments and cell nuclei showed that cells completely covered the electrodes in all media (Fig. 4.8 A-C). Seeding identical cell numbers in all media at high densities producing confluent cell layers immediately after seeding minimized differences of impedance values which are due to cell numbers but mainly reflects cell morpholoy and adhesion properties.

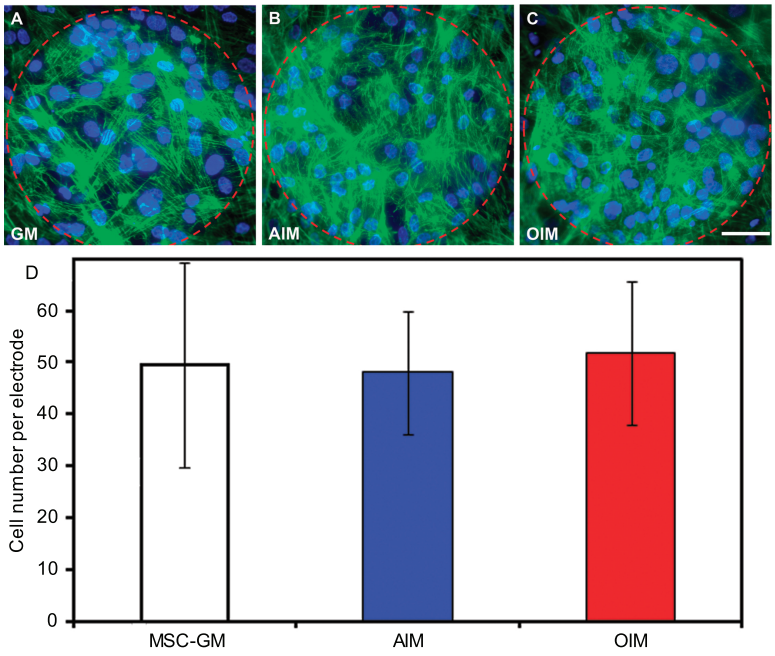

Figure 4.8: Cells on electrodes - Fluorescence microscopy of differentiating BMSCs on ECIS electrodes (red circles) after growth for 5 days in MSC-GM, AIM and OIM. Staining of actin filaments with phalloidin-FITC (green) and of cell nuclei (blue; Hoechst). Scale bar: 50 μm. (D) Cell numbers of BMSCs on ECIS electrodes after 5 days in MSC-GM, AIM and OIM determined by counting of Hoechst dye stained cell nuclei.

Determination of cell numbers on electrodes after cultivating cells for 5 days did show only neglitable, not significant variations of cells on the electrodes between the different media (Fig. 4.8 D). Generally, cell densities appeared slightly higher on gold than on the plastic surface, though reliable evaluation was hampered by the different plane of focus. While in MSC-GM cells were more spread than in AIM or OIM, apparent by flattened

nuclei and an extended actin cytoskeleton, in AIM cells appeared smaller and more roundish. The actin network was most pronounced in OIM revealing predominantly spindle shaped, often overlapping cells, whereas the heterogeneous morphology in MSC-GM was accompanied by sparser actin filaments.

Importantly, the impedance profiles fully corresponded to the differentiation levels at day 14, indicated by Oil Red lipid stain or mineralization (mainly calcium phosphates) by von Kossa stain and molecular markers (Fig. 4.9). While ORO was strongly positive throughout (Fig. 4.9 A-C), ASC-1 kept in OIM revealed at best marginal von Kossa staining (Fig. Fig. 4.9 F) compared to deposited calcium stained in BMSCs and ASC-2 samples (Fig. 4.9 E and G).

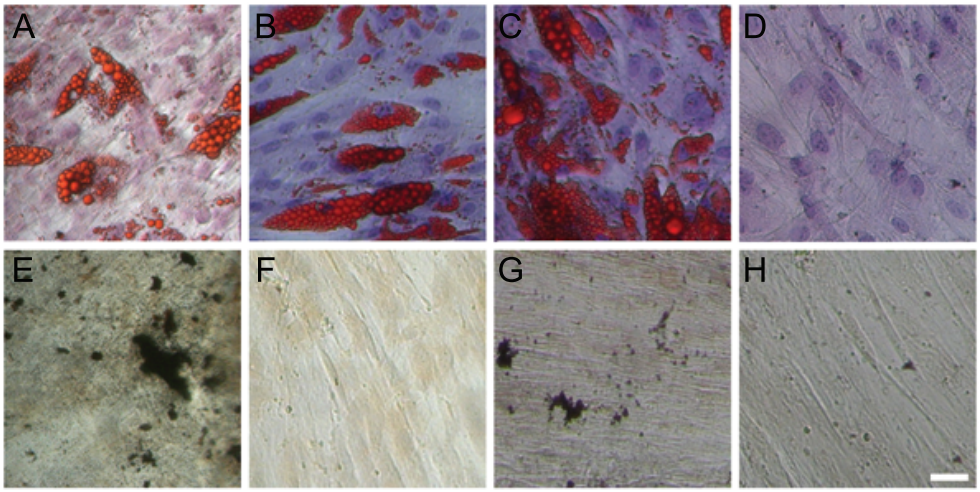

Figure 4.9: ORO and von Kossa stain of BMSCs and ASCs - ORO (A-D) and von Kossa (E-H) staining in ECIS-wells, respectively at end point (d14), for BMSCs (A, E), ASC-1 (B, F) and ASC-2 (C, G); negative controls shown for ASC-2 (D, H). Scale bar: 100 μm.

Western blots confirmed the actual course of differentiation at the protein level, as exemplified for BMSCs (ASC-2 similar, not shown), by detection of adipose differentiation related protein (ADRP) and perilipin (PERI) for adipogenic differentiation or late osteogenic marker bone sialoprotein (BSP) and osteopontin (OPN) for osteogenic differentiation (Mizuno and Kuboki, 2001), respectively (Fig. 4.10). Validating the value of impedance as measure for differentiation, in ASC-1 the low osteogenic profile (compare Fig. 4.7) correlated also to low expression of the osteogenic markers BSP and

osteopontin.

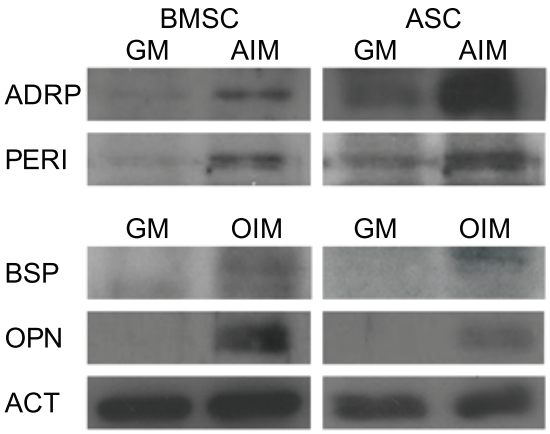

Figure 4.10: Western blot of differentiated MSCs - Western blots of 14 days cultures (induced vs. uninduced) showing adipophilin (ADRP) and perilipin (PERI) as adipogenic marker and for osteogenic differentiation bone sialoproten (BSP) and osteopontin (OPN) with β-actin (ACT) as loading control for the BMSC and the ASC-1 samples. Note that low OIM profile of ASC-1 corresponds to only marginal von Kossa stain and low BSP and osteopontin.

Specificity of adipogenic differentiation was underlined by RNA data (RT-qPCR) from cultures grown in alternating AIM and AMM, corresponding to significant time points of impedance profiles. This revealed a marked AIM-dependent induction of peroxisome proliferative activated receptor (PPAR)γ, and also for perilipin shown for samples of BMSC-1, -2, and -3 and ASC-1 (Fig. 4.11 A and B), which was inversely related to the oscillating impedance signals. Gene expression of late adipogenic marker adiponectin was highly expressed in all samples only in 14 day AIM-cultures (Fig. 4.11 C). The expression of all examined adipogenic differentiation related genes was quite variable between the samples, in general. RT-qPCR of osteogenic genes did not give reliable results although several primers and probes and combination of them have been tested.

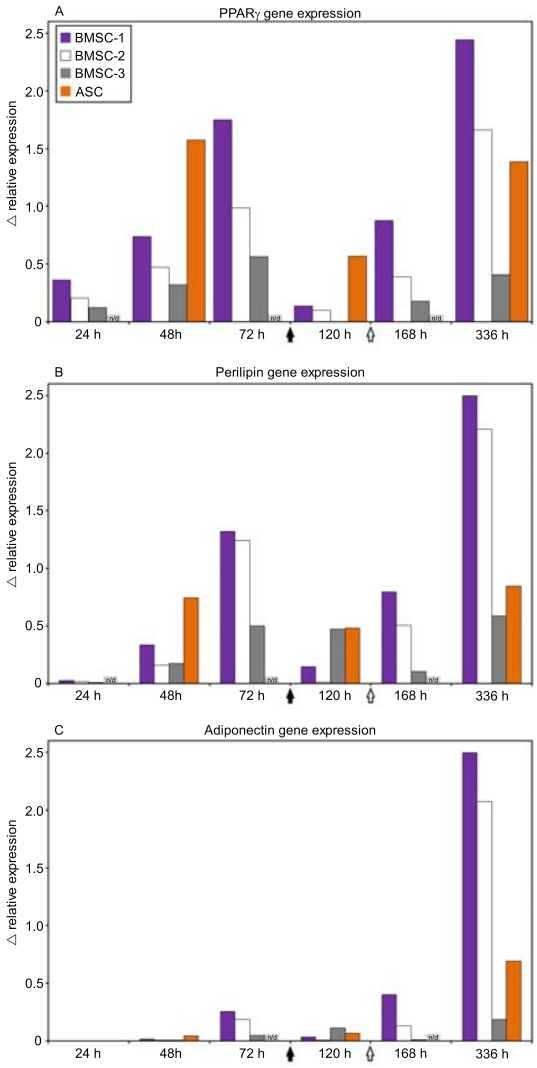

Figure 4.11: Adipogenic gene expression of BMSCs and ASCs - Relative gene expression (induced minus uninduced) of adipogenic markers (A) PPARγ, (B) perilipin and (C) adiponectin at different timepoints of the 3 different BMSC isolates (days 1, 2, 3, 5, 7 and 14) and ASC-1 (days 2, 5 and 14). After 3 days, induction medium was switched to maintenance medium (black arrow) and back to AIM again (white arrow), indicating the effect of induction/maintenance medium, obvious also in impedance profiles. All cells have been analyzed at population doublings below 20.

4.3 Cell adhesion on ECM proteins monitored by impedance measurements

Next the influence of interactions with proteins of the ECM on MSC behavior with consequences on impedance profiles was examined.

4.3.1 Extracellular matrix proteins affect MSC differentiation

For studying differentiation of MSCs on ECM proteins, BMSCs were cultured in vessels coated with collagen I, collagen IV, fibronectin or laminin. Seeding 2.5 x 10^4 cells/well (xCELLigence) impedance was measured for 96 hours (Fig. 4.12). Osteogenic induction caused steeply rising impedance profiles on collagen I or IV, while reaching markedly lower values with somewhat flattened slopes on fibronectin and particularly laminin, correlating to early morphological appearance of the cells (see also 4.16 and 4.17). Beyond 20 hours the shape of osteogenic curves was similar. Showing an almost as strong

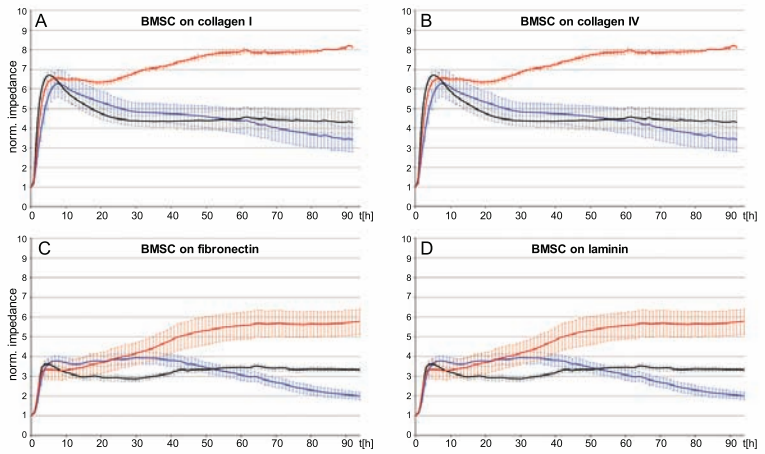

Figure 4.12: Extracellular matrix molecules influence impedance differentiation profiles of MSC - Impedance profiles of differentiating BMSCs on various ECM coatings: 2.5 x 10^4 cells/cm^2 were seeded on collagen I, collagen IV, fibronectin and laminin. Profiles are means of quadruplicates in differentiation media (OIM: red, AIM: blue) and control medium (black).

increase on the collagens, the adipogenic impedance profiles dropped on all matrices to levels far below the endpoints of osteogenic tracks. However, the initial reduction of the adipogenic curve was much less pronounced on fibronectin, exceeding the largely

reduced osteogenic profile for about 30 hours, before it dropped below the osteogenic profile which was steadily increasing. On laminin both curves reached similar, but further reduced levels while their shapes corresponded to those on fibronectin. Skin fibroblasts did not show very distinct profiles on those matrices in the various media, though the initial attachment peak was highest on collagens (Fig. 4.13 A and B) and markedly reduced on fibronectin in osteogenic medium (Fig. 4.13 C and D).

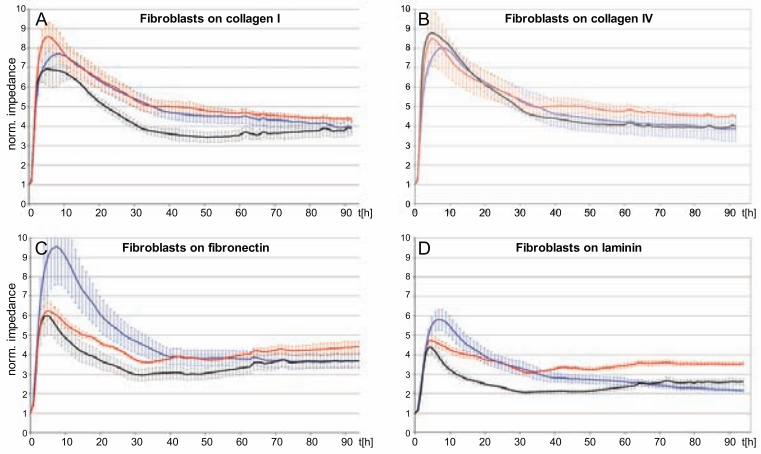

Figure 4.13: Fibroblasts on extracellular matrix molecules monitored via impedance - Impedance profiles of fibroblasts on various ECM coatings: 2.5 x 10^4 cells/cm^2 were seeded on (A) collagen I, (B) collagen IV, (C) fibronectin and (D) laminin. Profiles are means of quadruplicates in differentiation media (OIM: red, AIM: blue) and control medium (black) (xCELLigence system).

4.3.1.1 Adhesion on Collagen I depends on coating density

Impedance profiles of BMSCs were also affected by coating with different concentrations of collagen I. Adipogenic and osteogenic differentiation of BMSCs was induced in ECIS wells coated with 5, 10, 25 and 50 μg/cm^2 collagen I and impedance was recorded as described before. Impedance values rose with rising collagen I concentration peaking at 25 μg/cm^2 throughout all media and was very low for high concentration of 50 μg/cm^2 suggesting inhibiting influences on cell adhesion due to dense collagen coating. While in MSC-GM and AIM uncoated controls (Fig. 4.14 A and B) were quite similar to 10-25 μg/cm^2 coated samples, for osteogenic differentiation impedance of samples are in sequential order to rising collagen concentration, excepting highest collagen density

of 50 $\mu g/cm^2$, suggesting a supportive role of collagen I for adhesion of osteogenic cells. Quantification of lipid accumulation with Oil Red revealed further influence of collagen I on adipogenic differentiation of BMSCs being highest at 10 $\mu g/cm^2$, somewhat lower at 5 and 25 $\mu g/cm^2$ and low at 50 $\mu g/cm^2$ collagen I. High impedance values on 25 $\mu g/cm^2$ in AIM (Fig. 4.14 B) inversely correspond to low ORO staining after 5 days (Fig. 4.20).

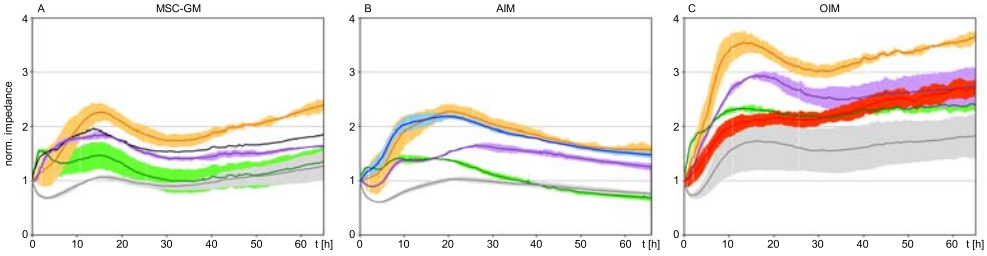

Figure 4.14: Concentration of collagen I affects impedance profiles - BMSCs were seeded on various collagen I concentration (5 (green), 10 (purple), 25 (orange) and 50 (gray) $\mu g/cm^2$) in AIM (B) and OIM (C) differentiation media and MSC-GM (A) as controls. Controls in uncoated wells were run in parallel in MSC-GM (A, black line), AIM (B, blue) and OIM (C, red).

To evaluate the influence of conformational state of proteins, wells were coated with collagen I in its native form as before, neither denatured nor being air-dried, and in contrast with collagen I which has been denatured by heating before coating. Impedance data of both conformations display similar profiles, where denatured collagen I resulted in higher initial peaks and higher impedance values in general compared to native collagen I (Fig. 4.15).

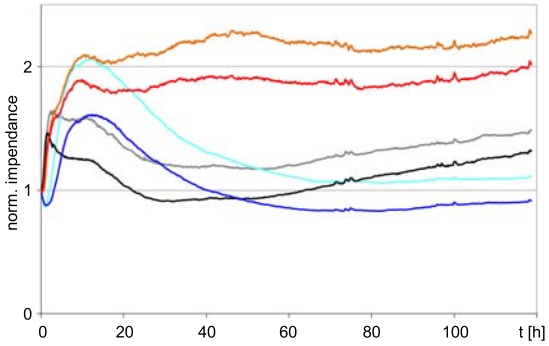

Figure 4.15: Denatured vs. native collagen I coating in impedance measurement - BMSCs were seeded in adipogenic (blue colors) and osteogenic (red colors) differentiation and control media (black or gray) on native and denatured collagen I coated wells. Impedance data of both conformations display similar profiles, with denatured collagen I having higher impedance values in general (AIM: light blue; OIM: orange; MSC-GM: gray, compared to native collagen I (AIM: blue; OIM: red; MSC-GM: black).

4.3.2 Confirmation and quantification of adipogenesis and osteogenesis

As possible morphological correlates phase contrast images of BMSCs revealed at 8 hours well spread cells without noticeable differences between applied media or matrices (Fig. 4.16 A, D, G and J). While after 24 hours spindle shaped morphology was largely retained, adipogenic cells showed prominent extensions and osteogenic cells markedly increased in density (Fig. 4.16 B, E, H and K). The differences became more striking at day 5, some cells in AIM containing also small lipid inclusion bodies (Fig. 4.16 C and F). These morphological manifestations were similarly seen on collagen I and fibronectin.

Additionally, for evaluation of cell morphology at early time points, cells suspended in the various media were plated on MSA containing ten different micro-spotted ECM proteins. After 4 hours cells were stained for actin and vimentin. Shape and quantity of attached BMSCs were further affected by differentiation media (examples of collagen I, collagen IV and fibronectin are shown in Fig. 4.17). While in GM high numbers of compact BMSCs were found on both collagens, on collagen I cells were widely spread in AIM and OIM. On collagen IV the attachment rate was higher, cells appearing smaller in OIM, much like in GM. By contrast, on fibronectin much fewer cells being extremely spread attached in all three media.

Adipogenic and osteogenic differentiation markers were determined for BMSCs grow-

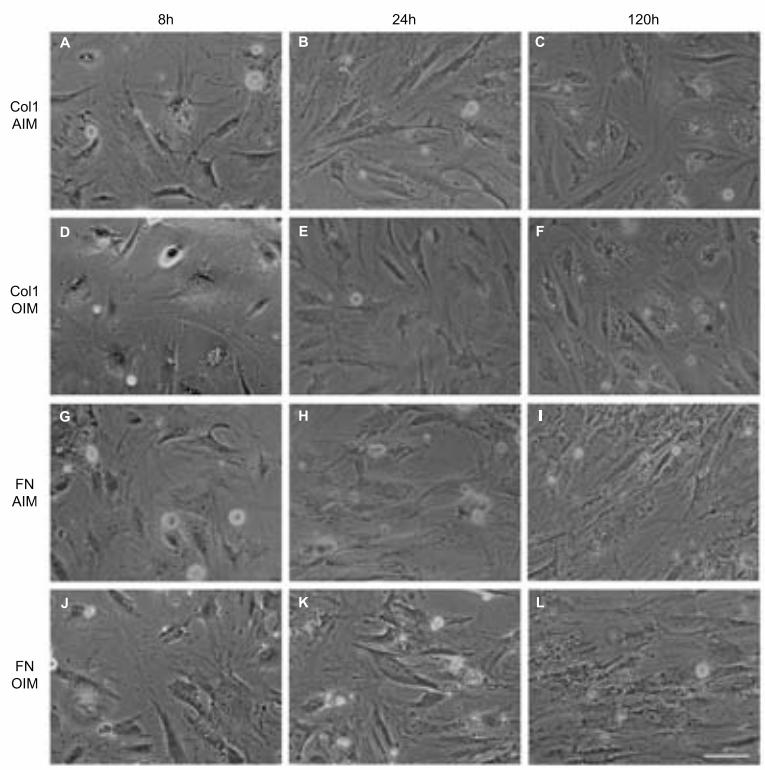

Figure 4.16: Phase contrast microscopy of BMSCs on ECM proteins - BMSCs were seeded on Collagen Type I and fibronectin in differentiation media and photos were taken after 8, 24 and 120 hours. Scale bar: 100 μm.

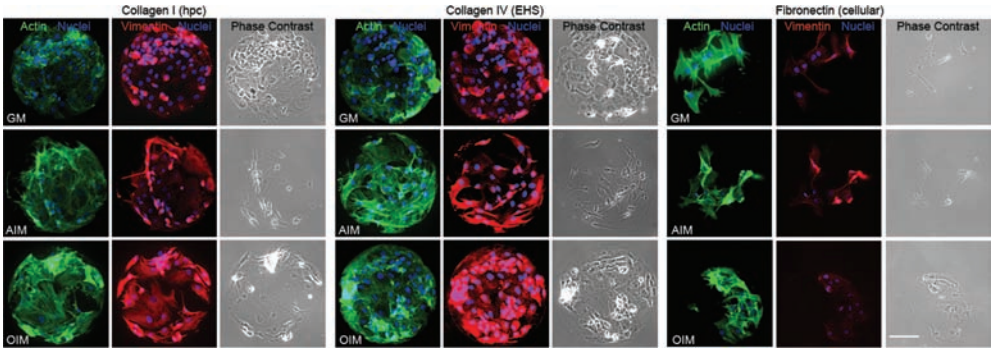

Figure 4.17: Attachment of BMSCs on MSA on different ECM-proteins - After incubation with 1 x 10^4 MSCs per well for 4 hours at 37°C cells were stained for actin (green), vimentin (red) and nuclei (blue; Hoechst dye). Cells on collagen I (left panel), collagen IV (middle) and fibronectin (right) were grown in GM, AIM and OIM; scale bar: 100 μm.

ing on ECM-coated cover slips. Five days after induction by AIM the highest number of cells with lipid droplets (ORO staining) was observed on fibronectin and collagen I followed by collagen IV, and being lowest on laminin (Fig. 4.18).

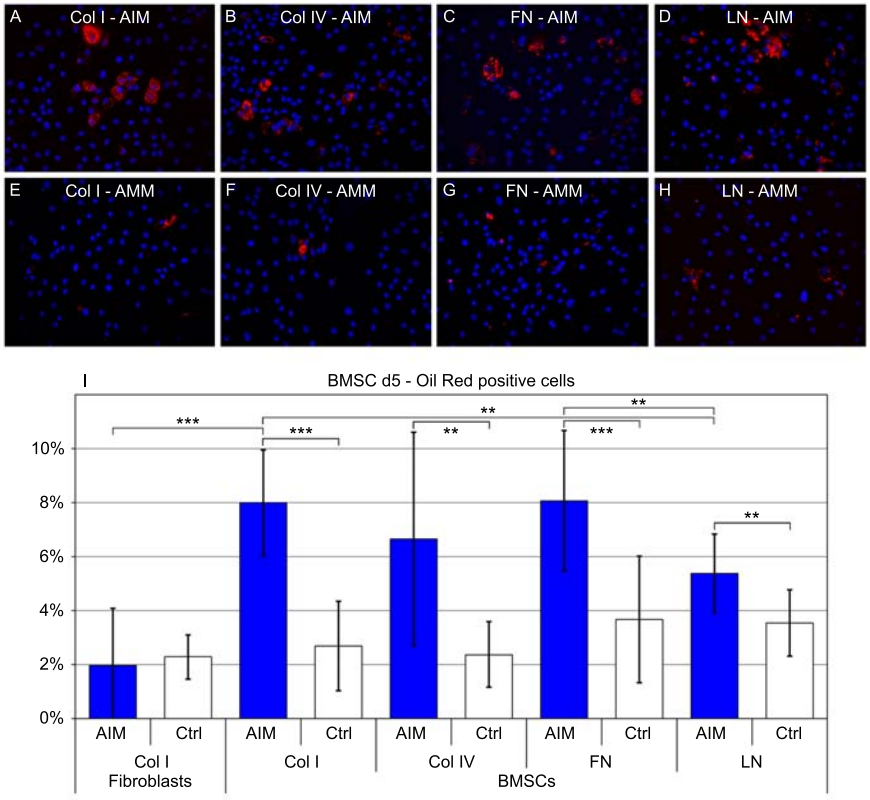

Figure 4.18: Matrix influence on early adipogenic differentiation - Fluorescence microscopy of adipogenic differentiation of BMSCs on ECM proteins 5 days after induction (A-D), showing ORO positive lipid droplets (nuclei, Hoechst stain) compared to controls (E-H); scale bar: 50 μm. (I) Histogram of percentage of positive cells (induced vs. uninduced) on various ECM coatings is at this stage already significantly different from controls. Fibroblast staining does not exceed levels of controls (* $p<0.05$; ** $p<0.01$; *** $p<0.001$; $n=10$).

But after 21 days positive cells rose to more than 80% on fibronectin and laminin, compared to about 60% on collagen I and IV showing also less lipid accumulations. Unexpectedly, without coating (PBS control) nearly 80% of cells were finally ORO positive presumably for soluble fibronectin and vitronectin in the media, firmly adhering to glass surfaces. These results were corroborated by strongly increased staining intensity at 21 days (Fig. 4.19 A-L) and image analysis which revealed a significantly stronger

signal on fibronectin compared to the other samples (Fig. 4.19 M). The staining of the high passaged BMSC (p16) was very low like seen in fibroblasts (compare Fig. 4.18).

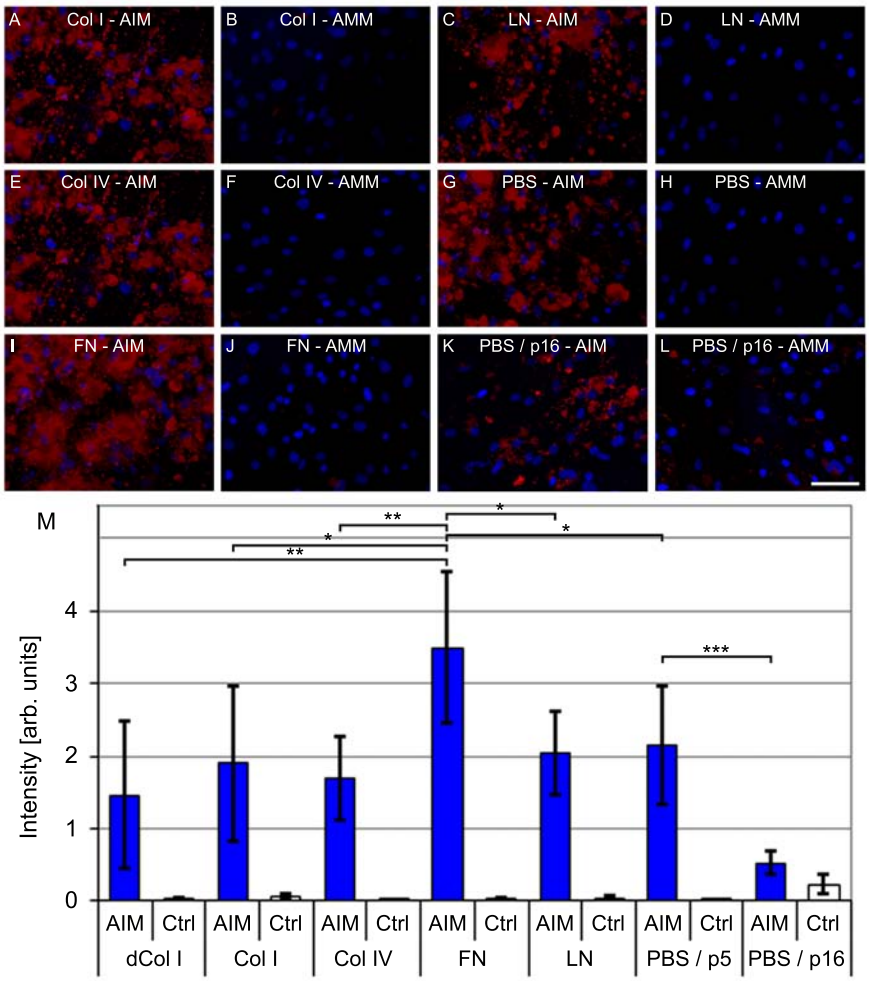

Figure 4.19: ORO staining of d21 samples - Fluorescence microscopy of lipid ORO staining (nuclei counterstained) of BMSCs after 21 days in AIM and control medium (Ctrl) cultivated on collagen I (A and B), collagen IV (E and F), fibronectin (I and J), laminin (C and D) and controls without protein coating (G and H) as well as high passaged (P16) cells (K and L); scale bar 50 μm. Intensity of ORO staining of BMSCs determined by image analysis. Intensity was significant higher on induced fibronectin samples compared to other matrices. High passaged MSCs showed significantly reduced intensity (* $p<0.05$; ** $p<0.01$; *** $p<0.001$; $n=10$).

Intensities of ORO staining of BMSCs 5 days after adipogenic induction on various collagen I concentrations (0-50 μg/cm^2) did not differ significantly. However, after 21 days of adipogenesis, ORO intensity of uncoated controls exceeded that of collagen I coated samples, which exhibit decreasing lipid staining when coating density was increased (Fig. 4.20).

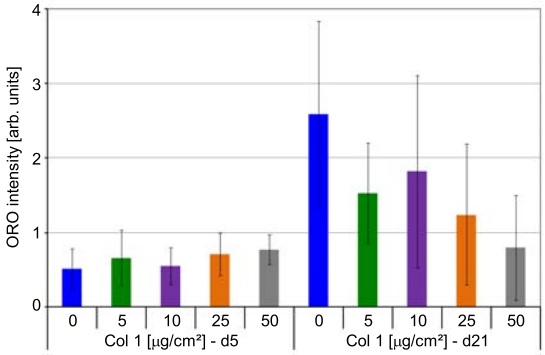

Figure 4.20: Quantification of ORO staining on various collagen I concentrations ORO staining of BMSCs differentiated into adipogenic cells was quantified after 5 and 21 days revealing influences of collagen I concentration on lipid accumulation in adipogenic cells.

Generally, the visible appearance of osteogenic markers took considerably more time. After 21 days in OIM cells showed distinct staining of calcium deposits on collagens, in general, partially less intense on collagen I, whereas staining was weaker on fibronectin and laminin (Fig. 4.21). This was compatible with the more pronounced impedance profiles of BMSCs on collagens in OIM (shown in Fig. 4.12). Although by and large reflecting microscopic observations, differences seen in quantification of Alizarin staining are not significant due to a very heterogeneous deposition of calcium throughout the culture resulting in high deviations (Fig. 4.21 M). Similar, quantification of calcium deposition on varying densities of collagen I coatings in ECIS wells reflect differences seen during impedance measurements (Fig. 4.14) but are not significant (Fig. 4.21 M).

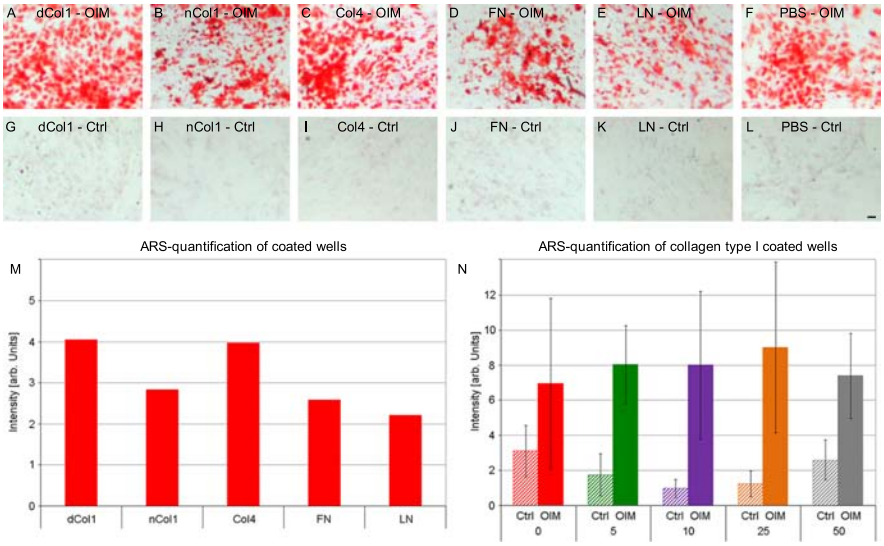

Figure 4.21: Extracellular matrix molecules influence MSC differentiation: osteogenesis - Light microscopy of Alizarin Red S staining detecting calcium deposits of osteogenic BMSCs on protein matrices (A-F) compared to not induced controls (G-K) after 21 days in culture; scale bar: 500 μm. (M) Quantification of alizarin staining shows differences on osteogenic differentiation of BMSCs on protein coatings. (N) Osteogenic induced cells compared to not induced cells on various concentrations of collagen 1 coatings (5-50 $\mu g/cm^2$) and uncoated control.

Again, expression of adipogenic genes were also determined in RT-qPCR experiments using the differentiation markers PPARγ, perilipin and adiponectin. While uncoated control samples resembled the expression profiles of PPARγ and perilipin as seen before (compare Fig. 4.11), decreasing expression of those genes in adipogenic maintenance medium (AMM), whereas high during induction cycle (AIM (Fig. 4.22 A and B blue bars), on ECM protein coats this oscillating expression was only detected for perilipin but not for PPARγ gene expression. After 14 days, also late adipogenic marker adiponectin could be detected at high levels (Fig. 4.22 C). Although surprising weak expression of adipogenic differentiation genes after 14 days for control samples comparable with laminin coated samples was detected, highest levels of gene expression was seen on fibronectin, followed by collagen I and somewhat weaker collagen IV, confirming quantification data of ORO lipid staining (Fig. 4.19).

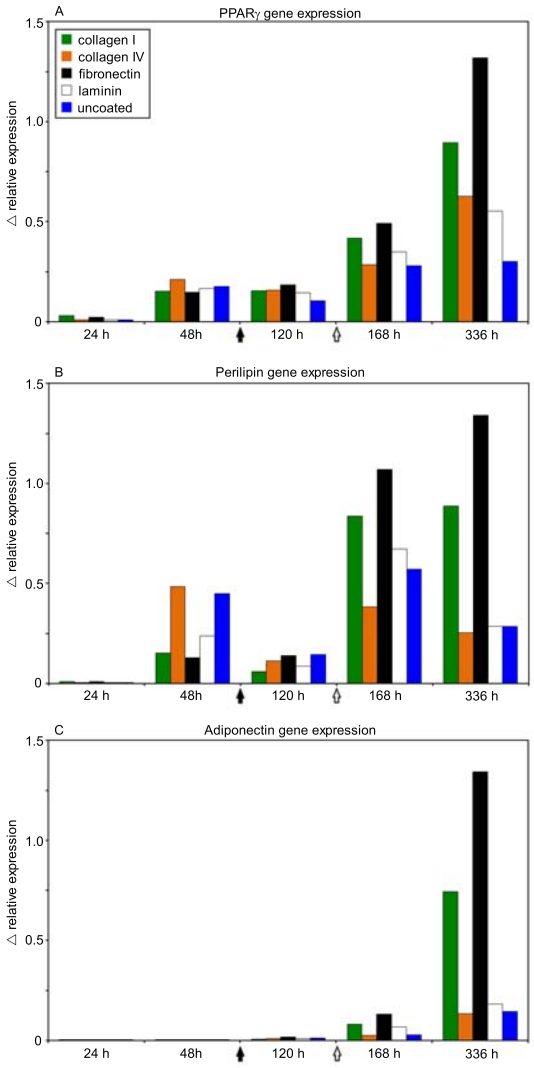

Figure 4.22: Relative gene expression of adipogenic markers on ECM coatings - Relative gene expression (induced minus uninduced) of adipogenic markers (A) PPARγ, (B) perilipin and (C) adiponectin at different timepoints during differentiation process on ECM proteins collagen I (green bars), collagen IV (orange), fibronectin (black), laminin (white) and uncoated control (blue). After 3 days, induction medium was switched to maintenance medium (black arrow) and back to AIM again (white arrow). All cells have been analyzed at population doublings below 20.

4.4 Cell migration monitored by impedance

To examine cell adhesion, migration and growth after wounding, cells were grown in multi-wells with one single electrode and after reaching confluence cell layers were wounded by a high voltage pulse resulting in a defined cell-free area surrounded by unaffected living cells. Repopulation of the cell free-electrodes were monitored by impedance recording.

4.4.1 Expression of adhesion molecule affects cell migration

Studying migration of keratinocytes into electrically wounded area further points on effects of nidogen-1 on cell adhesion and therefore migratory properties, reflected by prolonged recovery phase after wounding of nidogen-1 expressing keratinocytes compared to not induced cells (Fig. 4.23 A). Similar negative effects of nidogen expression on migration were also seen using mouse fibroblasts. Wild-type fibroblasts expressing nidogen were slower compared to double knockout fibroblasts in which expression of nidogen was abolished (Fig. 4.23 B).

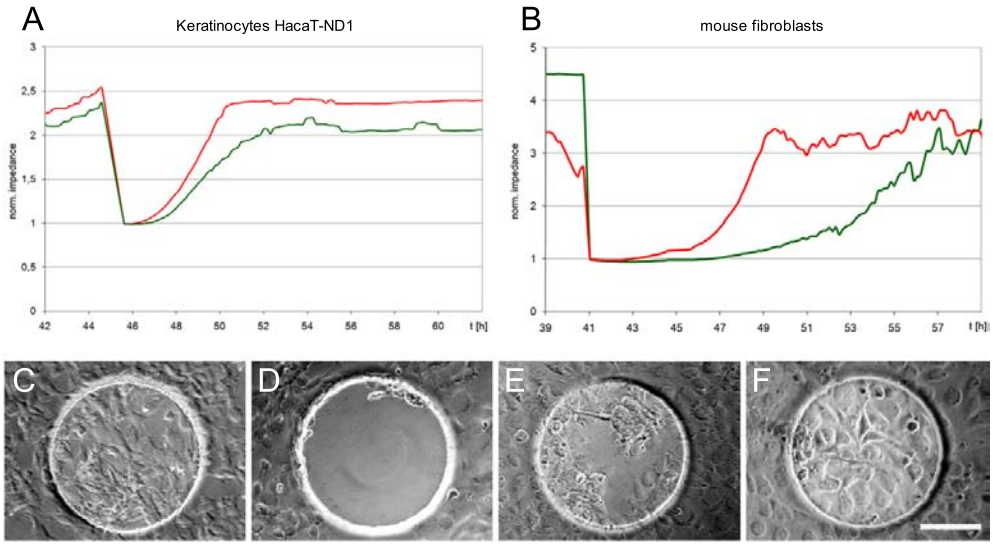

Figure 4.23: Wounding of HaCaT cells and fibroblasts - After reaching counfluency HaCaT ND1 cells were exposed to high voltage pulses (4V, 3x 20s) and repopulation of the electrodes was recorded. (A) Keratinocytes induced for nidogen-1 expression (green) migrated slower compared to non-induced cells (red). (B) Similar migratory behavior was observed in mouse fibroblasts. Repopulation of the electrodes took longer with wild-type fibroblasts naturally expressing nidogens (green) when compared to fibroblasts which lack nidogen-expression (red). Phasencontrast pictures of keratinocytes on electrodes (C) before, (D) immediately, and (E) 3 hours after wounding, and (F) when electrodes where fully repopulated after 10 hours; scale bar: 100 μm.

4.4.2 Migration of MSCs

Subjecting confluent BMSC (p6) cultures in the respective differentiation media to electrical wounding generated impedance signals like during initial cell attachment with flatter slope for adipogenic than for osteogenic cells (Fig. 4.24 A). For comparison, cells were grown upon confluency separated by a silicon insert. After removal of the separating wall, cells started to migrate into the gap to populate the cell-free area. Closing of cell layer was documented by microscopy followed by picture analysis. Results were similar to electrical wounding: adipogenic cells seem to be inhibited in growth and migration when compared to osteogenic and control cells (Fig. 4.24 B).

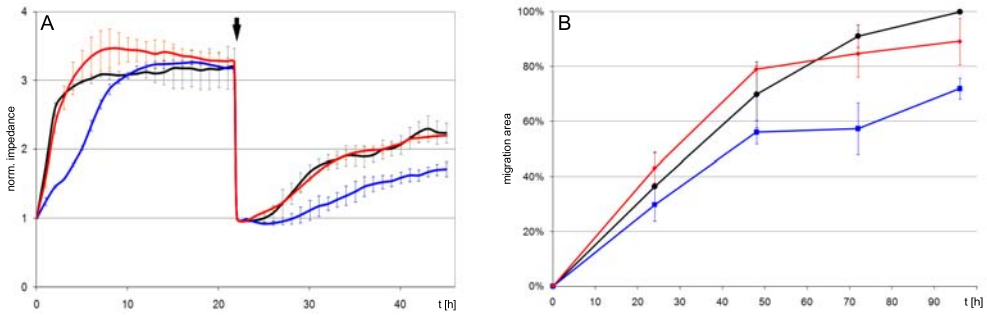

Figure 4.24: Migration of differentiating MSCs - BMSCs were seeded in differentiation medium (adipogenic: blue, osteogenic: red, control: black). For wounding (A) confluent cells were detached from electrodes by a 4V pulse (arrow), recording recovery by growth of BMSCs over the electrode, impedance data are normalized to start value. (B) BMSCs migration into the area of artificial gap from silicon inserts.

Furthermore, influence of single factors on MSC migration can be monitored by impedance. Therefore, factors like SDF-1, PDGF and tumor necrosis factor (TNF)α, which are closely related with MSC migration was monitored by electrical wounding but also again by insert-based migration assays. While SDF-1 and PDGF did not show significant differences to controls without additional factors, migration of cells treated with TNFα was significantly delayed in both assays (Fig. 4.25).

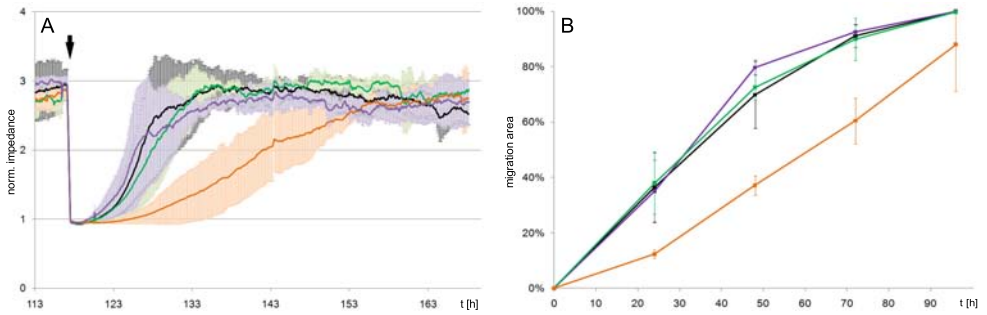

Figure 4.25: Migration factors influence on MSCs - BMSC in growth medium (black) and supplemented with SDF-1 (green), PDGF (purple) and TNFα (orange) were detached from electrodes by a 4V pulse (arrow), recording recovery by growth of BMSCs over the electrode. (B) MSCs migrate into the area of artificial gap from silicon inserts.

5 Discussion

Since their discovery, multipotent mesenchymal stromal cells (MSCs) have become attractive candidates for the regeneration of soft and solid tissues and their reconstruction *in vitro* by bioengineering. Thus, the ability of MSCs to differentiate *ex vivo* into multiple lineages upon specific induction has been shown in numerous studies (Prockop, 1997; Pittenger et al., 1999; Gregory et al., 2005; Nombela-Arrieta et al., 2011). Besides bone marrow, other tissues, like adipose tissue, umbilical cord blood or umbilical cord matrix were identified to harbor MSCs (Zuk et al., 2002; Bieback et al., 2004; Erices et al., 2000) and isolates of MSCs underwent extensive comparative analysis of proliferation, protein and gene expression, cell surface markers, or histochemical evaluation of their differentiation potential (Baksh et al., 2007; Wagner et al., 2005; Shetty et al., 2010; Banfi et al., 2000; Majumdar et al., 1998; Feldmann et al., 2005; Kern et al., 2006). Although the ISCT has defined minimal criteria for MSCs (Dominici et al., 2006), an unambiguous immunophenotype of MSCs can hardly be defined. Cell sorting of MSC isolates is hampered by the complexity of surface markers and particularly low cell yields due to the rare incidence of MSCs in tissue. Therefore descending from tissue isolates, MSC are commonly separated from their haematopoietic counterparts simply by their adhesive properties, resulting in mixtures of multipotent cells and progenitor or lineage committed cells. Isolates of MSCs vary depending on the donor, the donor age and the tissue MSCs originate from (Kretlow et al., 2008; Wagner et al., 2006), but also on the method of isolation and *in vitro* cultivation. Furthermore, extensive expansion of MSCs *in vitro* is often accompanied by the loss of differentiation potential (Kretlow et al., 2008). Opposing *in vitro* 'aging', maintenance of stemness is closely related to interactions with the environment, en gros defining the stem cell niche, and therein the role of cell interactions with the extracellular matrix (ECM) play a pivotal role (Volloch and Kaplan, 2002; Mauney et al., 2004, 2006). While differentiation in several directions, giving rise to osteogenic, adipogenic or chondrogenic lineages for example, has been

successfully established for *in vitro* cultures of MSCs (Prockop, 1997; Pittenger et al., 1999; Gregory et al., 2005; Nombela-Arrieta et al., 2011), the underlying mechanisms of the inducing chemical factors are not fully understood, since *in vivo* cells are apparently triggered by orchestration of many different stimuli. In addition, MSCs, transplanted into certain body sites, are not immune to differentiate into irregular or pathological tissue types (Breitbach et al., 2007) and occasionally MSCs have been also associated with conversion into CAFs in tumor stroma (Galiè et al., 2008; Mishra et al., 2009). Nevertheless, due to their versatile properties, ranging from immunosuppression and tissue regeneration to trophic functions, MSCs are a promising source for cell therapy (Sensebé et al., 2010; Zhao et al., 2010). However, this requires an improved understanding of how these cells maintain their stemness, how differentiation processes are guided and the assessment of risks, e.g. for developing cancer. Last not least standardized procedures and good manufacturing practices (GMPs) have to be established before broader usage of MSCs in regenerative medicine is indicated for safety and the unambiguous benefit of the patients.

In this thesis the differentiation of MSCs from different sources has been investigated in regard to specific inducing factors and cell-interactions with different ECM-molecules. For this purpose, the novel method of non-invasive impedance measurements on living cell layers was applied which allowed to monitor in real time early and late changes in MSC cultures undergoing differentiation. MSC cultures have been analyzed according to currently used clinical settings, being aware that they are heterogeneous mixtures of multipotent to lineage-committed progenitor cells, and their progeny.

Changes in morphology and adhesion during MSC differentiation

Morphology and adhesion properties of different cell types vary depending on their *in vivo* function. Thus, the overall cell-cell contacts of epithelial cells like keratinocytes *in vitro* are stronger than cell-substratum or cell-matrix interactions, respectively, due to the formation of high numbers of intercellular adherens and tight junctions and especially desmosomes. The situation is inverse for cells derived from connective tissue like fibroblasts or (multipotent) mesenchymal stromal cells. These cells secrete high amounts of various ECM proteins and form strong interactions with the substratum while direct cell-cell contacts are merely or not at all developed. These differences in cell

morphology, cell-cell and cell-matrix interactions are utilized for impedance monitoring of cell behavior.

For setting up the system, in a first round of experiments, cells of different cell types were seeded at various densities and impedance profiles were recorded (see Fig. 4.1). The impedance measurements showed over a wide range a strong correlation to cell numbers for each cell type but revealed also marked differences between MSCs, skin fibroblasts, and keratinocytes, underlining the effect of cell type-specific adhesion and shape in concord with the predictions and assay principle.

Accordingly, cells in the process of differentiation are subjected to rearrangements of cytoskeletal elements and adhesion structures both together leading to profound changes in cell morphology and interactions according to their differentiation fate. In order to explore this on multipotent stromal cells MSCs, isolated from bone marrow or adipose tissue, were seeded at high densities in media directing distinct tracks of differentiation or lacking inducing factors and impedance was recorded continuously. Samples from different donors and tissues as well as *in vitro* aged cells were compared and impedance profiles were correlated to the degree of differentiation, estimated by histochemical staining, gene expression profiling, and protein analysis.

Adipogenic differentiation

MSCs induced for adipogenic or osteogenic differentiation yielded highly specific and discriminatory impedance profiles. Shallower profile slopes in adipogenic medium (AIM) in the initial phase indicated delayed cell spreading, i.e. slower or less intense formation of adhesion contacts than in the other media (see Fig. 4.5 A). The effect and the responsiveness of cells became most apparent by following a cycling protocol for adipogenic differentiation. The impedance steeply increased when adding the maintenance medium AMM and promptly decreased upon switching again to AIM (Fig. 4.7). On the molecular basis, this was paralleled by inverse PPARγ and perilipin expression (shown by RT-qPCR; Fig. 4.11), which were determined at the corresponding time points. This strongly argues for fluctuations in cell interactions, whereas effects due to massive cell loss could also be excluded by counting nuclei positioned on the electrodes (Fig. 4.8). As a mechanistic explanation, IBMX and indomethacine in AIM reduces turnover of cAMP and the increased cAMP activates PKA. The observed impact on the actin

cytoskeleton may promote retraction of MSCs (Tio et al., 2010; Nombela-Arrieta et al., 2011), but in addition the stimulated synthesis of hyaluronan and chondroitin sulfate proteoglycan by activated PKA lowers cell contacts or widens spacing of cell-matrix adhesion (Calvo et al., 1991; Zizola et al., 2007). Underlining these mechanisms, the effects on cytoskeleton and cell morphology were only marginal for MSCs in AIM lacking IBMX or indomethacine, as judged by impedance recordings which rather resembled profiles of uninduced MSCs (see Fig. 4.6). Thus, according to the profiles the lack of the other inducing agents, dexamethasone and insulin did not affect adipogenic differentiation *per se*, indicating a more supportive or enhancing role, e.g. by stimulating the clonal amplification of committed cells.

The observed changes in cell morphology and cell-cell interactions during differentiation are in total agreement with a very recently published study further elucidating impedance measurements of MSC differentiation (Bagnaninchi and Drummond, 2011). By applying a more sophisticated ECIS-system impedance values could be broken down into their main contributing parameters of barrier resistance (R_b), cell membrane capacitance (C_m) and cell-substrate parameter α (Giaever and Keese, 1991; Lo et al., 1995; Bagnaninchi and Drummond, 2011). This uncovered definitely that the initial increase in OIM after induction was more due to enhanced cell-substrate interactions reflected by parameter α^2 but differences to adipogenic-induced cells were diminished over time. Supporting the here presented impedance data on fluctuations in cell interactions during cycling adipogenic differentiation, Bagnaninchi and Drummond (2011) demonstrated that after one day impedance was dominated by R_b values, reflecting the established intercellular junctions. In AIM this value was almost zero but regained after medium change to maintenance medium presumably by reestablishing loose cell-cell contacts due to changes in the cytoskeleton. This would explain why in AIM the MSCs spread initially more slowly and acquired finally a roundish, adipocyte-like morphology.

The finally really advanced adipogenic stage was confirmed in these experimental settings by intense ORO staining of lipid droplets, presence of ADRP and perilipin on western blots, and expression of the late adipogenic marker gene adiponectin besides PPARγ and perilipin. All those were detected by RT-qPCR in the MSC samples induced for adipogenesis at the end points (Fig. 4.9 - 4.11).

Osteogenic differentiation

The initially steeper osteogenic profiles reflect formation of strong cell adhesion, as demonstrated by high cell-substrate parameter α (Bagnaninchi and Drummond, 2011). Later on impedance is rising mostly due to firmly established intercellular junctions but also enhanced ECM deposition by osteogenic cells which further increases layer resistance R_b. This was confirmed by an additional report on higher impedance values of MSCs in OIM (Hildebrandt et al., 2010; Bagnaninchi and Drummond, 2011).

In this work, differentiation was finally verified histologically by Alizarin red S or von Kossa staining as well as detection of osteopontin and of late osteogenic marker BSP on western blots at end points. In this context, it has to be emphasized that the initial cell density matters tremendously when comparing results from different experimental settings. Seeding MSCs at densities beyond confluency apparently saturates coverage of the cell substratum or matrix support while also minimizing proliferation due to contact inhibition, which is leading to signal saturation visible by impedance plateaus. Contrarily, gain of impedance was much higher under conditions allowing to start with lower number of MSCs (2.5 x 10^4 cells/cm^2; xCELLigence system). Presumably both delayed contact inhibition of proliferation and less restricted spreading contributed to steeper impedance curves shown herein, a view supported by reports on enhanced expression of adhesion receptors (e.g. integrins) in OIM (Mizuno et al., 2000; Warstat et al., 2010).

Underlining the value of this method, impedance curves clearly distinguished non-differentiated from differentiating osteogenic or adipogenic cells and allowed a level of quantification at early time points of differentiation (Fig. 4.7). This was true for high passage versus low passage cells as well as for the comparison of MSCs from different tissues or donors. Thus, comparing two MSC strains from adipose tissue, ASC-1 cells showed in contrast to the fully potent ASC-2 cells merely a weak osteogenic impedance profile (Fig. 4.7 C and D) which correlated to the at best marginal von Kossa staining after 14 days (Fig. 4.9) and only a very faint osteopontin band on western blot.

Application of cells from different tissues

Up-to-now, only cells from bone marrow or adipose tissue were successfully used in impedance-monitored differentiation experiments. Since cells from umbilical cord blood

tested so far, showed distinct growth behavior, rather colony-like pattern than forming confluent cell layers (not shown), no reliable impedance measurements for umbilical cord blood cells was applicable. Therefore, the usage of impedance measurements has to be tested for other cell sources than bone marrow or adipose tissue. Whether the height or profile course of impedance can also be extrapolated to the degree of differentiation potential has to be evaluated in future studies with larger sample cohorts and with samples from various tissues.

As proof of principle for concept of impedance sensing even minutes changes due to small molecular variations, a keratinocyte line (HaCaT cells), with inducible expression was employed. These epidermal cells usually not expressing nidogen, could be forced to express this adhesion molecule (present in BM) via doxycycline inducible vector. Secretion of nidogen provided the cells increased adhesive properties, which were reflected by impedance measurements (Fig. 4.3). Furthermore, like the induced HaCaT cells also wild-type fibroblasts expressing genuine nidogen showed delayed repopulation of the wounded electrodes compared to non-induced cells or nidogen-knock out fibroblasts (Fig. 4.23). As a caveat, differences seen for fibroblasts should be considered with some caution since those cells can vary from isolate to isolate and in addition undergo changes during cultivation. Contrarily, the results of migration experiments with stable HaCaT cell line, representing a rather homogeneous cell population, apparently just evoked from their response to nidogen induction. Certainly, the molecular processes in these manipulated nidogen-expressing keratinocytes need to be addressed in future studies to elucidate the role of nidogen on changes in adhesion, cytoskeletal rearrangements, and further consequences like delayed migration. Nevertheless, this emphasizes the sensitivity of impedance measurement, being able to detect little changes caused on the molecular level.

Migration of MSCs during differentiation

Differentiation finally leading to a basic change in cell functions, not only has a high impact on morphology or adhesion of cells but also on their migratory behavior. Though being one of the major characteristics of MSCs, their ability to differentiate into multiple lineages might not be their major contribution to tissue repair *in vivo*. Rather than being a source of new tissue or cell mass, there are cues that MSC contribution to

tissue repair may largely occur through a more indirect, trophic functional manner. Thus, upon recruitment to injured or inflammatory tissue MSCs secrete cytokines or growth factors which stimulate resident stromal cells to proliferate and to secrete ECM and other proteins, thus participating in or enhancing wound healing. But for this scenario, first of all MSCs have to be either mobilized from their stem cell niche or recruited from the blood flow to the wounded tissue, followed by final attachment and homing there. To accomplish that, chemokines and growth factors are released from inflammatory sites and distributed via the blood flow towards the stem cell niches where they mobilize the MSCs (Ji et al., 2004; Sordi et al., 2005). The recruitment of circulating MSCs to wound or inflammatory sites may occur by mechanisms shared with lymphocytes, the elucidation of which will require further extensive research. To study certain aspects of the migratory behavior of MSCs, cells were seeded at confluent densities and repopulation of electrically wounded cell-free areas (high voltage pulse at sensing electrode) was monitored by impedance recordings. Alternatively closing of an artificial cell free area by surrounding MSCs was recorded at certain time points by photomicrographs. Both showed distinct migratory behavior in response to initiation of differentiation or to agents for stimulating cell migration (Fig. 4.24 and 4.25).

A key player in cell migration is RhoA, a member of the RhoGTPase family. It regulates the cross-linking of actin and myosin filaments into stress fibers and functions in actin stabilization. RhoA also takes part in the formation of focal contacts by clustering integrins and associated molecules, which are essential processes for migration, too. Accordingly, inhibition of RhoA was leading to reduced MSC migration (Lee et al., 2008; Raheja et al., 2011). In contrast, overstimulation with forced constitutively active RhoA inhibited MSC migration (Jaganathan et al., 2007). While high levels of RhoA correlated with osteogenic differentiation, the levels were lowered during adipogenesis (McBeath et al., 2004). In turn this might contribute to decreased migratory properties in adipogenic cells, in accord with the migration assays presented herein (Fig. 4.24). For this test, the high seeding numbers gave rise to confluent cell layers which did not reveal any significant variations in cell numbers in the different media as evaluated by counting cell nuclei (Fig. 4.8). Therefore the number of cells surrounding the wound area was very similar in all media and thus, the delay in wound recovery directly correlated to lower MSC migration in AIM (Fig. 4.24.The other way around, the impact on the actin cytoskeleton, seen by fluorescence microscopy, accompanying adipogenic

differentiation could be indirectly influenced by expression of RhoA, apart from regulating cell migration. Lower migration of adipogenic cells compared to osteogenic or undifferentiated cells replicates the *in vivo* situation. While there is no further need for adipogenic cells to migrate within adipose tissue, the initial function of MSCs crucially depends on migration towards injured tissue sites which could be also modulated by ECM composition as discussed below. What osteogenesis is concerned, the continuous turnover of bones relies on a fine-tuned interplay of osteoblasts and osteoclasts. Bone matrix gets degraded by osteoclasts, followed by immigration of osteoblasts into the degraded bone mass. The osteoblasts then rebuild bone structure by deposition and reassembly of new organic and inorganic matrix material.

Low chemokinetic effects on MSC migration

To recruit cells, like MSCs, macrophages or neutrophils, for wound healing, chemokines and cytokines but also specific growth factors are secreted from tissue cells at injured or inflammatory sites *in vivo*. Several factors have been connected to the promotion of MSC migration including SDF-1α, PDGF-AB, epidermal growth factor (EGF), insulin-like growth factor-1, hepatocyte growth factor (HGF), interleukin (IL)-8, CCL5 (also known as RANTES), monocyte chemotactic protein 1 (MCP-1) or vascular endothelial growth factor (VEGF) (Ponte et al., 2007; Ringe et al., 2007; Spaeth et al., 2008). However, the effects of the examined factors PDGF-AB or SDF-1α on migration were quite low compared to standard growth medium (Fig. 4.25). This was in marked contrast to previous studies claiming that these factors are highly potent inducers of MSC migration (Ponte et al., 2007; Ringe et al., 2007; Ryu et al., 2010; Xu et al., 2010). But in general, former studies have been performed in trans-well chambers, studying cell migration towards a gradient of chemotactic agents. Contrarily, migration assays herein were more likely to reflect chemokinetic or adhesion related effects on the cells apparently hardly or not at all influenced by PDGF or SDF-1 (Fig. 4.25). Whether these factors act on mobilization of MSCs from the stem cell niche or direct only circulating cells from the peripheral blood has not been clarified yet. TNFα seems to act more indirectly on MSC migration. It upregulates the expression of several chemokine receptors increasing the response of MSCs to several factors and cytokines like CCL5 or TNF-related apoptosis-inducing ligand (TRAIL) which increase cell migration (Corallini et al., 2010; Hemeda

et al., 2010; Ponte et al., 2007). But the role of TNFα on adhesion molecules seems to be of ambivalent nature. It increases expression of ICAM-1 which can activate Rho-like GTPases and it interacts on actin organization, both being important players in migration themselves (Fu et al., 2009). Contrarily, TNFα increased homing of rat MSCs to cardiac microvascular endothelium which as shown to be mediated by VCAM-1 (Segers et al., 2006). Therefore, the application of TNFα solely, without addition of other chemokines might increase the adhesion of MSCs whereas Rho-like GTPase activation is less efficient through TNFα leading to slower repopulation of 'wounded', cell free areas as indicated by the MSC migration assays herein (Fig. 4.25).

Results of MSC migration experiments in response to chemokine stimulation show the limits of electric wounding assay. Since MSC migration is usually more towards a gradient of chemokines, this assay is more dedicated to study adhesion-related effects on migration and to identify involved receptors than to evaluate chemokine stimulation of MSCs. However, studies with impedance measurements in transwell chamber experiments are also under development or even already available and may facilitate the analysis of chemokine-mediated migration and high-throughput screening of various factors.

ECM proteins affect MSC differentiation

For studying the influence of specific cell-matrix interactions during differentiation, the concept of monitoring MSC differentiation with impedance recording was extended: Culture vessels were precoated with the ECM proteins collagen I, collagen IV, fibronectin, or laminin before the cells were seeded and differentiation was initiated. For MSCs, interactions with ECM proteins are crucial for the maintenance of their differentiation potential *in vitro* (Mauney et al., 2005, 2006), which mirrors the role of ECM in the stem cell niche or also for homing in target tissues. But ECM interactions can also promote or inhibit distinct differentiation pathways (Mizuno et al., 2000; Mizuno and Kuboki, 2001; Salasznyk et al., 2004; Mauney and Volloch, 2009, 2010), according to some reports even without addition of specific inducing factors (Mizuno et al., 2000; Klees et al., 2005). This is in line with herein presented findings that impedance values increased when inducing the osteogenic track in OIM on collagen I or IV coatings, whereas the drop of profiles in AIM typical for adipogenic differentiation was far less

pronounced (Fig. 4.12). Reduced adipogenesis on collagen matrix was confirmed by the weak ORO staining after 21 days, whereas Alizarin Red S staining was more pronounced on collagens (see Figs. 4.19 and 4.21). These data were in accordance with previous reports on the effect of collagen I and IV on osteogenic and adipogenic differentiation (Mauney and Volloch, 2009, 2010).

Applying collagen I in different densities, ranging from 0-50 $\mu g/cm^2$ revealed only marginal differences in ORO stain 5 days after adipogenic induction, whereas lipid accumulation was lowered after 21 days at all collagen concentrations, supporting previous results of negative effects of collagen I on adipogenesis. Corresponding impedance data in AIM or MSC-GM were more ambiguous, coating with 25 $\mu g/cm^2$ showed highest impedance values in all media, likely reflecting best adhesion on this matrix (Fig. 4.14). Higher coating density using 50 $\mu g/cm^2$ reversed this effect, showing surprising low impedance data, pointing to oversaturation of matrix coating and blocking of cell adhesion sites instead of providing support. This is also reflected in OIM, were impedance profiles are in sequential order to increasing collagen matrix density, exempted 50 $\mu g/cm^2$, and although not significant, the same tendencies were observed by Alizarin Red S staining for calcium deposition. Overall this provides further evidence for the hypothesis that increased adhesive properties which are reflected by high impedance values might be supportive for osteogenic differentiation.

The situation is even more complex for fibronectin, which has been thought formerly to be a negative effector of adipogenesis due to its strong cell spreading effect. But this inhibition can be principally reversed by high insulin levels (Spiegelman and Ginty, 1983) as it is applied in our experiments by AIM. Apparently, fibronectin supported long lasting spreading of MSCs reflected by the delayed decrease of impedance in the first 40 hours. Differentiation into adipogenic lineage was initiated afterwards, changing morphology into round cell bodies over time and correlating to continuously declining impedance. For comparison, similar curves but lower impedance levels on laminin inferred weaker adhesion as observed for other mesenchymal cells like fibroblasts. Principally, the degree of cell adhesion and spreading is inversely related to adipogenic differentiation where a more roundish cell shape is acquired which correlates with lipid droplet accumulation (McBeath et al., 2004; Park et al., 2009). Interestingly, numbers of ORO positive cells on fibronectin and laminin coats after 21 days of differentiation

in AIM did not differ from uncoated controls, which presumably reflects deposition of fibronectin or vitronectin from the FCS containing media as well as ECM secretion by the MSCs themselves. The effect became even more striking by image analysis of the average intensity of ORO staining which was markedly higher on fibronectin than on the other matrices. Thus, fibronectin coating in our experiments did not prevent but rather delayed adipogenic differentiation by increasing cell-substrate interactions, reflected by an extended plateau and delayed drop of the impedance profile.

The degree of differentiation or its inhibition apparently depends, apart from possible concentration effects, on conformation or structure of protein coatings (Mauney and Volloch, 2009, 2010). For those experiments, wells were coated with a film of native ECM proteins and in addition for comparison of protein conformation with denatured collagen I. Compared to its native counterpart denatured collagen I exhibits a more relaxed conformation, exposing other 'cryptic' binding site for $\alpha v\beta 3$ integrin while binding sites for $\alpha 1\beta 1$ and $\alpha 2\beta 1$ integrins are masked (Davis, 1992). Altered adhesion properties match the impedance data of native versus denatured collagen I coating, while the overall profile of the graphs on both conformations remained identical. But on the latter matrix higher impedance values were noted in all media, which argues for increased adhesion of MSCs on denatured collagen I in general (see Fig. 4.15). As already discussed above, increased adhesion is related to a decrease in adipogenesis and improved osteogenesis, as confirmed by lipid and calcium staining, respectively. However, these results are in contrast to a previous study, claiming efficient p38 kinase regulated adipogenesis but inefficient osteogenesis in a Hsp90-independent manner on denatured collagen I. One explanation of this discrepancy be a harsher treatment for collagen denaturation in that study, possibly leading to molecular damage and a gelatin like material with adverse properties. The finding of an inverse relation on native collagen I by the authors (Mauney and Volloch, 2009) is in line with the data for native collagen I presented above. Also in harmony with the results on collagen IV Mauney and Volloch (2010) found a negative influence of native collagen IV on adipogenesis, though it was again highly efficient on denatured collagen IV matrices.

Requirements for cell therapies with MSCs

The herein presented results support former findings of varying potential of MSC isolates and underline the regulatory role of cell-matrix contacts for maintenance of stemness and differentiation processes. Thus, to generate more homogeneous, standardized MSC populations for research and therapeutic application, methods for MSC isolation and conditions for *in vitro* cultivation need to be optimized and better standardized. This also implicates the general need for the development of GMPs. On the one hand, optimized media and a growth environment for the maintenance of stem cell properties like self-renewal and differentiation potential are required, which on the other hand the development of culture conditions for most efficient lineage commitment and differentiation, e.g. for cell replacement therapies, are desirable. Therein, the quality of cultivation medium plays a pivotal role. Although *in vitro* propagated, autologous MSCs do not provoke alloreactivity themselves after *in vivo* transplantation, some recipients of MSCs formed antibodies against FCS, a common supplement of standard media for *ex vivo* culturing of cells (Sundin et al., 2007), which might provoke side-effects in patients. This underlines the necessity to optimize and standardize *in vitro* cultivation, which ensures MSC functionality without bearing biohazards. Chemically defined media, human AB serum or thrombin-activated platelet-rich plasma as alternatives to FCS supplemented media, are currently under investigation (Kocaoemer et al., 2007) and will gain importance in future MSC research and especially for cell therapy.

Herein, impedance based assays can not only be used for studying proliferation, but furthermore impedance can help to assess the impact of distinct media on stemness and differentiation potential. As far as shown in this thesis, the fate of MSCs - maintenance of stemness, tissue homing and differentiation - also depends on extracellular matrix contacts. Structured coating with RGD peptide, generating a pattern with defined molecular spacing has demonstrated that this governs outside-in signaling through the integrins bound to these ligands which can have dramatic consequences for cellular fate (Selhuber-Unkel et al., 2010). Future experiments with combinations of varying proteins of the ECM or with bioactive peptides and synthetic compounds will help to identify receptor molecules to correlate impedance profiles with patterns of cell receptors responsible for maintenance of stemness or guiding MSC differentiation. Identification of these receptors, e.g. by blocking with specific antibodies or RNAi techniques, will not

only improve the definition of the stem cell niche but also provide information how cells maintain vitality and their properties while traveling in the circulation. For that goal mimicking of more *in vivo*-like conditions is required. Thus, more complex ECM scaffolds, MSC growth and differentiation in three-dimensional cultures or cultivation under hypoxic conditions need to be tested and which may provide new insights especially into cell-matrix interactions.

Conclusions

In this work the behavior and differentiation potential of multipotent mesenchymal stromal cells (MSCs) have been investigated in response to inducing agents and under particular consideration of cell adhesion and cell-matrix interactions. For this task monitoring live cells by electrical cell impedance sensing (ECIS) was adapted and optimized, verifying the tracks of adipogenic or osteogenic differentiation by light microscopy, analysis of gene expression and marker proteins as well as histological and fluorescence staining. Establishing this continuous real-time and non-invasive method with different cell types clearly showed distinct impedance profiles closely correlating to cell numbers in general and specifically adhesive properties of the various cells types which were changing according to the specific differentiation modes as shown herein in great detail for MSCs. Furthermore, according to those ECIS recordings a marked variation of differentiation potential has been found depending on donors, tissue of origin and number of cell passages *in vitro* confirming former findings by other methods (Sekiya et al., 2002; Bonab et al., 2006; Kretlow et al., 2008).

During differentiation MSCs change, together with function and morphology, their contacts with neighboring cells and matrix proteins both of which adding to the fate of MSCs in return. As shown herein, osteogenesis is favored on collagen matrices, while fibronectin was promoting adipogenic differentiation *in vitro*, an issue under controversial debate in the past. Corresponding to overall changes in expression of genes and proteins in each stage of differentiation, patterns of matrix receptor molecules, largely integrins, undergo profound alterations. These cell-matrix interactions trigger further signaling pathways (outside-in signaling) which in turn contribute to differentiation modes and cell behavior in general. Identification of these receptors and the changes within receptor expression is essential to gain new information on the mechanism involved in homing of MSCs at specific tissue sites or stem cell niches, including the maintenance of stemness and guidance of differentiation. The fact that also very early changes with onset of MSC differentiation are detectable by impedance measurements, which can neither be addressed reliably by histochemistry nor by profiling of gene expression or cell surface markers, recommends this method for further research on these processes involving cell attachment and specific interactions. A better understanding of the underlying cell biology will certainly boost therapeutic applications.

However, for treatment of patients in particular but also to make research results of MSC preparations better comparable, methods for isolation and *in vitro* cultivation have to be further optimized and standardized, generally implied in the development of good manufacturing practices (GMPs). This emphasizes the importance of specific cell isolation procedures and especially directed amplification (e.g. by cell-matrix interactions) with regard to maintenance or lineage commitment of the cells before broader application in research or clinical trials. For this purpose impedance sensing qualifies as particularly suitable quality control for the screening of larger MSC sample cohorts, which can also be combined with microscopy directly or in parallel applying advanced imaging techniques.

In this thesis the impedance measurements have been demonstrated to represent a non-invasive real time technique for monitoring early steps in cell attachment and further interactions and the fate of MSCs. Based on the stability of the method to clearly discriminate MSCs from other cell types and to display typical profiles of osteo- and adipogenic differentiation, this method may be considered as a valuable tool for screening large panels of inducing factors or support matrices, but last not least for quality control of MSC preparations. This work should also provide a basis for future investigations on adhesion related cell behavior and identification of receptors contributing to the intracellular signaling, analyzing these processes in a label-free and continuous, non-invasive manner.

References

B. Alberts, A. Johnson, J. Lewis, M. Raff, K. Roberts, and Walter P. *Molecular Biology of the Cell*. Garland Science, Fifth edition, 2007.

M. Angstmann. Forced nidogen-1 and -2 expression in human epidermal cell line HaCaT. *Diploma Thesis, Mannheim University of Applied Science*, 2007.

F. Arnalich-Montiel, S. Pastor, A. Blazquez-Martinez, J. Fernandez-Delgado, M. Nistal, J. L. Alio, and M. P. De Miguel. Adipose-derived stem cells are a source for cell therapy of the corneal stroma. *Stem Cells*, 26(2):570–579, 2008.

J. M. Atienza, J. Zhu, X. Wang, X. Xu, and Y. Abassi. Dynamic monitoring of cell adhesion and spreading on microelectronic sensor arrays. *Journal of Biomolecular Screening*, 10(8): 795–805, 2005.

J. E. Aubin. Regulation of osteoblast formation and function. *Rev Endocr Metab Disord*, 2(1): 81–94, 2001.

M. Aumailley and P. Rousselle. Laminins of the dermo-epidermal junction. *Matrix Biology*, 18 (1):19–28, 1999.

M. Aumailley, L. Bruckner-Tuderman, W. G. Carter, R. Deutzmann, D. Edgar, P. Ekblom, J. Engel, E. Engvall, E. Hohenester, J. C. R. Jones, H. K. Kleinman, M. P. Marinkovich, G. R. Martin, U. Mayer, G. Meneguzzi, J. H. Miner, K. Miyazaki, M. Patarroyo, M. Paulsson, V. Quaranta, J. R. Sanes, T. Sasaki, K. Sekiguchi, L. M. Sorokin, J. F. Talts, K. Tryggvason, J. Uitto, I. Virtanen, K. von der Mark, U. M. Wewer, Y. Yamada, and P. D. Yurchenco. A simplified laminin nomenclature. *Matrix Biology*, 24(5):326–332, 2005.

P. O. Bagnaninchi and N. Drummond. Real-time label-free monitoring of adipose-derived stem cell differentiation with electric cell-substrate impedance sensing. *Proceedings of the National Academy of Sciences*, 108(16):6462–6467, 2011.

D. Baksh, R. Yao, and R. S. Tuan. Comparison of proliferative and multilineage differentiation potential of human mesenchymal stem cells derived from umbilical cord and bone marrow. *Stem Cells*, 25(6):1384–92, 2007.

A. Banas, T. Teratani, Y. Yamamoto, M. Tokuhara, F. Takeshita, G. Quinn, H. Okochi, and T. Ochiya. Adipose tissue-derived mesenchymal stem cells as a source of human hepatocytes. *Hepatology*, 46(1):219–228, 2007.

A. Banfi, A. Muraglia, B. Dozin, M. Mastrogiacomo, R. Cancedda, and R. Quarto. Proliferation kinetics and differentiation potential of ex vivo expanded human bone marrow stromal cells: Implications for their use in cell therapy. *Exp Hematol*, 28(6):707–15, 2000.

D. Bexell, S. Gunnarsson, A. Tormin, A. Darabi, D. Gisselsson, L. Roybon, S. Scheding, and J. Bengzon. Bone marrow multipotent mesenchymal stroma cells act as pericyte-like migratory vehicles in experimental gliomas. *Mol Ther*, 17(1):183–90, 2009.

P. Bianco, P. Gehron Robey, I. Saggio, and M. Riminucci. "Mesenchymal" stem cells in human bone marrow (skeletal stem cells) — a critical discussion of their nature, identity, and significance in incurable skeletal disease. *Human Gene Therapy*, 21(9):1057–1066, 2010.

K. Bieback, S. Kern, H. Klüter, and H. Eichler. Critical parameters for the isolation of mesenchymal stem cells from umbilical cord blood. *Stem Cells*, 22(4):625–34, 2004.

K. Bieback, A. Hecker, A. Kocaömer, H. Lannert, K. Schallmoser, D Strunk, and H. Klüter. Human alternatives to fetal bovine serum for the expansion of mesenchymal stromal cells from bone marrow. *Stem Cells*, 27(9):2331–41, 2009.

K. Bieback, V. A. Ha, A. Hecker, M. Grassl, S. Kinzebach, H. Solz, C. Sticht, H. Klüter, and P. Bugert. Altered gene expression in human adipose stem cells cultured with fetal bovine serum compared to human supplements. *Tissue Engineering Part A*, 16(11):3467–3484, 2010.

M. M. Bonab, K. Alimoghaddam, F. Talebian, S. H. Ghaffari, A. Ghavamzadeh, and B. Nikbin. Aging of mesenchymal stem cell in vitro. *BMC Cell Biol*, 7:14, 2006.

P. Boukamp, R. T. Dzarlieva-Petrusevska, D. Breitkreutz, J. Hornung, A. Markham, and N. E. Fusenig. Normal keratinization in a spontaneously immortalized aneuploid human keratinocyte cell line. *J Cell Biol*, 106(3):761–71, 1988.

B. Brachvogel, H. Moch, F. Pausch, U. Schlötzer-Schrehardt, C. Hofmann, R. Hallmann, K. von der Mark, T. Winkler, and E. Pöschl. Perivascular cells expressing annexin a5 define a novel mesenchymal stem cell-like population with the capacity to differentiate into multiple mesenchymal lineages. *Development*, 132(11):2657–2668, 2005.

M. Breitbach, T. Bostani, W. Roell, Y. Xia, O. Dewald, J. M. Nygren, J. W. U. Fries, K. Tiemann, H. Bohlen, J. Hescheler, A. Welz, W. Bloch, S. E. W. Jacobsen, and B. K. Fleischmann. Potential risks of bone marrow cell transplantation into infarcted hearts. *Blood*, 110(4):1362–1369, 2007.

D. Breitkreutz, N. Mirancea, C. Schmidt, R. Beck, U. Werner, H. J. Stark, M. Gerl, and N. E. Fusenig. Inhibition of basement membrane formation by a nidogen-binding laminin gamma1-chain fragment in human skin-organotypic cocultures. *J Cell Sci*, 117(Pt 12):2611–22, 2004.

J. C. Calvo, D. Rodbard, A. Katki, S. Chernick, and M. Yanagishita. Differentiation of 3T3-L1 preadipocytes with 3-isobutyl-1-methylxanthine and dexamethasone stimulates cell-associated and soluble chondroitin 4-sulfate proteoglycans. *Journal of Biological Chemistry*, 266(17):11237–11244, 1991.

A. I. Caplan. Mesenchymal stem cells. *J Orthop Res.*, 9(5):641–650, 1991.

D. Chan, S. R. Lamande, W. G. Cole, and J. F. Bateman. Regulation of procollagen synthesis and processing during ascorbate-induced extracellular matrix accumulation in vitro. *Biochem J*, 269(1):175–81, 1990.

L. Chen, E. E. Tredget, P. Y. G. Wu, and Y. Wu. Paracrine factors of mesenchymal stem cells recruit macrophages and endothelial lineage cells and enhance wound healing. *PLoS ONE*, 3(4):e1886, 2008.

D. C. Colter, R. Class, C. M. DiGirolamo, and D. J. Prockop. Rapid expansion of recycling stem cells in cultures of plastic-adherent cells from human bone marrow. *Proc Natl Acad Sci U S A*, 97(7):3213–8, 2000.

F. Corallini, P. Secchiero, A. P. Beltrami, D. Cesselli, E. Puppato, R. Ferrari, C. A. Beltrami, and G. Zauli. TNF-alpha modulates the migratory response of mesenchymal stem cells to trail. *Cell Mol Life Sci*, 67(8):1307–14, 2010.

George E. Davis. Affinity of integrins for damaged extracellular matrix: [alpha]v[beta]3 binds to denatured collagen type I through rgd sites. *Biochemical and Biophysical Research Communications*, 182(3):1025–1031, 1992.

D. L. Diefenderfer, A. M. Osyczka, G. C. Reilly, and P. S. Leboy. BMP responsiveness in human mesenchymal stem cells. *Connective Tissue Research*, 44(1):305–311, 2003.

M. Dominici, K. Le Blanc, I. Mueller, I. Slaper-Cortenbach, F. Marini, D. Krause, R. Deans, A. Keating, D. J. Prockop, and E. Horwitz. Minimal criteria for defining multipotent mesenchymal stromal cells. The International Society for Cellular Therapy position statement. *Cytotherapy*, 8(4):315–7, 2006.

P. Ducy, R. Zhang, V. Geoffroy, A. L. Ridall, and G. Karsenty. Osf2/Cbfa1: A transcriptional activator of osteoblast differentiation. *Cell*, 89(5):747–754, 1997.

A. J. Engler, S. Sen, H. L. Sweeney, and D. E. Discher. Matrix elasticity directs stem cell lineage specification. *Cell*, 126(4):677–89, 2006.

A. Erices, P. Conget, and J. J. Minguell. Mesenchymal progenitor cells in human umbilical cord blood. *Br J Haematol*, 109(1):235–42, 2000.

Jr. Feldmann, R. E., K. Bieback, M. H. Maurer, A. Kalenka, H. F. Burgers, B. Gross, C. Hunzinger, H. Kluter, W. Kuschinsky, and H. Eichler. Stem cell proteomes: a profile of human

mesenchymal stem cells derived from umbilical cord blood. *Electrophoresis*, 26(14):2749–58, 2005.

A. J. Friedenstein, R. K. Chailakhjan, and K. S. Lalykina. The development of fibroblast colonies in monolayer cultures of guinea-pig bone marrow and spleen cells. *Cell Tissue Kinet.*, 3(4):393–403, 1970.

X. Fu, B. Han, S. Cai, Y. Lei, T. Sun, and Z. Sheng. Migration of bone marrow-derived mesenchymal stem cells induced by tumor necrosis factor-alpha and its possible role in wound healing. *Wound Repair Regen*, 17(2):185–91, 2009.

M. Galiè, G. Konstantinidou, D. Peroni, I. Scambi, C. Marchini, V. Lisi, M. Krampera, P. Magnani, F. Merigo, M. Montani, F. Boschi, P. Marzola, R. Orrù, P. Farace, A. Sbarbati, and A. Amic. Mesenchymal stem cells share molecular signature with mesenchymal tumor cells and favor early tumor growth in syngeneic mice. *Oncogene*, 27(18):2542–2545, 2008.

S. Garcia, M. C. Martín, R. de la Fuente, J. C. Cigudosa, J. Garcia-Castro, and A. Bernad. Pitfalls in spontaneous in vitro transformation of human mesenchymal stem cells. *Experimental Cell Research*, 316(9):1648–1650, 2010.

E.L. George, E.N. Georges-Labouesse, R.S. Patel-King, H. Rayburn, and R.O. Hynes. Defects in mesoderm, neural tube and vascular development in mouse embryos lacking fibronectin. *Development*, 119(4):1079–1091, 1993.

R. F. Ghohestani, K. Li, P. Rousselle, and J. Uitto. Molecular organization of the cutaneous basement membrane zone. *Clinics in Dermatology*, 19(5):551–562, 2001.

I. Giaever and C. R. Keese. Monitoring fibroblast behavior in tissue culture with an applied electric field. *Proc Natl Acad Sci U S A*, 81(12):3761–4, 1984.

I. Giaever and C. R. Keese. Micromotion of mammalian cells measured electrically. *Proc Natl Acad Sci U S A*, 88(17):7896–900, 1991.

I. Giaever and C. R. Keese. A morphological biosensor for mammalian cells. *Nature*, 366(6455): 591–2, 1993.

F. M. Gregoire, C. M. Smas, and H. S. Sul. Understanding adipocyte differentiation. *Physiol Rev*, 78(3):783–809, 1998.

C. A. Gregory, W. G. Gunn, A. Peister, and D. J. Prockop. An alizarin red-based assay of mineralization by adherent cells in culture: comparison with cetylpyridinium chloride extraction. *Anal Biochem*, 329(1):77–84, 2004.

C. A. Gregory, D. J. Prockop, and J. L. Spees. Non-hematopoietic bone marrow stem cells: molecular control of expansion and differentiation. *Exp Cell Res*, 306(2):330–5, 2005.

B. Hall, J. Dembinski, A. K. Sasser, M. Studeny, M. Andreeff, and F. Marini. Mesenchymal stem cells in cancer: tumor-associated fibroblasts and cell-based delivery vehicles. *Int J Hematol*, 86(1):8–16, 2007.

K. Hanada, J. E. Dennis, and A. I. Caplan. Stimulatory effects of basic fibroblast growth factor and bone morphogenetic protein-2 on osteogenic differentiation of rat bone marrow-derived mesenchymal stem cells. *Journal of Bone and Mineral Research*, 12(10):1606–1614, 1997.

H. Hemeda, M. Jakob, A. K. Ludwig, B. Giebel, S. Lang, and S. Brandau. Interferon-gamma and tumor necrosis factor-alpha differentially affect cytokine expression and migration properties of mesenchymal stem cells. *Stem Cells Dev*, 19(5):693–706, 2010.

P. Hernigou, A. Poignard, F. Beaujean, and H. Rouard. Percutaneous autologous bone-marrow grafting for nonunions. influence of the number and concentration of progenitor cells. *J Bone Joint Surg Am.*, 87(7):1430–1437, 2005.

C. Hildebrandt, H. Büth, S. Cho, Impidjati, and H. Thielecke. Detection of the osteogenic differentiation of mesenchymal stem cells in 2D and 3D cultures by electrochemical impedance spectroscopy. *Journal of Biotechnology*, 148(1):83–90, 2010.

E. M. Horwitz, P. L. Gordon, W. K. K. Koo, J. C. Marx, M. D. Neel, R. Y. McNall, L. Muul, and T. Hofmann. Isolated allogeneic bone marrow-derived mesenchymal cells engraft and stimulate growth in children with osteogenesis imperfecta: Implications for cell therapy of bone. *Proceedings of the National Academy of Sciences*, 99(13):8932–8937, 2002.

T. Hoshiba, N. Kawazoe, T. Tateishi, and G. Chen. Development of stepwise osteogenesis-mimicking matrices for the regulation of mesenchymal stem cell functions. *Journal of Biological Chemistry*, 284(45):31164–31173, 2009.

J. D. Humphries, A. Byron, and M. J. Humphries. Integrin ligands at a glance. *Journal of Cell Science*, 119(19):3901–3903, 2006.

C. Hung, C. Yao, F. Cheng, M. Wu, T. Wang, and S. Hwang. Establishment of immortalized mesenchymal stromal cells with red fluorescence protein expression for in vivo transplantation and tracing in the rat model with traumatic brain injury. *Cytotherapy*, 12(4):455–465, 2010.

B. G. Jaganathan, B. Ruester, L. Dressel, S. Stein, M. Grez, E. Seifried, and R. Henschler. Rho inhibition induces migration of mesenchymal stromal cells. *Stem Cells*, 25(8):1966–1974, 2007.

J. F. Ji, B. P. He, S. T. Dheen, and S. S. Tay. Interactions of chemokines and chemokine receptors mediate the migration of mesenchymal stem cells to the impaired site in the brain after hypoglossal nerve injury. *Stem Cells*, 22(3):415–27, 2004.

N. R. Jørgensen, Z. Henriksen, O. H. Sørensen, and R. Civitelli. Dexamethasone, BMP-2, and 1,25-dihydroxyvitamin D enhance a more differentiated osteoblast phenotype: validation of an in vitro model for human bone marrow-derived primary osteoblasts. *Steroids*, 69(4): 219–226, 2004.

C. R. Keese, J. Wegener, S. R. Walker, and I. Giaever. Electrical wound-healing assay for cells in vitro. *Proc Natl Acad Sci U S A*, 101(6):1554–9, 2004.

S. Kern, H. Eichler, J. Stoeve, H. Kluter, and K. Bieback. Comperative analysis of mesenchymal stem cells from bone marrow, umbilical cord blood, or adipose tissue. *Stem Cells*, 24(5):1294–1301, 2006.

J. Khoshnoodi, V. Pedchenko, and B. G. Hudson. Mammalian collagen IV. *Microscopy Research and Technique*, 71(5):357–370, 2008.

D. W. Kim, Y. J. Chung, T. G. Kim, Y. L. Kim, and I. H. Oh. Cotransplantation of third-party mesenchymal stromal cells can alleviate single-donor predominance and increase engraftment from double cord transplantation. *Blood*, 103(5):1941–8, 2004.

S. L. Kirstein, J. M. Atienza, B. Xi, J. Zhu, N. Yu, X. Wang, X. Xu, and Y. A. Abassi. Live cell quality control and utility of real-time cell electronic sensing for assay development. *Assay Drug Dev Technol.*, 4(5):545–553, 2006.

R. F. Klees, R. M. Salasznyk, K. Kingsley, W. A. Williams, A. Boskey, and G. E. Plopper. Laminin-5 induces osteogenic gene expression in human mesenchymal stem cells through an ERK-dependent pathway. *Mol Biol Cell*, 16(2):881–90, 2005.

A. Kocaoemer, S. Kern, H. Kluter, and K. Bieback. Human AB serum and thrombin-activated platelet-rich plasma are suitable alternatives to fetal calf serum for the expansion of mesenchymal stem cells from adipose tissue. *Stem Cells*, 25(5):1270–8, 2007.

T. Komori, H. Yagi, S. Nomura, A. Yamaguchi, K. Sasaki, K. Deguchi, Y. Shimizu, R. T. Bronson, Y. H. Gao, M. Inada, M. Sato, R. Okamoto, Y. Kitamura, S. Yoshiki, and T. Kishimoto. Targeted disruption of Cbfa1 results in a complete lack of bone formation owing to maturational arrest of osteoblasts. *Cell*, 89(5):755–764, 1997.

R. Koopman, G. Schaart, and M. K. Hesselink. Optimisation of oil red O staining permits combination with immunofluorescence and automated quantification of lipids. *Histochem Cell Biol*, 116(1):63–8, 2001.

T. Kreis and R. Vale. In: Guidebook to the extracellular matrix, anchor and adhesion proteins. *Oxford University Press*, 2nd Edition, 1999.

J. D. Kretlow, Y. Q. Jin, W. Liu, W. J. Zhang, T. H. Hong, G. Zhou, L. S. Baggett, A. G. Mikos, and Y. Cao. Donor age and cell passage affects differentiation potential of murine bone marrow-derived stem cells. *BMC Cell Biol*, 9:60, 2008.

K. Kühn. Basement membrane (type IV) collagen. *Matrix Biology*, 14(6):439–445, 1995.

K. Le Blanc, F. Frassoni, L. Ball, F. Locatelli, H. Roelofs, I. Lewis, E. Lanino, B. Sundberg, M. E. Bernardo, M. Remberger, G. Dini, R. M. Egeler, A. Bacigalupo, W. Fibbe, and O. Ringden. Mesenchymal stem cells for treatment of steroid-resistant, severe, acute graft-versus-host disease: a phase II study. *Lancet*, 371(9624):1579–86, 2008.

K. S. Lee, H. J. Kim, Q. L. Li, X. Z. Chi, C. Ueta, T. Komori, J. M. Wozney, E. G. Kim, J. Y. Choi, H. M. Ryoo, and S. C. Bae. Runx2 is a common target of transforming growth factor beta1 and bone morphogenetic protein 2, and cooperation between Runx2 and Smad5 induces osteoblast-specific gene expression in the pluripotent mesenchymal precursor cell line c2c12. *Mol Cell Biol*, 20(23):8783–92, 2000.

M. J. Lee, E. S. Jeon, J. S. Lee, M. Cho, D. S. Suh, C. L. Chang, and J. H. Kim. Lysophosphatidic acid in malignant ascites stimulates migration of human mesenchymal stem cells. *Journal of Cellular Biochemistry*, 104(2):499–510, 2008.

J. M. Lehmann, J. M. Lenhard, B. B. Oliver, G. M. Ringold, and S. A. Kliewer. Peroxisome proliferator-activated receptors alpha and gamma are activated by indomethacin and other non-steroidal anti-inflammatory drugs. *J Biol Chem*, 272(6):3406–10, 1997.

M. Leiss, K. Beckmann, A. Girós, M. Costell, and R. Fässler. The role of integrin binding sites in fibronectin matrix assembly in vivo. *Current Opinion in Cell Biology*, 20(5):502–507, 2008.

J. Liu and S. R. Farmer. Regulating the balance between peroxisome proliferator-activated receptor γ and β-catenin signaling during adipogenesis. *Journal of Biological Chemistry*, 279 (43):45020–45027, 2004.

C. M. Lo, C. R. Keese, and I. Giaever. Impedance analysis of MDCK cells measured by electric cell-substrate impedance sensing. *Biophys J*, 69(6):2800–7, 1995.

M. K. Majumdar, M. A. Thiede, J. D. Mosca, M. Moorman, and S. L. Gerson. Phenotypic and functional comparison of cultures of marrow-derived mesenchymal stem cells (MSCs) and stromal cells. *Journal of Cellular Physiology*, 176(1):57–66, 1998.

S. Makino, K. Fukuda, S. Miyoshi, F. Konishi, H. Kodama, J. Pan, M. Sano, T. Takahashi, S. Hori, H. Abe, J. Hata, A. Umezawa, and S. Ogawa. Cardiomyocytes can be generated from marrow stromal cells in vitro. *The Journal of Clinical Investigation*, 103(5):697–705, 1999.

C. Maniatopoulos, J. Sodek, and A. H. Melcher. Bone formation in vitro by stromal cells obtained from bone marrow of young adult rats. *Cell and Tissue Research*, 254(2):317–330, 1988.

Y. Mao and J. E. Schwarzbauer. Fibronectin fibrillogenesis, a cell-mediated matrix assembly process. *Matrix Biology*, 24(6):389–399, 2005.

J. Mauney and V. Volloch. Progression of human bone marrow stromal cells into both osteogenic and adipogenic lineages is differentially regulated by structural conformation of collagen I matrix via distinct signaling pathways. *Matrix Biol*, 28(5):239–50, 2009.

J. Mauney and V. Volloch. Human bone marrow-derived stromal cells show highly efficient stress-resistant adipogenesis on denatured collagen IV matrix but not on its native counterpart: implications for obesity. *Matrix Biol*, 29(1):9–14, 2010.

J. R. Mauney, D. L. Kaplan, and V. Volloch. Matrix-mediated retention of osteogenic differentiation potential by human adult bone marrow stromal cells during ex vivo expansion. *Biomaterials*, 25(16):3233–43, 2004.

J. R. Mauney, V. Volloch, and D. L. Kaplan. Matrix-mediated retention of adipogenic differentiation potential by human adult bone marrow-derived mesenchymal stem cells during ex vivo expansion. *Biomaterials*, 26(31):6167–75, 2005.

J. R. Mauney, C. Kirker-Head, L. Abrahamson, G. Gronowicz, V. Volloch, and D. L. Kaplan. Matrix-mediated retention of in vitro osteogenic differentiation potential and in vivo bone-forming capacity by human adult bone marrow-derived mesenchymal stem cells during ex vivo expansion. *J Biomed Mater Res A*, 79(3):464–75, 2006.

R. McBeath, D. M. Pirone, C. M. Nelson, K. Bhadriraju, and C. S. Chen. Cell shape, cytoskeletal tension, and RhoA regulate stem cell lineage commitment. *Dev Cell*, 6(4):483–95, 2004.

J. A. McDonald. Extracellular matrix assembly. *Annual Review of Cell Biology*, 4(1):183–207, 1988.

J. R. McMillan, M. Akiyama, and H. Shimizu. Ultrastructural orientation of laminin 5 in the epidermal basement membrane: an updated model for basement membrane organization. *J Histochem Cytochem*, 51(10):1299–306, 2003.

R. P. Mecham. The extracellular matrix: An overview. *Springer*, 1st Edition, 2011.

J. Miner and P. Yurchenco. Laminin functions in tissue morphogenesis. *Annual Review of Cell and Developmental Biology*, 20(1):255–284, 2004.

J. H. Miner. Basement membranes; in: The extracellular matrix: An overview; Mecham R. P. *Springer*, 1st Edition, 2011.

P. J. Mishra, J. W. Glod, and D. Banerjee. Mesenchymal stem cells: flip side of the coin. *Cancer Res*, 69(4):1255–8, 2009.

M. Mizuno and Y. Kuboki. Osteoblast-related gene expression of bone marrow cells during the osteoblastic differentiation induced by type I collagen. *J Biochem*, 129(1):133–8, 2001.

M. Mizuno, R. Fujisawa, and Y. Kuboki. Type I collagen-induced osteoblastic differentiation of bone-marrow cells mediated by collagen-alpha2beta1 integrin interaction. *J Cell Physiol*, 184(2):207–13, 2000.

I. Muller, S. Kordowich, C. Holzwarth, G. Isensee, P. Lang, F. Neunhoeffer, M. Dominici, J. Greil, and R. Handgretinger. Application of multipotent mesenchymal stromal cells in pediatric patients following allogeneic stem cell transplantation. *Blood Cells Mol Dis*, 40(1): 25–32, 2008.

H. Ni, P. S. T. Yuen, J. M. Papalia, J. E. Trevithick, T. Sakai, R. Fässler, R. O. Hynes, and D. D. Wagner. Plasma fibronectin promotes thrombus growth and stability in injured arterioles. *Proceedings of the National Academy of Sciences*, 100(5):2415–2419, 2003.

R. Nischt, C. Schmidt, N. Mirancea, A. Baranowsky, S. Mokkapati, N. Smyth, E. C. Woenne, H. J. Stark, P. Boukamp, and D. Breitkreutz. Lack of nidogen-1 and -2 prevents basement membrane assembly in skin-organotypic coculture. *J Invest Dermatol*, 127(3):545–54, 2007.

C. Nombela-Arrieta, J. Ritz, and L. E. Silberstein. The elusive nature and function of mesenchymal stem cells. *Nat Rev Mol Cell Biol*, 12(2):126–131, 2011.

J. Y. Oh, M. K. Kim, M. S. Shin, H. J. Lee, J. H. Ko, W. R. Wee, and J. H. Lee. The anti-inflammatory and anti-angiogenic role of mesenchymal stem cells in corneal wound healing following chemical injury. *Stem Cells*, 26(4):1047–1055, 2008.

A. Orimo, P. B. Gupta, D. C. Sgroi, F. Arenzana-Seisdedos, T. Delaunay, R. Naeem, V. J. Carey, A. L. Richardson, and R. A. Weinberg. Stromal fibroblasts present in invasive human breast carcinomas promote tumor growth and angiogenesis through elevated SDF-1/CXCL12 secretion. *Cell*, 121(3):335–48, 2005.

F. Otto, A. P. Thornell, T. Crompton, A. Denzel, K. C. Gilmour, I. R. Rosewell, G. W. H. Stamp, R. S. P. Beddington, S. Mundlos, B. R. Olsen, P. B. Selby, and M. J. Owen. Cbfa1, a candidate gene for cleidocranial dysplasia syndrome, is essential for osteoblast differentiation and bone development. *Cell*, 89(5):765–771, 1997.

J. Pairault and H. Green. A study of the adipose conversion of suspended 3T3 cells by using glycerophosphate dehydrogenase as differentiation marker. *Proc Natl Acad Sci U S A*, 76 (10):5138–42, 1979.

S. Paquet-Fifield, H. Schlüter, A. Li, T. Aitken, P. Gangatirkar, D. Blashki, R. Koelmeyer, N. Pouliot, M. Palatsides, S. Ellis, N. Brouard, A. Zannettino, N. Saunders, N. Thompson, J. Li, and P. Kaur. A role for pericytes as microenvironmental regulators of human skin tissue regeneration. *J Clin Invest.*, 119(9):2795–2806, 2009.

I. S. Park, M. Han, J. W. Rhie, S. H. Kim, Y. Jung, and I. H. Kim. The correlation between human adipose-derived stem cells differentiation and cell adhesion mechanism. *Biomaterials*, 30(36):6835–43, 2009.

R. F. Pereira, K. W. Halford, M. D. O'Hara, D. B. Leeper, B. P. Sokolov, M. D. Pollard, O. Bagasra, and D. J. Prockop. Cultured adherent cells from marrow can serve as long-lasting precursor cells for bone, cartilage, and lung in irradiated mice. *Proc Natl Acad Sci U S A*, 92(11):4857–61, 1995.

M. F. Pittenger, A. M. Mackay, S. C. Beck, R. K. Jaiswal, R. Douglas, J. D. Mosca, M. A. Moorman, D. W. Simonetti, S. Craig, and D. R. Marshak. Multilineage potential of adult human mesenchymal stem cells. *Science*, 284(5411):143–7, 1999.

V. Planat-Benard, C. Menard, M. Andre, M. Puceat, A. Perez, J.-M. Garcia-Verdugo, L. Penicaud, and L. Casteilla. Spontaneous cardiomyocyte differentiation from adipose tissue stroma cells. *Circ Res*, 94(2):223–229, 2004a.

V. Planat-Benard, J. S. Silvestre, B. Cousin, M. Andre, M. Nibbelink, R. Tamarat, M. Clergue, C. Manneville, C. Saillan-Barreau, M. Duriez, A. Tedgui, B. Levy, L. Penicaud, and L. Casteilla. Plasticity of human adipose lineage cells toward endothelial cells: Physiological and therapeutic perspectives. *Circulation*, 109(5):656–663, 2004b.

A. L. Ponte, E. Marais, N. Gallay, A. Langonné, B. Delorme, O. Hérault, P. Charbord, and J. Domenech. The in vitro migration capacity of human bone marrow mesenchymal stem cells: Comparison of chemokine and growth factor chemotactic activities. *Stem Cells*, 25(7): 1737–1745, 2007.

D. J. Prockop. Marrow stromal cells as stem cells for nonhematopoietic tissues. *Science*, 276 (5309):71–4, 1997.

R. Quarto, M. Mastrogiacomo, R. Cancedda, S. M. Kutepov, V. Mukhachev, A. Lavroukov, E. Kon, and M. Marcacci. Repair of large bone defects with the use of autologous bone marrow stromal cells. *New England Journal of Medicine*, 344(5):385–386, 2001.

L. F. Raheja, D. C. Genetos, A. Wong, and C. E. Yellowley. Hypoxic regulation of mesenchymal stem cell migration: the role of RhoA and HIF-1alpha. *Cell Biol Int.*, In press, 2011.

I. T. Rebustini, V. N. Patel, J. S. Stewart, A. Layvey, E. N. Georges-Labouesse, J. H. Miner, and M. P. Hoffman. Laminin [alpha]5 is necessary for submandibular gland epithelial morphogenesis and influences fgfr expression through [beta]1 integrin signaling. *Developmental Biology*, 308(1):15–29, 2007.

G. Regl, G. W. Neill, T. Eichberger, M. Kasper, M. S. Ikram, J. Koller, H. Hintner, A. G. Quinn, A. M. Frischauf, and F. Aberger. Human GLI2 and GLI1 are part of a positive feedback mechanism in basal cell carcinoma. *Oncogene*, 21(36):5529–5539, 2002.

J. Ringe, S. Strassburg, K. Neumann, M. Endres, M. Notter, G. Burmester, C. Kaps, and M. Sittinger. Towards in situ tissue repair: Human mesenchymal stem cells express chemokine receptors CXCR1, CXCR2 and CCR2, and migrate upon stimulation with CXCL8 but not CCL2. *Journal of Cellular Biochemistry*, 101(1):135–146, 2007.

A. S. Rowlands, P. A. George, and J. J. Cooper-White. Directing osteogenic and myogenic differentiation of MSCs: interplay of stiffness and adhesive ligand presentation. *Am J Physiol Cell Physiol*, 295(4):C1037–44, 2008.

D. Rubio, S. Garcia, T. De la Cueva, M. F. Paz, A. C. Lloyd, A. Bernad, and J. Garcia-Castro. Human mesenchymal stem cell transformation is associated with a mesenchymal-epithelial transition. *Exp Cell Res*, 314(4):691–8, 2008.

C. H. Ryu, S. A. Park, S. M. Kim, J. Y. Lim, C. H. Jeong, J. A. Jun, J. H. Oh, S. H. Park, W. I. Oh, and S. S. Jeun. Migration of human umbilical cord blood mesenchymal stem cells mediated by stromal cell-derived factor-1/CXCR4 axis via Akt, ERK, and p38 signal transduction pathways. *Biochem Biophys Res Commun*, 398(1):105–10, 2010.

K. M. Safford, S. D. Safford, J. M. Gimble, A. K. Shetty, and H. E. Rice. Characterization of neuronal/glial differentiation of murine adipose-derived adult stromal cells. *Experimental Neurology*, 187(2):319–328, 2004.

R. M. Salasznyk, W. A. Williams, A. Boskey, A. Batorsky, and G. E. Plopper. Adhesion to vitronectin and collagen I promotes osteogenic differentiation of human mesenchymal stem cells. *J Biomed Biotechnol*, 2004(1):24–34, 2004.

J. A. Santiago, R. Pogemiller, and B. M. Ogle. Heterogeneous differentiation of human mesenchymal stem cells in response to extended culture in extracellular matrices. *Tissue Eng Part A*, 15(12):3911–22, 2009.

V. F. M. Segers, I. Van Riet, L. J. Andries, K. Lemmens, M. J. Demolder, A. J. M. L. De Becker, M. M. Kockx, and G. W. De Keulenaer. Mesenchymal stem cell adhesion to cardiac microvascular endothelium: activators and mechanisms. *American Journal of Physiology - Heart and Circulatory Physiology*, 290(4):H1370–H1377, 2006.

I. Sekiya, B. L. Larson, J. R. Smith, R. Pochampally, J. G. Cui, and D. J. Prockop. Expansion of human adult stem cells from bone marrow stroma: conditions that maximize the yields of early progenitors and evaluate their quality. *Stem Cells*, 20(6):530–41, 2002.

C. Selhuber-Unkel, T. Erdmann, M. Lopez-Garcia, H. Kessler, U. S. Schwarz, and J. P. Spatz. Cell adhesion strength is controlled by intermolecular spacing of adhesion receptors. *Biophys J*, 98(4):543–51, 2010.

L. Sensebé, M. Krampera, H. Schrezenmeier, P. Bourin, and R. Giordano. Mesenchymal stem cells for clinical application. *Vox Sang*, 98(2):93–107, 2010.

M. J. Seo, S. Y. Suh, Y. C. Bae, and J. S. Jung. Differentiation of human adipose stromal cells into hepatic lineage in vitro and in vivo. *Biochemical and Biophysical Research Communications*, 328(1):258–264, 2005.

P. Shetty, K. Cooper, and C. Viswanathan. Comparison of proliferative and multilineage differentiation potentials of cord matrix, cord blood, and bone marrow mesenchymal stem cells. *Asian J Transfus Sci*, 4(1):14–24, 2010.

P. Singh, C. Carraher, and J. E. Schwarzbauer. Assembly of fibronectin extracellular matrix. *Annual Review of Cell and Developmental Biology*, 26(1):397–419, 2010.

H. Smola, G. Thiekotter, and N. E. Fusenig. Mutual induction of growth factor gene expression by epidermal-dermal cell interaction. *J Cell Biol*, 122(2):417–29, 1993.

V. Sordi, M. L. Malosio, F. Marchesi, A. Mercalli, R. Melzi, T. Giordano, N. Belmonte, G. Ferrari, B. E. Leone, F. Bertuzzi, G. Zerbini, P. Allavena, E. Bonifacio, and L. Piemonti. Bone marrow mesenchymal stem cells express a restricted set of functionally active chemokine receptors capable of promoting migration to pancreatic islets. *Blood*, 106(2):419–27, 2005.

E. Spaeth, A. Klopp, J. Dembinski, M. Andreeff, and F. Marini. Inflammation and tumor microenvironments: defining the migratory itinerary of mesenchymal stem cells. *Gene Ther*, 15(10):730–8, 2008.

B. M. Spiegelman and C. A. Ginty. Fibronectin modulation of cell shape and lipogenic gene expression in 3T3-adipocytes. *Cell*, 35(3 Pt 2):657–66, 1983.

W. D. Staatz, K. F. Fok, M. M. Zutter, S. P. Adams, B. A. Rodriguez, and S. A. Santoro. Identification of a tetrapeptide recognition sequence for the alpha 2 beta 1 integrin in collagen. *Journal of Biological Chemistry*, 266(12):7363–7367, 1991.

C. M. Stanford, P. A. Jacobson, E. D. Eanes, L. A. Lembke, and R. J. Midura. Rapidly forming apatitic mineral in an osteoblastic cell line (UMR 106_01 BSP). *Journal of Biological Chemistry*, 270(16):9420–9428, 1995.

M. Styner, B. Sen, Z. Xie, N. Case, and J. Rubin. Indomethacin promotes adipogenesis of mesenchymal stem cells through a cyclooxygenase independent mechanism. *J Cell Biochem*, 111(4):1042–50, 2010.

M. Sundin, O. Ringden, B. Sundberg, S. Nava, C. Gotherstrom, and K. Le Blanc. No alloantibodies against mesenchymal stromal cells, but presence of anti-fetal calf serum antibodies, after transplantation in allogeneic hematopoietic stem cell recipients. *Haematologica*, 92(9): 1208–15, 2007.

E. Thedinga, A. Kob, H. Holst, A. Keuer, S. Drechsler, R. Niendorf, W. Baumann, I. Freund, M. Lehmann, and R. Ehret. Online monitoring of cell metabolism for studying pharmacodynamic effects. *Toxicology and Applied Pharmacology*, 220(1):33–44, 2007.

K. Timper, D. Seboek, M. Eberhardt, P. Linscheid, M. Christ-Crain, U. Keller, B. Müller, and H. Zulewski. Human adipose tissue-derived mesenchymal stem cells differentiate into insulin, somatostatin, and glucagon expressing cells. *Biochemical and Biophysical Research Communications*, 341(4):1135–1140, 2006.

R. Timpl, H. Wiedemann, V. Van Delden, H. Furthmayr, and K. Kühn. A network model for the organization of type IV collagen molecules in basement membranes. *European Journal of Biochemistry*, 120(2):203–211, 1981.

M. Tio, K. H. Tan, W. Lee, T. T. Wang, and G. Udolph. Roles of db-cAMP, IBMX and RA in aspects of neural differentiation of cord blood derived mesenchymal-like stem cells. *PLoS ONE*, 5(2):e9398, 2010.

I. Titorencu, V. Jinga, E. Constantinescu, A. Gafencu, C. Ciohodaru, I. Manolescu, C. Zaharia, and M. Simionescu. Proliferation, differentiation and characterization of osteoblasts from human BM mesenchymal cells. *Cytotherapy*, 9(7):682–696, 2007.

S. Tomita, R. K. Li, R. D. Weisel, D. A. G. Mickle, E. J. Kim, T. Sakai, and Z. Q. Jia. Autologous transplantation of bone marrow cells improves damaged heart function. *Circulation*, 100(90002):II–247–256, 1999.

J. Vandesompele, K. De Preter, F. Pattyn, B. Poppe, N. Van Roy, A. De Paepe, and F. Speleman. Accurate normalization of real-time quantitative RT-PCR data by geometric averaging of multiple internal control genes. *Genome Biology*, 3(7):research0034.1 – research0034.11, 2002.

V. Volloch and D. Kaplan. Matrix-mediated cellular rejuvenation. *Matrix Biol*, 21(6):533–43, 2002.

W. Wagner, F. Wein, A. Seckinger, M. Frankhauser, U. Wirkner, U. Krause, J. Blake, C. Schwager, V. Eckstein, W. Ansorge, and A. D. Ho. Comparative characteristics of mesenchymal stem cells from human bone marrow, adipose tissue, and umbilical cord blood. *Exp Hematol*, 33(11):1402–16, 2005.

W. Wagner, Jr. Feldmann, R. E., A. Seckinger, M. H. Maurer, F. Wein, J. Blake, U. Krause, A. Kalenka, H. F. Burgers, R. Saffrich, P. Wuchter, W. Kuschinsky, and A. D. Ho. The heterogeneity of human mesenchymal stem cell preparations–evidence from simultaneous analysis of proteomes and transcriptomes. *Exp Hematol*, 34(4):536–48, 2006.

K. Warstat, D. Meckbach, M. Weis-Klemm, A. Hack, G. Klein, P. de Zwart, and W. K. Aicher. TGF-beta enhances the integrin alpha2beta1-mediated attachment of mesenchymal stem cells to type I collagen. *Stem Cells Dev*, 19(5):645–56, 2010.

J. Wiest, T. Stadthagen, M. Schmidhuber, M. Brischwein, J. Ressler, U. Raeder, H. Grothe, A. Melzer, and B. Wolf. Intelligent mobile lab for metabolics in environmental monitoring. *Analytical Letters*, 39:1759–1771, 2006.

F. Xu, J Shi, B Yu, W. Ni, X. Wu, and Z Gu. Chemokines mediate mesenchymal stem cell migration toward gliomas in vitro. *Oncol Rep.*, 23(6):1561–1567, 2010.

J. Xu, E. Bae, Q. Zhang, D. S. Annis, H. P. Erickson, and D. F. Mosher. Display of cell surface sites for fibronectin assembly is modulated by cell adherence to 1F3 and C-terminal modules of fibronectin. *PLoS ONE*, 4(1):e4113, 2009.

F. Yao, T. Svensjö, T. Winkler, M. Lu, C. Eriksson, and E. Eriksson. Tetracycline repressor, tetR, rather than the tetR-mammalian cell transcription factor fusion derivatives, regulates inducible gene expression in mammalian cells. *Human Gene Therapy*, 9(13):1939–1950, 1998.

K. Yoshimura, K. Sato, N. Aoi, M. Kurita, K. Inoue, H. Suga, H.i Eto, H. Kato, T. Hirohi, and K. Harii. Cell-assisted lipotransfer for facial lipoatrophy: Efficacy of clinical use of adipose-derived stem cells. *Dermatologic Surgery*, 34(9):1178–1185, 2008.

S. Zhao, R. Wehner, M. Bornhauser, R. Wassmuth, M. Bachmann, and M. Schmitz. Immunomodulatory properties of mesenchymal stromal cells and their therapeutic consequences for immune-mediated disorders. *Stem Cells Dev*, 19(5):607–14, 2010.

C. F. Zizola, V. Julianelli, G. Bertolesi, M. Yanagishita, and J. C. Calvo. Role of versican and hyaluronan in the differentiation of 3T3-L1 cells into preadipocytes and mature adipocytes. *Matrix Biology*, 26(6):419–430, 2007.

P. A. Zuk, M. Zhu, H. Mizuno, J. Huang, J. W. Futrell, A. J. Katz, P. Benhaim, H. P. Lorenz, and M. H. Hedrick. Multilineage cells from human adipose tissue: implications for cell-based therapies. *Tissue Eng*, 7(2):211–28, 2001.

P. A. Zuk, M. Zhu, P. Ashjian, D. A. De Ugarte, J. I. Huang, H. Mizuno, Z. C. Alfonso, J. K. Fraser, P. Benhaim, and M. H. Hedrick. Human adipose tissue is a source of multipotent stem cells. *Mol Biol Cell*, 13(12):4279–95, 2002.

Appendix

Scientific publication

Angstmann M, Brinkmann I, Bieback K, Breitkreutz D, Maercker C.; Monitoring human mesenchymal stromal cell differentiation by electrochemical impedance sensing. Cytotherapy. 2011 May 30. [Epub ahead of print]

Oral Presentation

Michael Angstmann; Monitoring human mesenchymal stem cell differentiation in live cell chips; 20th Annual Conference of the German Society for Cytometry; Leipzig; 2010, October 13-15.

Poster Presentations

Michael Angstmann, Christian Maercker, Petra Boukamp, Roswitha Nischt, Dirk Breitkreutz; Inducible Nidogen Expression in Epidermal HaCaT Cells; XIIIth International Symposium on Basement Membranes; Cologne; 2007 September 19-22.

Michael Angstmann, Ariane Tomsche, Claudia Soldner, Chris Rippolz, Armin Bieser, Petra Boukamp, Margareta Müller, Roswitha Nischt, Karen Bieback, Dirk Breitkreutz, Christian Maercker; Characterization of mesenchymal stem cells by electric cell-substrate impedance sensing (ECIS); Biotechtag, University of Applied Science, Mannheim; 2007 October 10.

Michael Angstmann, Christian Maercker, Roswitha Nischt, Harald Schnidar, Fritz Aberger, Petra Boukamp, Dirk Breitkreutz Inducible Nidogen Expression in Epidermal HaCaT Cells; 31th Annual Meeting of the German Society of Cell Biology (DGZ); Marburg, 2008 March 12-15.

Michael Angstmann, Armin Bieser, Karen Bieback, Dirk Breitkreutz, Christian Maercker; Monitoring of mesenchymal stem cell differentiation by electric cell-substrate impedance sensing (ECIS); Europ J Cell Biol 87(S58) 16 (2008) (P); 31th Annual Meeting of the German Society of Cell Biology (DGZ); Marburg, 2008 March 12-15.

M. Angstmann, F. Graf, C. Maercker, D. Breitkreutz; Induction of mesenchymal stem cell differentiation - early changes in cell substrate/-extracellular matrix interactions; EJCB European Journal of Cell Biology 88S1, Suppl. 59 (2009 March) MS3-1; 32th Annual Meeting of the German Society of Cell Biology (DGZ); Konstanz; 2009 March 24-27.

M. Angstmann, F. Graf, K. Bieback, D. Breitkreutz, C. Maercker; Induction of mesenchymal stem cell differentiation - early changes in cell substrate/extracellular matrix interactions (cell adhesion, impedance); 3rd International Workshop "Multipotent Stromal Cells (MSCs) for Regenerative Medicine and Immune Regulation", Frankfurt; 2009 June 12-13.

Michael Angstmann, Fabian Graf, Karen Bieback, Dirk Breitkreutz, Christian Maercker; Monitoring of mesenchymal stem cell differentiation; Biotechtag, University of Applied Science, Mannheim; 2009 November 03.

Michael Angstmann, Karen Bieback, Dirk Breitkreutz, Christian Maercker; Induction of Mesenchymal Stem Cell Differentiation - Early Changes in Cell-Substrate/-Extracellular Matrix Interactions; 33rd Annual Meeting of the German Society of Cell Biology (DGZ); Regensburg; 2010 March 10-13.

Contributions to abstracts

Michael Angstmann, Karen Bieback, Dirk Breitkreutz, Christian Maercker; Translating functional genomics into the clinics: Characterization and isolation of differentiating mesenchymal stem cells in live cell chips; 14th Human genome meeting (HGM); Montpellier, France; 2010 May 18-20.

Michael Angstmann, Irena Brinkmann, Karen Bieback, Dirk Breitkreutz, Christian Maercker; Monitoring of mesenchymal stem cell differentiation; 34th Annual Meeting of the German Society of Cell Biology (DGZ); Bonn; 2011 March 30 - April 2.

Irena Brinkmann, **Michael Angstmann**, Christian Maercker, Dirk Breitkreutz, Karen Bieback; Electrochemical impedance sensing to non-invasive monitor mesenchymal stromal cell differentiation potential; 44th Annual Meeting of the German Society of Transfusion Medicine and Hemotherapy (DGTI); Hannover; 2011 September 27-30.

Michael Angstmann, Haotian Wang, Achim Breiling, Karen Bieback, Dirk Breitkreutz, Frank Lyko, Christian Maercker; Cell adhesion as a marker for molecular processes during stem cell differentiation; 1st Joint CSH Asia/ISSCR Conference on Cellular Programs and Reprogramming; Suzhou, China; 2011 October 24-27.

Declaration

I hereby declare that this thesis has been prepared by me without the prohibited assistance of third parties and without making use of aids other than those specified. This thesis has not previously been presented in identical or similar form to any other German or foreign examination board.

Heidelberg, 14^{th} of July 2011

(Michael Angstmann)